

Time resolution of silicon sensors

Werner Riegler, CERN, werner.riegler@cern.ch

October 15, 2021

Abstract

Precision timing with solid state detectors is being employed in many areas of particle physics instrumentation. Applications for pileup rejection and time of flight measurements at the LHC are just two of many notable examples.

During the past years the principal contributions to the time resolution for various types of silicon sensors have been studied. The principal contributors to the time resolution are Landau fluctuations, electronics noise, signal shape fluctuations due to a varying pad response function as well as gain fluctuations.

We discuss silicon pad and silicon pixel sensors, LGAD sensors as well as SPADs and SiPMs. These sensors have been simulated using the Garfield++ toolkit. The analytic statistical analysis of the contributions to the time resolution has been performed, resulting in elementary expressions for the timing performance of these sensors. These expressions show the basic directions for optimization of these sensors as well as the fundamental limits to the time resolution.

Outline

- Time resolution of 'standard' planar silicon detectors
- Signal processing and center of gravity (c.o.g.) time of a signal
- Contribution from noise, optimum filters
- Contributions from 'weighting fields'
- Time resolution of MAPS sensors
- Time resolution Low Gain Avalanche Diodes (LGADS)
- Single Photon Avalanche Diodes (SPADs), Silicon Photomultipliers (SiPMs)
- SPAD time resolution and efficiency for photons and charged particles

References for this talk

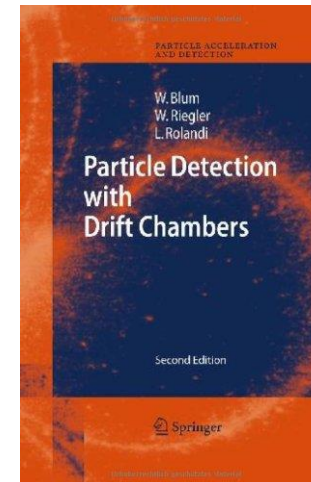
W. Riegler and G. Aglieri Rinella, **Time resolution of silicon pixel sensors**, JINST 12 (2017) P11017

W. Riegler and G. Aglieri Rinella, **Point Charge Potential and Weighting field of a Pixel or Pad in a Plane Condenser**, NIMA 767 (2014) 267-27

W. Riegler, P. Windischhofer, **Time resolution and efficiency of SPADs and SiPMs for photons and charged particles**, NIMA 1003 (2021) 165265

P. Windischhofer, W. Riegler, **The statistics of electron–hole avalanches**, NIMA 1003 (2021) 165327

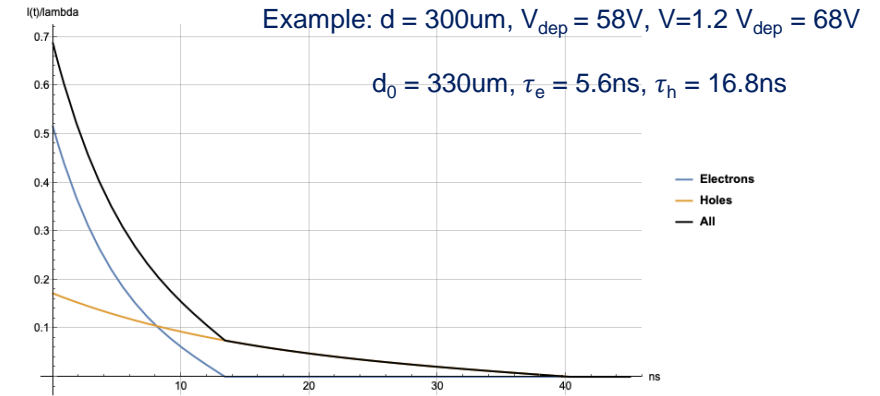
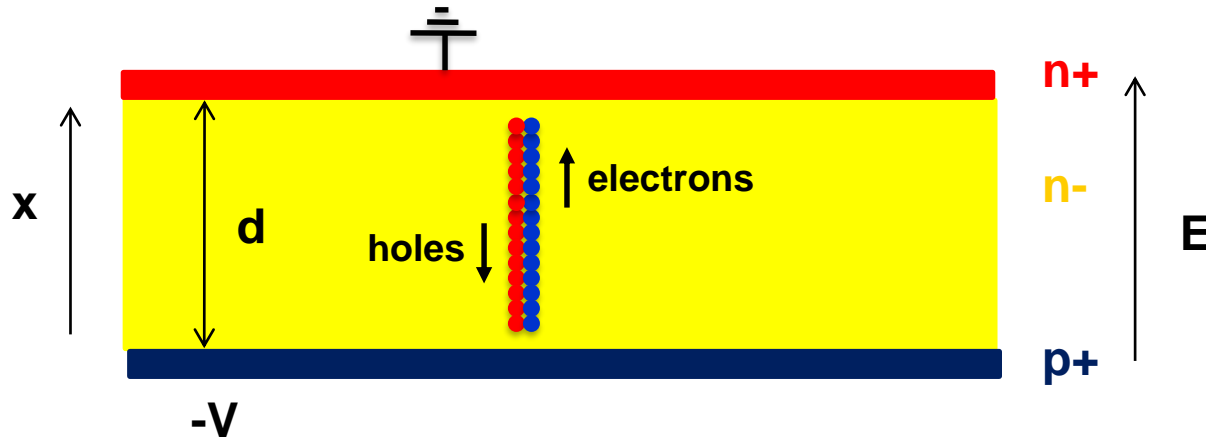
W. Blum, W. Riegler, L. Rolandi, **Particle Detection with Drift Chambers**, Springer 2008, ISBN: 978-3-540-76683-4



Signal Processing,
Noise, optimum filters
etc.

Time resolution of 'standard' silicon sensors

Intrinsic time resolution of a 'large' silicon pad detector



In silicon sensors the signal edge is instantaneous (i.e. sub ps level)

- acceleration of electrons to 10^7cm/s in vacuum is 0.14ps
- passage of the particle through a 50 μm sensor takes 0.16ps

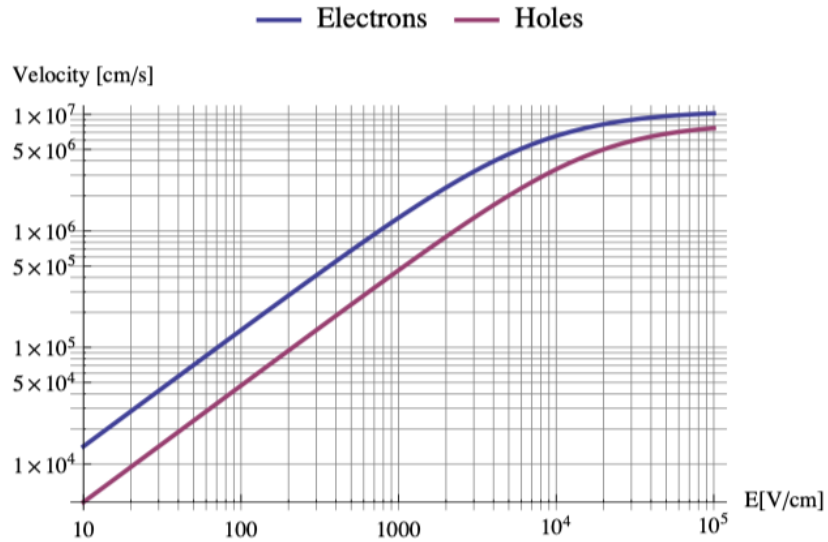
In Wire Chambers the electrons first have to move to the wires before an avalanche at the wire leads to an appreciable signal
→ intrinsic resolution limit.

In RPCs the avalanche starts instantly, but it still takes some time until the signal reaches the threshold
→ intrinsic resolution limit.

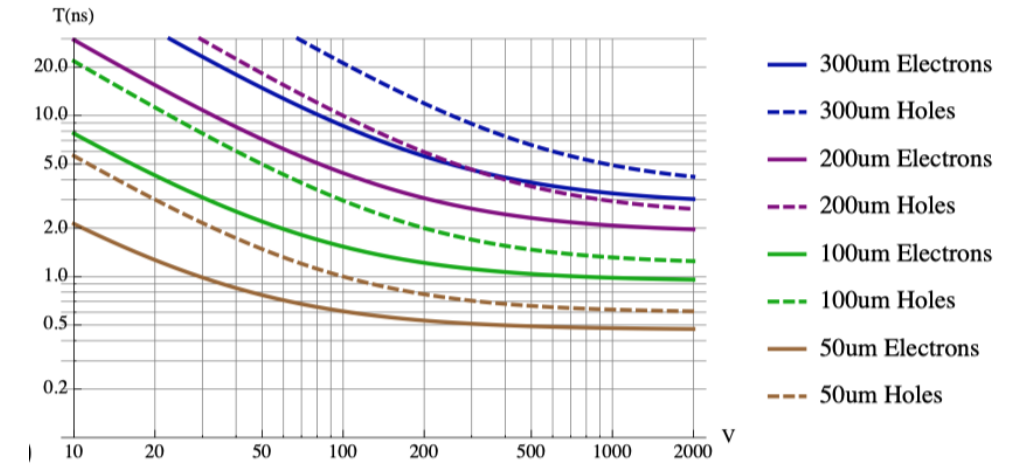
→ The intrinsic time resolution of a silicon sensor is infinite (sub ps).

→ The time resolution in a planar silicon sensor without gain is a question of signal/noise/electronics and specifically the Landau fluctuations within the electronics integration time.

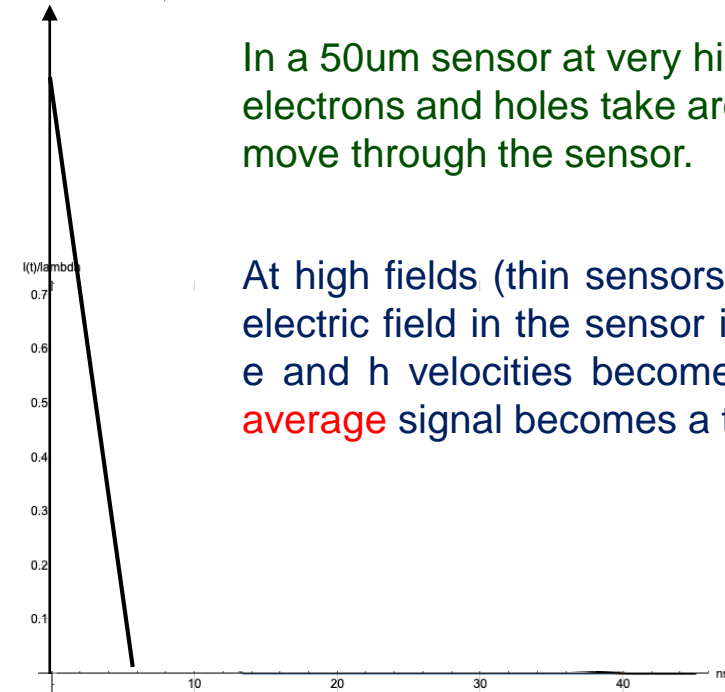
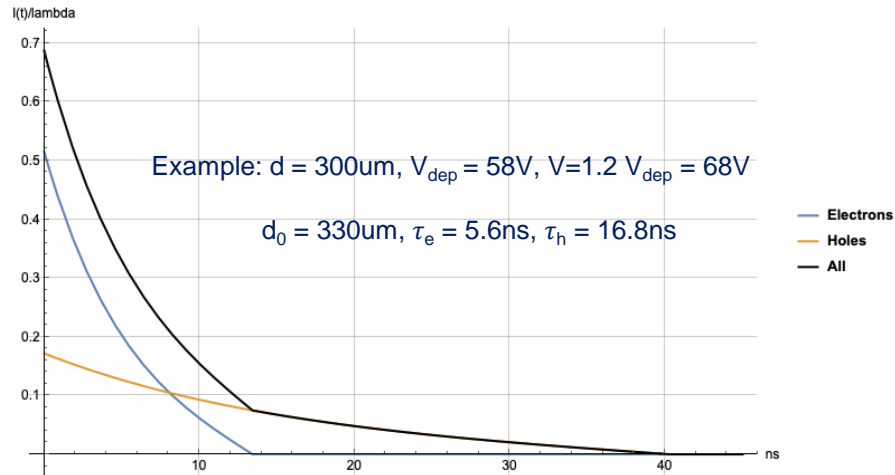
Total drift time of electrons and holes in the silicon sensor



At high electric fields, the drift-velocity saturates around 10^7 cm/s = $0.1 \mu\text{m}/\text{ps}$ for both, electrons and holes.

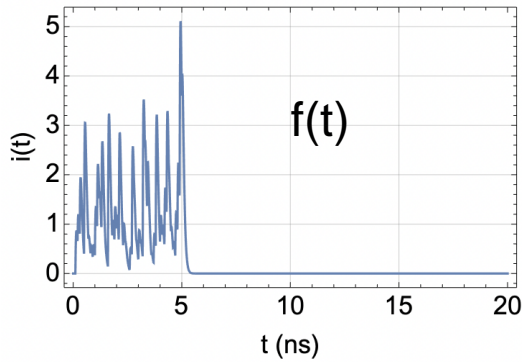


In a 50um sensor at very high voltage the electrons and holes take around 500ps to move through the sensor.



At high fields (thin sensors, large voltage), the electric field in the sensor is close to constant, e and h velocities become saturated and the **average** signal becomes a triangle.

Electronics processing of a detector signal



Frontend delta response:

$$h(t) = \left(\frac{t}{t_p}\right)^n e^{n(1-t/t_p)} \Theta(t)$$

Corresponding transfer function:

$$H(\omega) = \frac{t_p e^n n!}{(n + i\omega t_p)^{n+1}}$$

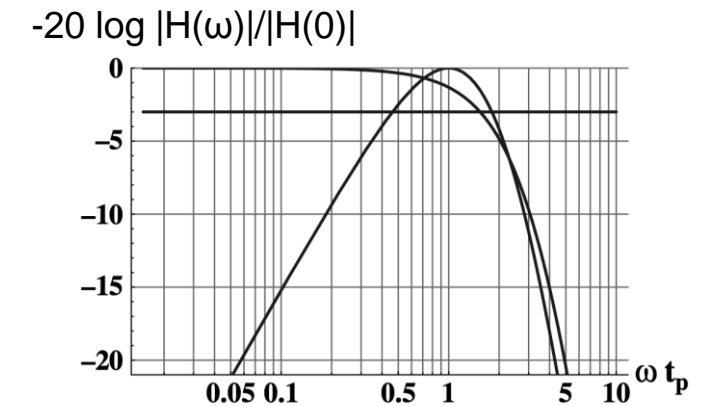
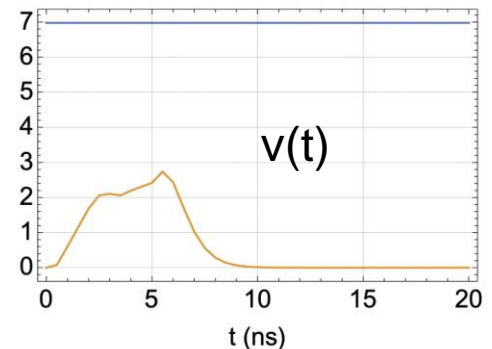
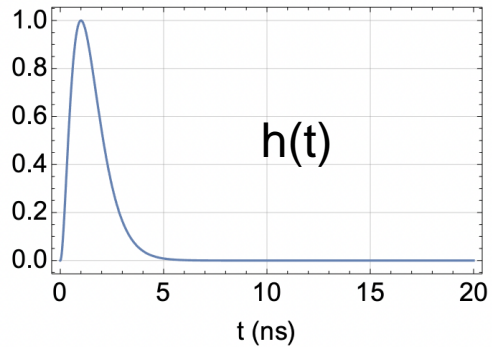
$$v(t) = \int_0^t h(t - t') f(t') dt'$$

$$\Theta(t) = \begin{cases} 0 & x < 0 \\ 1 & x > 0 \end{cases}$$

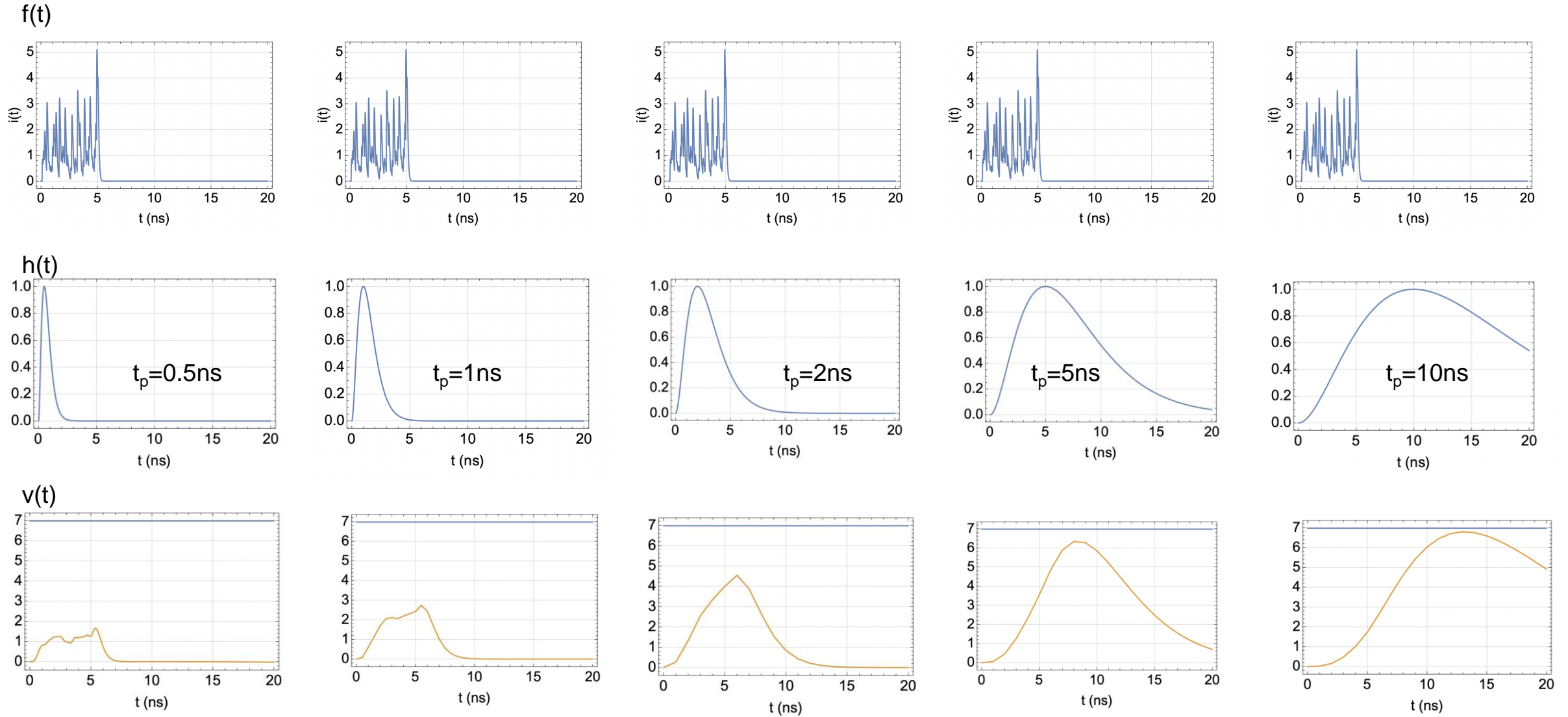
$$\omega_{bw} = n \sqrt{2^{1/(n+1)} - 1} / t_p$$

$$\approx 1.54/t_p \text{ for } n = 4$$

$$t_p = 1 \text{ ns} \quad f_{bw} \sim 250 \text{ MHz}$$



Electronics processing of a detector signal



If the peaking time t_p becomes larger than the signal length, the peak of the output signal approaches the total charge. What else ... ?

Electronics processing of a detector signal

Signal duration of T i.e. $f(t) = 0$ for $t > T$

Electronics peaking time $t_p \gg T$

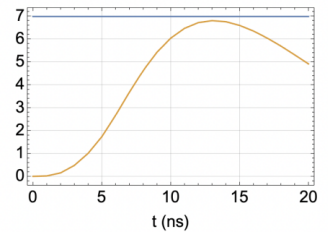
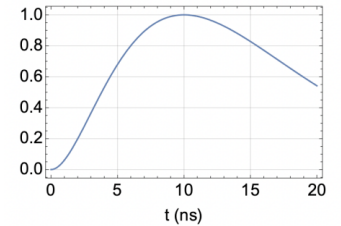
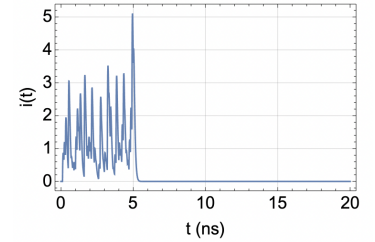
We are interested in times $t > T$

$$\begin{aligned}v(t) &= \int_0^t h(t-t') f(t') dt' \\&\approx \int_0^T [h(t) - h'(t)t'] f(t') dt' \\&= h(t) \int_0^T f(t') dt' - h'(t) \int_0^T t' f(t') dt' \\&= \int_0^T f(t') dt' \left[h(t) - h'(t) \frac{\int_0^T t' f(t') dt'}{\int_0^T f(t') dt'} \right] \\&= q [h(t) - h'(t)t_{cog}] \\&= \underline{q h(t - t_{cog})}\end{aligned}$$

In case the electronics peaking time t_p is longer than the signal duration T, the electronics output signal has

- the same shape as the delta response
- a pulse-height equal to the total charge of the signal
- a 'time displacement' of this delta response by the center of gravity time t_{cog} of the signal.

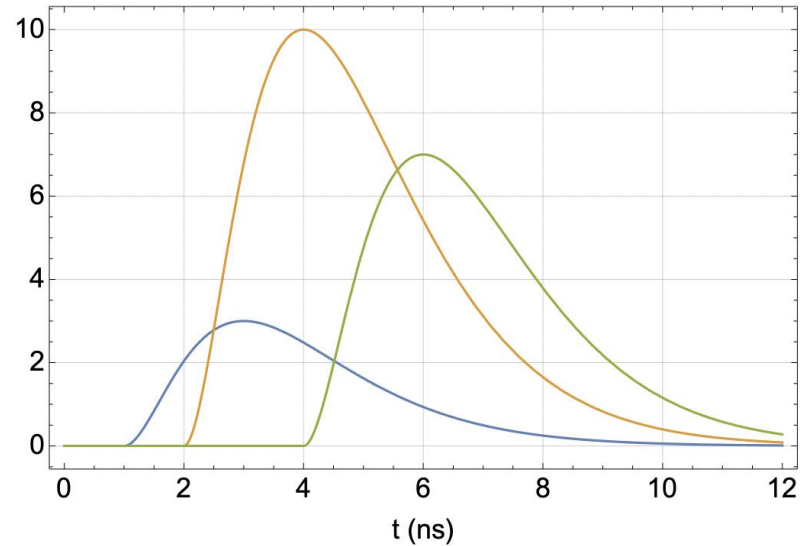
→ An amplifier that is 'slower' than the signal measures the center of gravity time of the signal



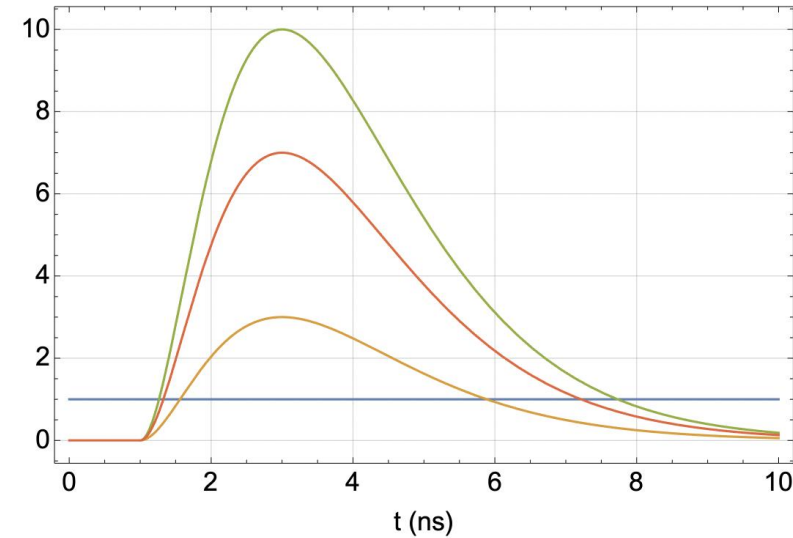
$$q = \int_0^T f(t') dt' \quad t_{cog} = \frac{\int_0^T t' f(t') dt'}{\int_0^T f(t') dt'} = \frac{1}{q} \int_0^T t' f(t') dt'$$

Electronics 'slower' than the detector signal, time slewing

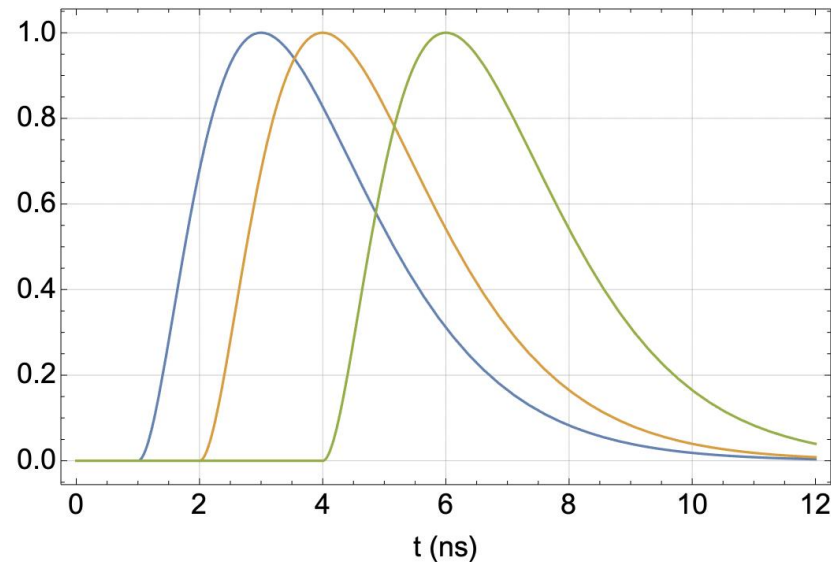
Delta response shifted by t_{cog} and scaled by Q



'time slewing'



Signal normalized to same amplitude \rightarrow time

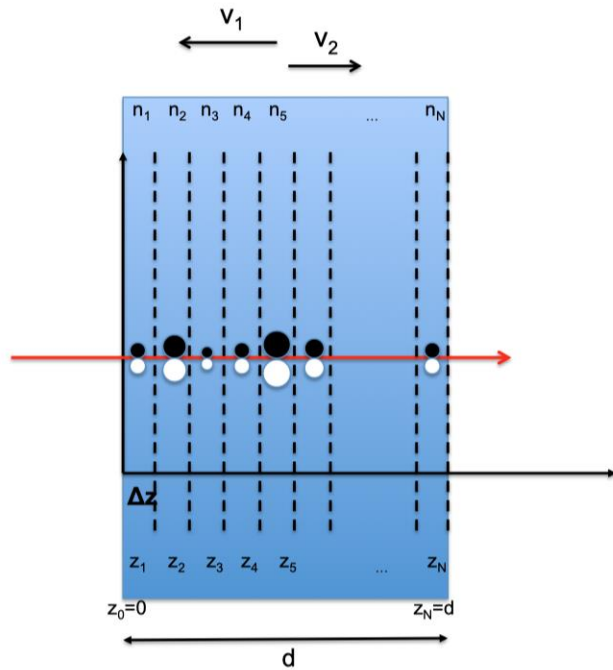


There are many different ways to correct for this slewing effect

- Constant Fraction discrimination
- Standard discrimination using time over threshold to correct for pulse-height
- Standard discrimination + pulseheight to correct for pulse-height
- Standard discrimination + total charge to correct for pulse-height
- Multiple sampling and 'fitting' the know signal shape
-

\rightarrow What is the c.o.g. time resolution of a silicon sensor ?

Energy deposit in silicon



A high energy particle passing the sensor will experience primary interactions, with an average distance of around $\lambda=0.21\mu\text{m}$. In each interaction there is a probability $p_{clu}(n)$ to produce a cluster of n electrons. The probability $p(n, \Delta z)$ have n e-h pairs in Δz is therefore

$$p(n, \Delta z)dn = \left(1 - \frac{\Delta z}{\lambda}\right) \delta(n)dn + \frac{\Delta z}{\lambda} p_{clu}(n)dn$$

$$P(s, d) = \mathcal{L}[p(n, d)] = \mathcal{L}[p(n, \Delta z)]^N = \left(1 + \frac{d}{\lambda N} (P_{clu}(s) - 1)\right)^N$$

The probability to have n e-h pairs in the sensor of thickness d , $p(n, d)$ is then

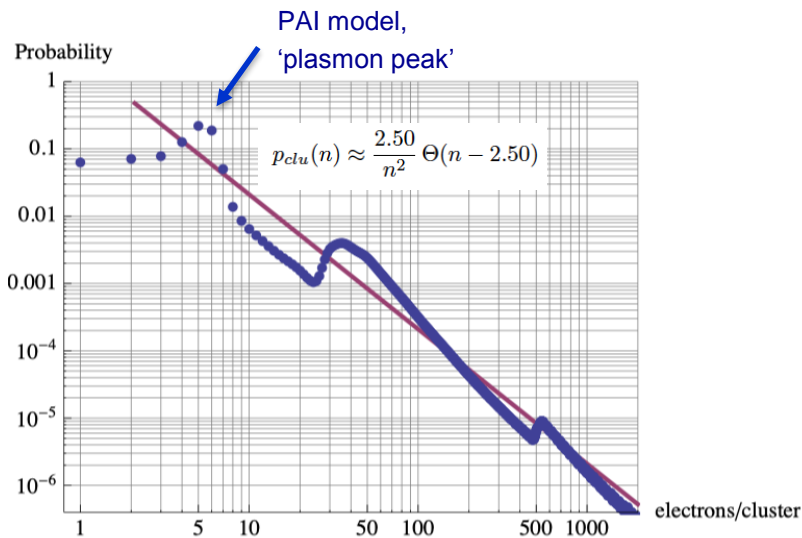
$$p(n, d) = \mathcal{L}^{-1} \left[e^{d/\lambda (P_{clu}(s) - 1)} \right]$$

The cluster size distribution is $p_{clu}(n)$ is typically calculated using the PAI model. Landau's approach assumes a $1/E^2$ distribution for the energy transfer in accordance with Rutherford scattering, which leads to an $1/n^2$ distribution for the e-h pairs

$$p_{clu}(n) \approx \frac{2.50}{n^2} \Theta(n - 2.50)$$

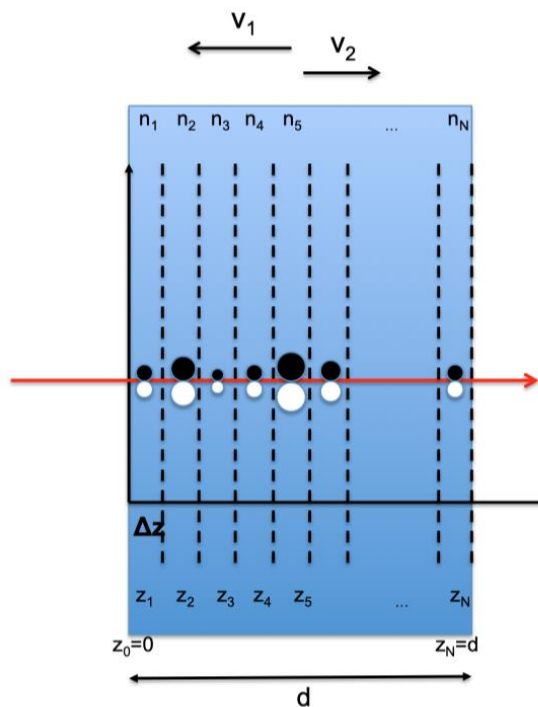
$$p(n, d)dn = \frac{\lambda}{2.50 d} L \left(\frac{\lambda}{2.50 d} n + C_\gamma - 1 - \log \frac{d}{\lambda} \right) dn$$

$$L(x) = \frac{1}{\pi} \int_0^\infty e^{-t \log t - x t} \sin(\pi t) dt$$



→ Landau distribution

Energy deposit in silicon



Most probable number of e-h pairs:

$$n_{MP} \approx \frac{2.50 d}{\lambda} \left(0.2 + \log \frac{d}{\lambda} \right)$$

Full width of half maximum

$$\frac{\Delta n_{FWHM}}{n_{MP}} \approx \frac{4.02}{0.2 + \log d/\lambda}$$

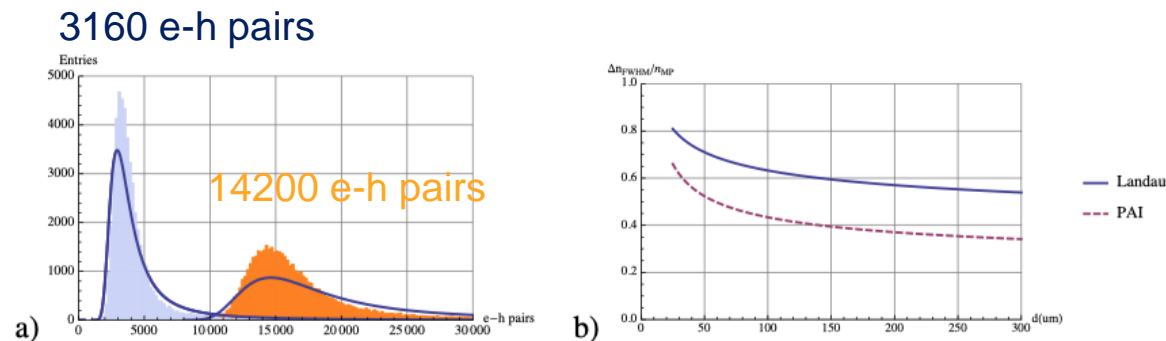
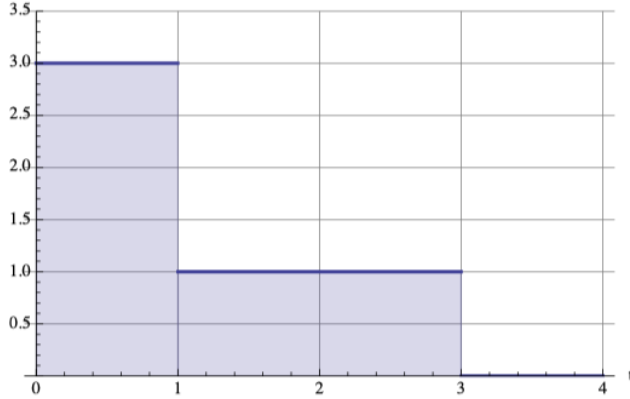


Figure 2. a) Distribution of the number of e-h pairs in 50 μm (blue) and 200 μm of silicon. The histograms show the PAI model, the solid lines show the Landau theory. b) Ratio of full width half maximum and most probable values for the Landau and PAI model for different values of silicon thickness. The Landau theory overestimates the fluctuations by 25–35%.

Figure 2a shows the distribution of e-h pairs in a 50 μm and a 200 μm sensor for the PAI model together with the curves from the Landau theory. As seen in figure 2b the Landau theory overestimates the fluctuations by 25–35%. The PAI model predicts a most probable number of 3160, 6710, 14200, 21900 e-h pairs in 50, 100, 200, 300 μm of silicon, which is within 10% of the values from the Landau theory when assuming a cutoff of $n_0 = 2.2$. We will use both models for evaluation of the time resolution in the following.

Center of gravity time of a silicon detector signal

Single e-h pair



$$i(t) = -\frac{qv_1}{d}\Theta(z/v_1 - t) - \frac{qv_2}{d}\Theta((d-z)/v_2 - t) \quad (4.1)$$

with $\Theta(t)$ being the Heaviside step function. An example is shown in figure 3b. We have $\int i(t)dt = -q$ and according to eq. (3.1) the centroid time of this signal is then

$$\tau = \frac{1}{2d} \left[\frac{z^2}{v_1} + \frac{(d-z)^2}{v_2} \right] \quad (4.2)$$

If n_1, n_2, \dots, n_N charges are produced at positions z_1, z_2, \dots, z_N and are moving to the electrodes with v_1 and v_2 , the resulting centroid time of the signal is

$$\tau(n_1, n_2, \dots, n_N) = \frac{1}{2d \left(\sum_{k=1}^N n_k \right)} \sum_{k=1}^N n_k \left[\frac{z_k^2}{v_1} + \frac{(d-z_k)^2}{v_2} \right] \quad (4.3)$$

We now divide the sensor of thickness d into N slices of $\Delta z = d/N$ as shown in figure 1. The probability to have n_k e/h pairs in slice k is given by the Landau distribution $p(n_k, \Delta z)$ and if we

After some lengthy evaluation:

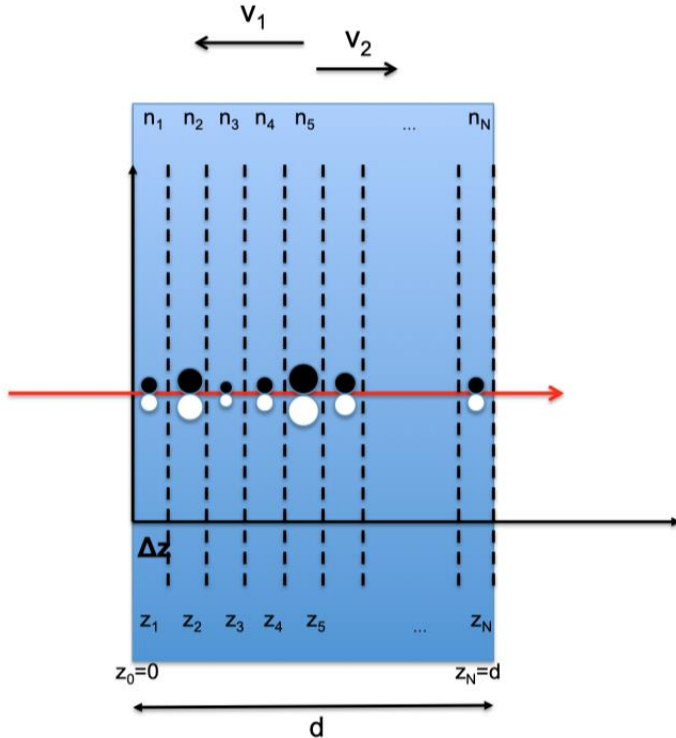
$$\Delta_\tau^2 = \overline{\tau^2} - \bar{\tau}^2 \quad (4.4)$$

with $\bar{\tau}$ and $\overline{\tau^2}$ being the average and the second moment of τ . The evaluation is given in B and we find

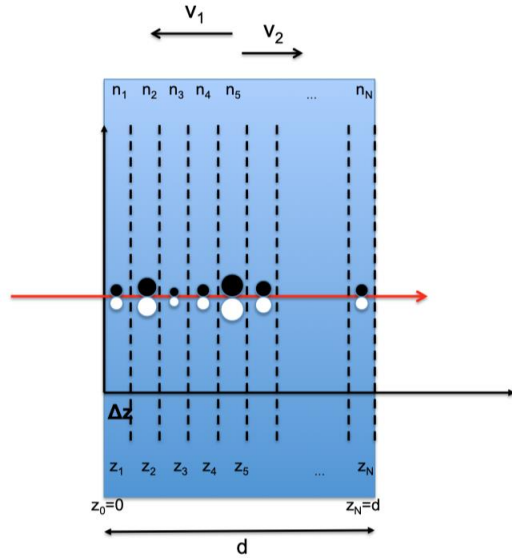
$$\Delta_\tau = w(d) \sqrt{\frac{4}{180} \frac{d^2}{v_1^2} - \frac{7}{180} \frac{d^2}{v_1 v_2} + \frac{4}{180} \frac{d^2}{v_2^2}} \quad (4.5)$$

with

$$w(d)^2 = \frac{d}{\lambda} \int_0^\infty \left[\int_0^\infty \frac{n_1^2 p_{clu}(n_1)}{(n_1 + n)^2} dn_1 \right] p(n, d) dn \quad (4.6)$$



Centroid time of a silicon detector signal



$$\Delta\tau = w(d) \sqrt{\frac{4}{180} \frac{d^2}{v_1^2} - \frac{7}{180} \frac{d^2}{v_1 v_2} + \frac{4}{180} \frac{d^2}{v_2^2}}$$

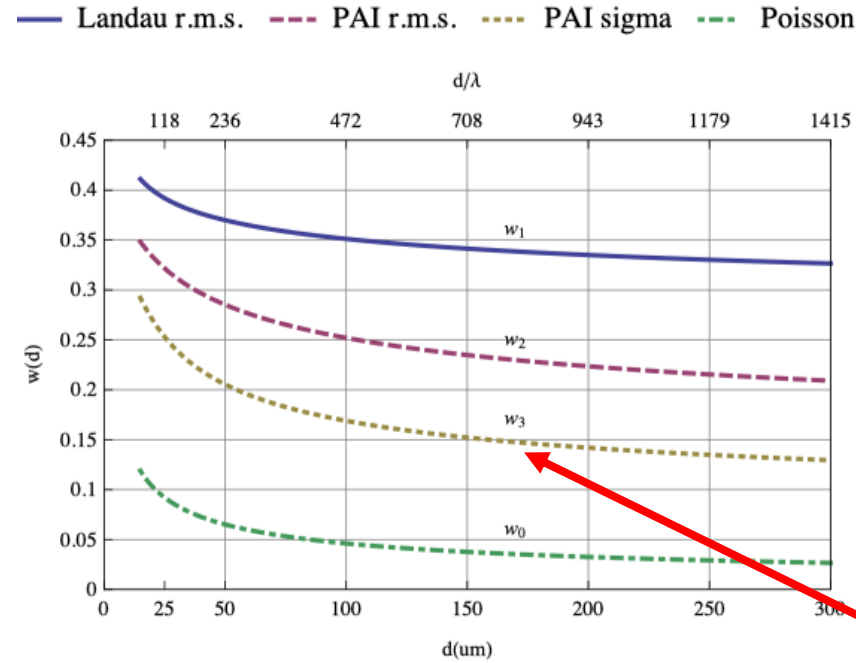
$$w(d)^2 = \frac{d}{\lambda} \int_0^\infty \left[\int_0^\infty \frac{n_1^2 p_{clu}(n_1)}{(n_1 + n)^2} dn_1 \right] p(n, d) dn$$

For $v_1=v_2$

$$\Delta_t = w(d) \frac{1}{\sqrt{180}} \frac{d}{v} \approx 0.075 w(d) T$$

50um sensor: $0.075 \times 0.2 \times 650\text{ps} = 10\text{ps}$

T= total e- drift time = total h drift time
= total width of the 'triangle'



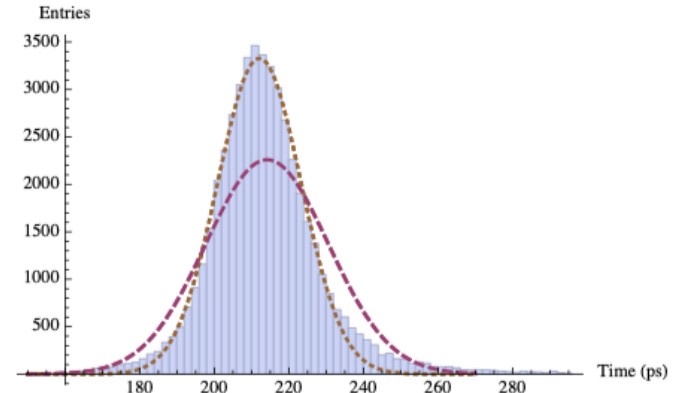
For the Landau Theory

$$w(d)^2 = \frac{1}{\ln(d/\lambda)} \quad d/\lambda \rightarrow \infty$$

For a thinner sensor – the contribution from Landau fluctuation increases.

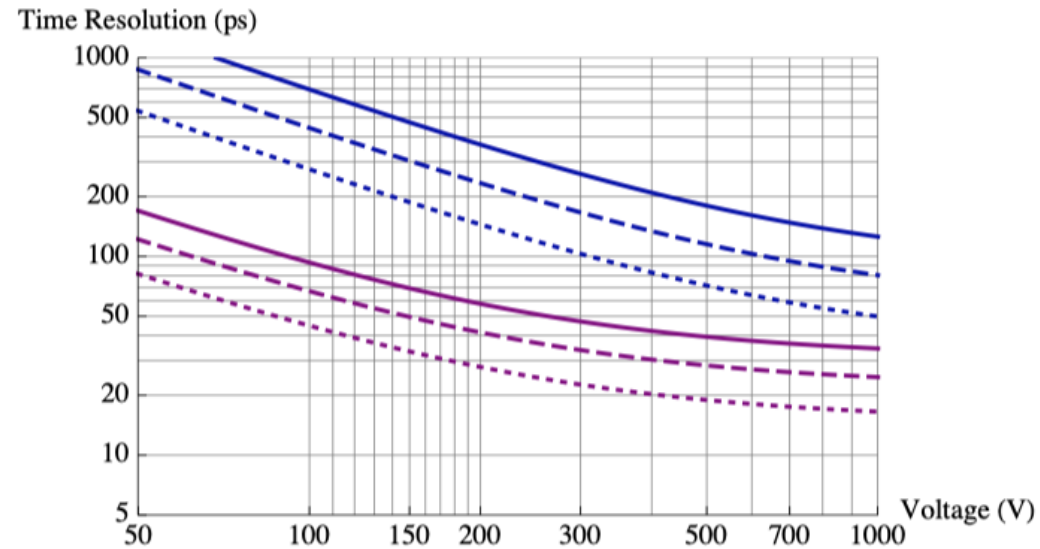
This worsening of the resolution is superseded by the decrease of e-h drift times.

For Si sensors: Important difference between r.m.s. time resolution and the σ of the core of the distribution.

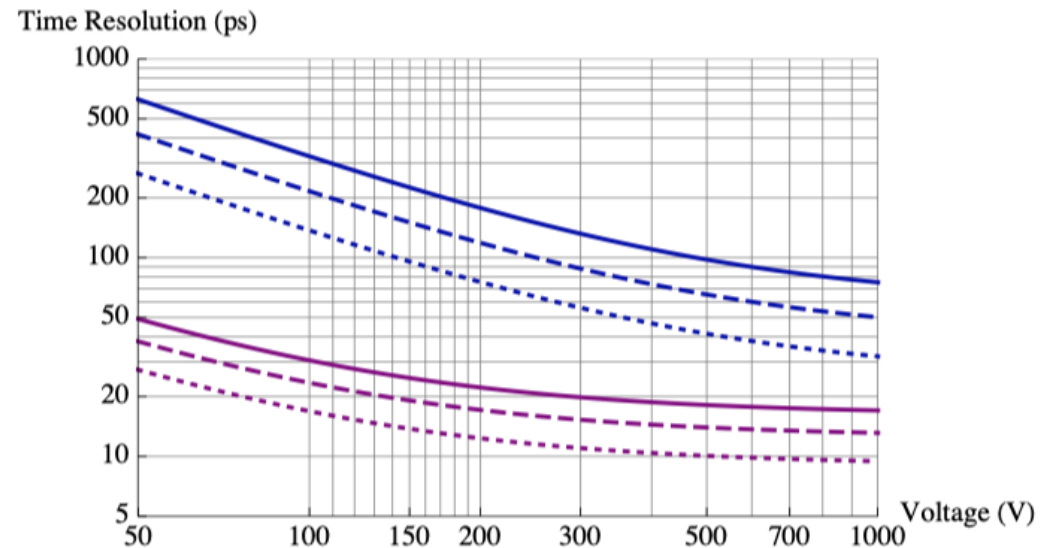


PAI model, Gauss fit

Center of gravity time resolution for silicon sensors



- d=300um, Landau r.m.s.
- - d=300um, PAI r.m.s.
- ... d=300um, PAI sigma
- d=100um, Landau r.m.s.
- - d=100um, PAI r.m.s.
- ... d=100um, PAI sigma



- d=200um, Landau r.m.s.
- - d=200um, PAI r.m.s.
- ... d=200um, PAI sigma
- d=50um, Landau r.m.s.
- - d=50um, PAI r.m.s.
- ... d=50um, PAI sigma

50um sensor, 10ps

Leading edge discrimination

$$f(x) = x^n e^{n(1-x)} \quad (4.61)$$

The amplifier output signal is then given by the convolution of the induced signal and the amplifier delta response

$$s(n_1, n_2, \dots, n_N, x, y, t) = c \int_0^t f\left(\frac{t-t'}{t_p}\right) i(n_1, n_2, \dots, n_N, x, y, t') dt' \quad (4.62)$$

$$= c q \sum_{k=1}^N n_k g(x, y, k \Delta z, t) \quad (4.63)$$

where $g(x, y, z, t)$ is

$$g(x, y, z, t) = \Theta(z - v_1 t) \int_{\frac{z-v_1 t}{d}}^{\frac{z}{d}} f\left(\frac{v_1 t - z + ud}{v_1 t_p}\right) E_w^z(x/d, y/d, u, w_x/d, w_y/d, 1) du \quad (4.64)$$

$$+ \Theta(v_1 t - z) \int_0^{\frac{z}{d}} f\left(\frac{v_1 t - z + ud}{v_1 t_p}\right) E_w^z(x/d, y/d, u, w_x/d, w_y/d, 1) du$$

$$+ \Theta[(d - z) - v_2 t] \int_{\frac{z}{d}}^{\frac{z+v_2 t}{d}} f\left(\frac{v_2 t + z - ud}{v_2 t_p}\right) E_w^z(x/d, y/d, u, w_x/d, w_y/d, 1) du$$

$$+ \Theta[v_2 t - (d - z)] \int_{\frac{z}{d}}^1 f\left(\frac{v_2 t + z - ud}{v_2 t_p}\right) E_w^z(x/d, y/d, u, w_x/d, w_y/d, 1) du$$

$$\bar{h}(t) = \frac{c}{w_x w_y} \iint \left[\int_0^1 g(x, y, sd, t) ds \right] dx dy \quad (4.66)$$

and

$$\Delta_h^2(t) = w(d)^2 \frac{c^2}{w_x w_y} \iint \left[\int_0^1 g(x, y, sd, t)^2 ds - \left(\int_0^1 g(x, y, sd, t) ds \right)^2 \right] dx dy \quad (4.67)$$

$$+ \frac{c^2}{w_x w_y} \iint \left[\left(\int_0^1 g(x, y, sd, t) ds \right)^2 dx dy - \left[\frac{c}{w_x w_y} \iint \left(\int_0^1 g(x, y, sd, t) ds \right) dx dy \right]^2 \right]$$

The time resolution is then defined by (figure 18b)

$$\sigma_t = \frac{\Delta_h(t)}{\bar{h}'(t)} \quad (4.68)$$

Here we just discuss the example of an infinitely extended pixel i.e. we use $E_w^z(x, y, z, w_x, w_y, d) = 1/d$, which evaluates $g(x, y, z, t)$ to

$$\frac{n^{n+1}}{e^n} \frac{d}{t_p} g(x, y, z, t) = v_1 \Theta(z - v_1 t) [n! - \Gamma(n+1, t/t_p)]$$

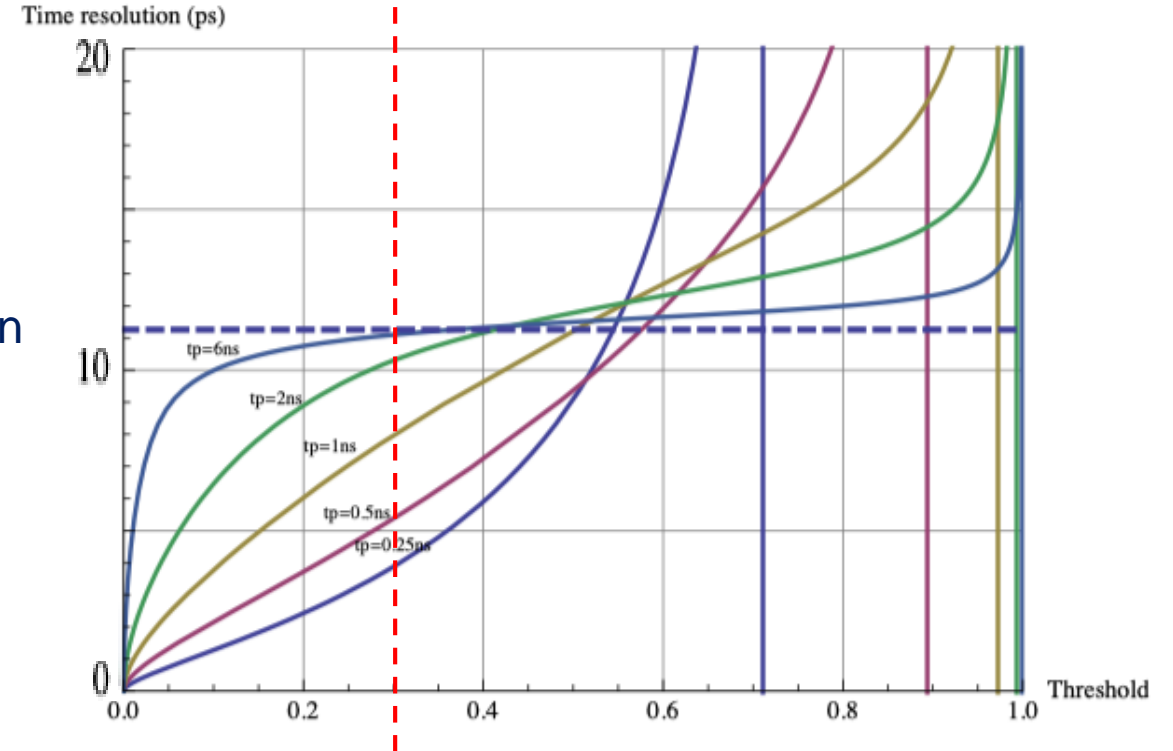
$$- v_1 \Theta(v_1 t - z) [\Gamma(n+1, t/t_p) - \Gamma(n+1, -(z - v_1 t)/(t_p v_1))]$$

$$+ v_2 \Theta((d - z) - v_2 t) [n! - \Gamma(n+1, t/t_p)]$$

$$- v_2 \Theta(v_2 t - (d - z)) [\Gamma(n+1, t/t_p) - \Gamma(n+1, -(d - z - v_2 t)/(t_p v_2))]$$

c.o.g. time resolution

50um sensor at 200V for different peaking times and constant fraction discrimination T=0.8ns



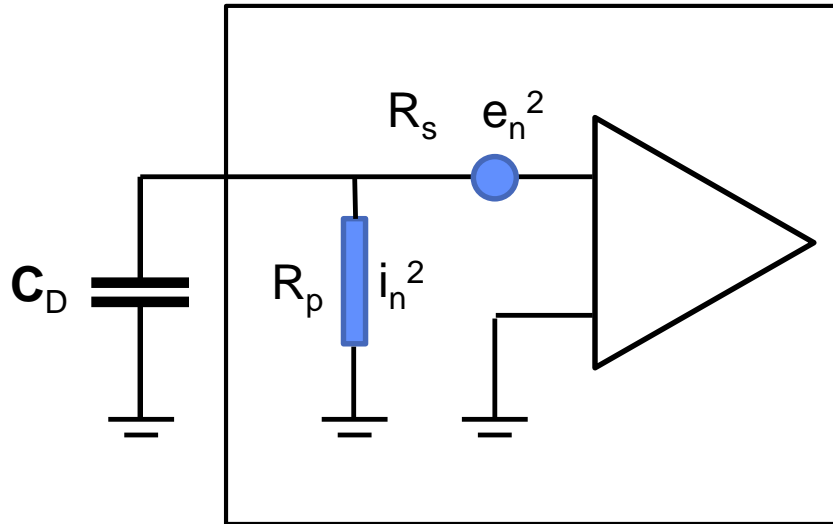
Leading edge discrimination on the signal that is normalized to the total deposited charge.

50um sensor, $t_p=0.5ns$, threshold at 30% of the charge

→ 5ps time resolution BUT this is unrealistic since S/N becomes too small → Noise will dominate !

Noise

For a sensor that is represented by a capacitance, the noise is determined by the amplifier only. The amplifier noise can be characterized by the parallel and series noise power spectrum.



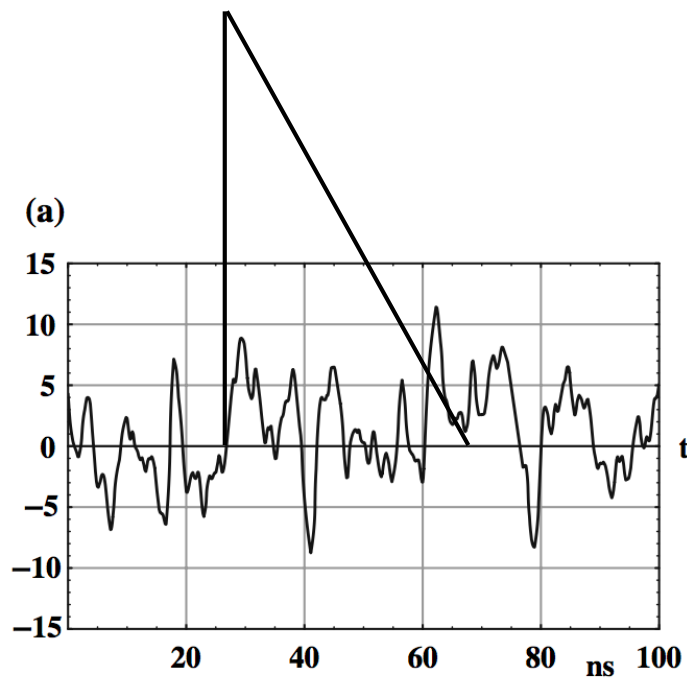
In case the parallel and series noise power spectra are 'white' we can formulate this as noise resistance R_s and R_p .

The level of this noise is a specification of the amplifier, there is no intrinsic noise in the sensor.

This noise level is very specific to the technology, but in general, lower noise requires more power (current through the input transistor etc.).

This places practical limits on the achievable noise level in systems with high granularity i.e. many channels on a small surface.

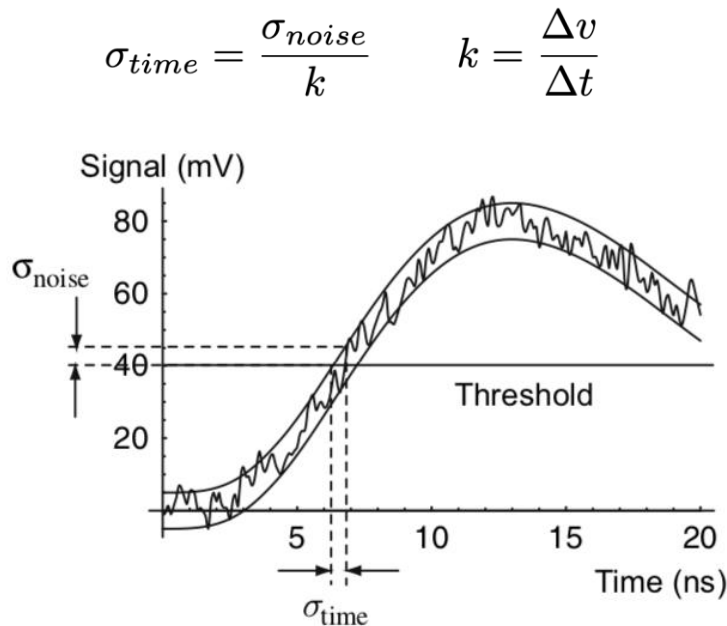
Noise and Optimum filters



Let us assume we have a signal $f(t)$ with superimposed noise of a given noise power spectrum and we want to find the amplifier transfer function that **maximizes**

- the **signal to noise** ratio for the best amplitude measurement, or
- the **slope to noise** ratio for the best time measurement

→ Theory of optimum filters



Optimum filter for best signal to noise ratio

A signal $f(t)$ superimposed to a noise with a noise power spectrum $w(\omega)$ is processed by a filter with transfer function $H(i\omega)$. The output signal and output noise r.m.s. are

$$g(t) = \frac{1}{2\pi} \int_{-\infty}^{\infty} F(i\omega) H(i\omega) e^{i\omega t} d\omega \quad \sigma^2 = \frac{1}{2\pi} \int_0^{\infty} w(\omega) |H(i\omega)|^2 d\omega.$$

The signal to noise ration is then

$$\left(\frac{S}{N}\right)^2 = \left(\frac{g(t_m)}{\sigma}\right)^2 = \frac{1}{\pi} \frac{\left| \int_{-\infty}^{\infty} F(i\omega) H(i\omega) e^{i\omega t_m} d\omega \right|^2}{\int_{-\infty}^{\infty} w(\omega) |H(i\omega)|^2 d\omega}.$$

The expression has an upper limit given by the Schwartz inequality, which relates two complex valued functions according to

$$\left| \int_a^b \psi^*(x) \phi(x) dx \right|^2 \leq \int_a^b |\psi(x)|^2 dx \int_a^b |\phi(x)|^2 dx,$$

We insert

$$\psi(\omega) = \frac{F^*(i\omega)}{\sqrt{w(\omega)}} e^{-i\omega t_m} \quad \phi(\omega) = \sqrt{w(\omega)} H(i\omega)$$

and have

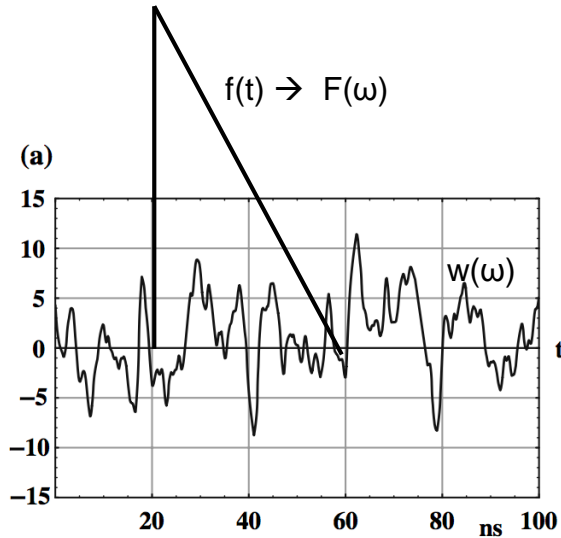
$$\left(\frac{S}{N}\right)^2 \leq \frac{1}{\pi} \int_{-\infty}^{\infty} \frac{|F(i\omega)|^2}{w(\omega)} d\omega = \frac{2}{\pi} \int_0^{\infty} \frac{|F(i\omega)|^2}{w(\omega)} d\omega.$$

The equal sign applies if $\psi = c_1 \phi$ and we have the optimum filter transfer function

$$\frac{F^*(i\omega)}{\sqrt{w(\omega)}} e^{-i\omega t_m} = c_1 \sqrt{w(\omega)} H(i\omega) \rightarrow H(i\omega) = \frac{1}{c_1} \frac{F^*(i\omega)}{w(\omega)} e^{-i\omega t_m}.$$

The output signal is

$$G(i\omega) = F(i\omega) H(i\omega) = \frac{|F(i\omega)|^2}{w(\omega)} \quad g(t) = \mathcal{F}^{-1}[G(i\omega)].$$



Optimum filter for best slope to noise ratio

We want to minimise the time resolution i.e. maximise the slope to noise

$$\left(\frac{k}{\sigma}\right)^2 = \left(\frac{g'(t_m)}{\sigma}\right)^2 = \frac{1}{\pi} \frac{\left(\int_{-\infty}^{\infty} i\omega F(i\omega) H(i\omega) e^{i\omega t_m} d\omega\right)^2}{\int_{-\infty}^{\infty} w(\omega) |H(i\omega)|^2 d\omega}.$$

Following the steps from before we find an upper bound for the slope to noise ratio of

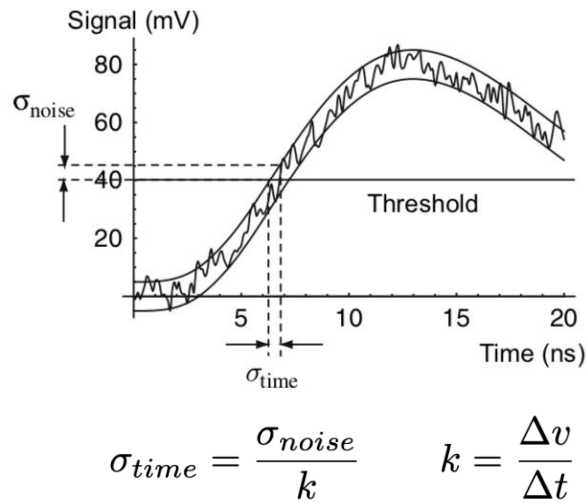
$$\left(\frac{k}{\sigma}\right)^2 \leq \frac{2}{\pi} \int_0^{\infty} \frac{|\omega F(i\omega)|^2}{w(\omega)} d\omega$$

And the optimum transfer function as well as the output signal are

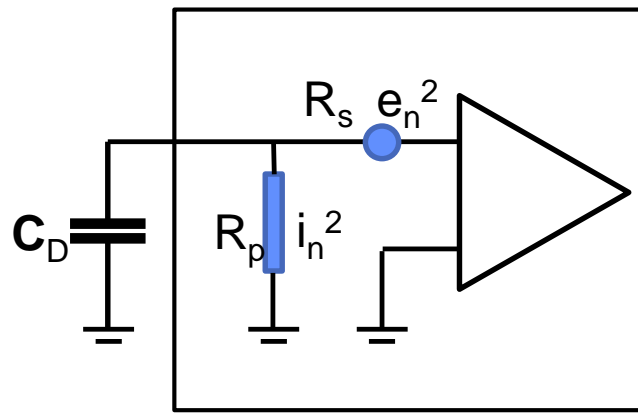
$$H(i\omega) = i\omega \frac{F^*(i\omega)}{w(\omega)} e^{-i\omega t_m} \quad G(i\omega) = i\omega \frac{|F(i\omega)|^2}{w(\omega)} e^{-it_m \omega}.$$

Since multiplication with $i\omega$ refers to the derivative in the time domain we have the following relation:

The filter maximising the slope to noise ratio, i.e. the filter giving the best time resolution, is equal to the time derivative of the filter that maximises the signal to noise ratio !



Optimum filter for best timing



Assuming a silicon sensor with negligible depletion voltage and saturated drift-velocity, the signal shape is a triangle:

$$f(t) = \frac{2Q_0}{T} \left(1 - \frac{t}{T}\right) \quad F(i\omega) = \frac{2Q_0}{\omega^2 T^2} (1 - e^{-i\omega T} - i\omega T)$$

For the noise we assume series noise and parallel noise together with a detector capacitance C_D

$$w(\omega) = \frac{4kT}{R_p} + 4kTR_s C_D^2 \omega^2 = a^2 + b^2 \omega^2 \quad e_n^2(\omega) = 4kTR_s \quad i_n^2(\omega) = \frac{4kT}{R_p}$$

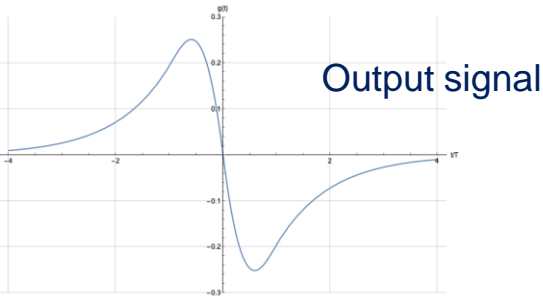
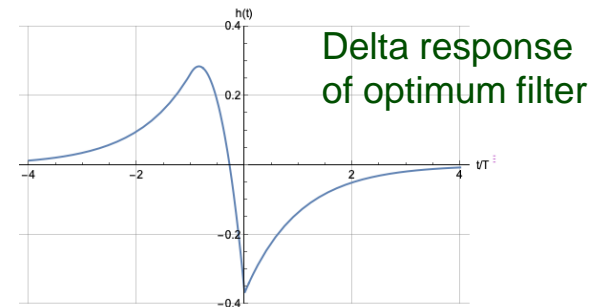
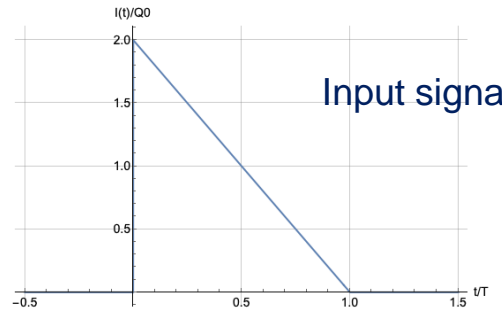
The maximum slope to noise ratio is

$$\left(\frac{k}{\sigma}\right)^2 \leq \frac{4Q_0^2}{a^3 T^4} \left(2e^{-aT/b}(b + aT) + \frac{a^2 T^2}{b} - 2b\right)$$

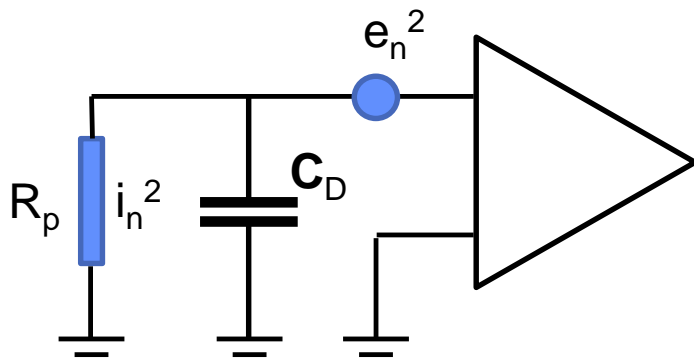
If we neglect parallel noise we have

$$\left(\frac{k}{\sigma}\right)^2 \leq \frac{8Q_0^2}{3b^2 T}$$

This filter is a-causal and can only be approximated in practise.



Realistic preamp transfer function



Preamp delta response

$$h(t) = e^n n^{-n} \left(\frac{nt}{t_p} \right)^n e^{-nt/t_p} \quad H(i\omega) = \frac{t_p e^n n!}{(n + i\omega t_p)^{n+1}}$$

For the noise we assume series noise and parallel noise together with a detector capacitance C_D

$$\sigma^2(t_p) = \frac{1}{2\pi} \int_0^\infty w(\omega) |H(i\omega)|^2 d\omega = a^2 K_p t_p + b^2 \frac{K_s}{t_p}$$

$$K_p = \frac{1}{2} \left(\frac{e}{2n} \right)^{2n} (2n-1)!$$

$$K_s = \frac{1}{2} \left(\frac{e}{2n} \right)^{2n} n^2 (2n-2)!$$

The output signal is

$$g(t) = \int_0^t h(t-t') g(t') dt'$$

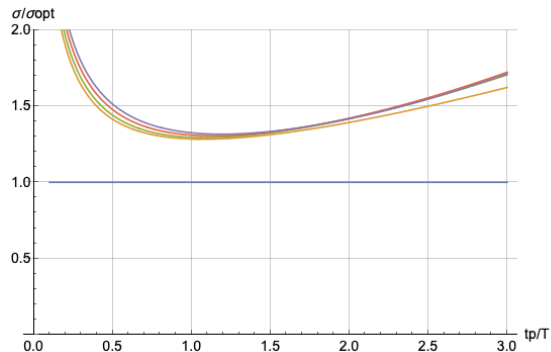
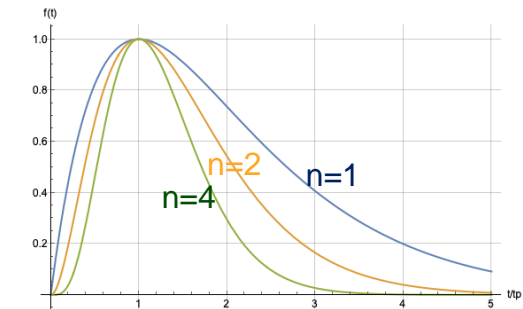
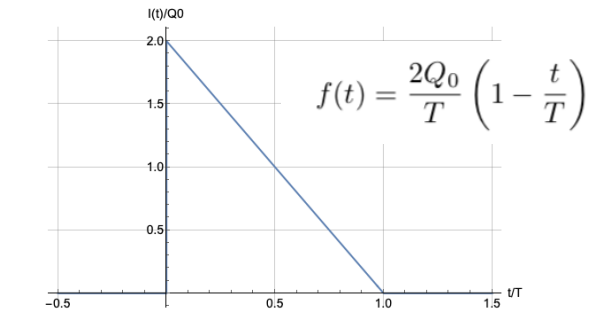
And the maximum slope evaluates to

$$k(t_p) = \frac{2Q_0}{T^2} \frac{e^n}{n^{n+1}} \left(e^{-nt/t_p} n T (nt/t_p)^n - t_p n! + t_p \Gamma(n+1, nt/t_p) \right)$$

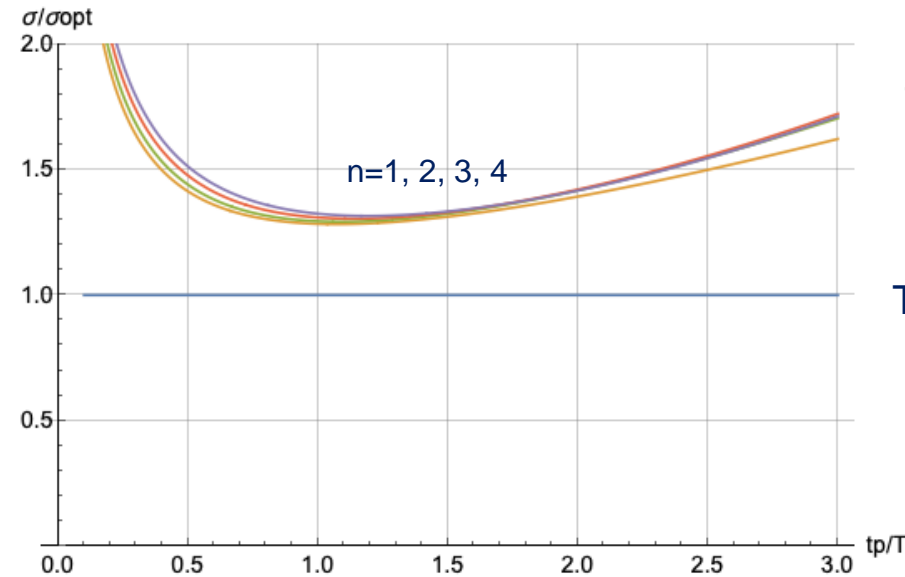
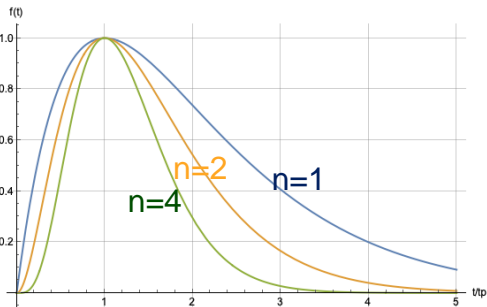
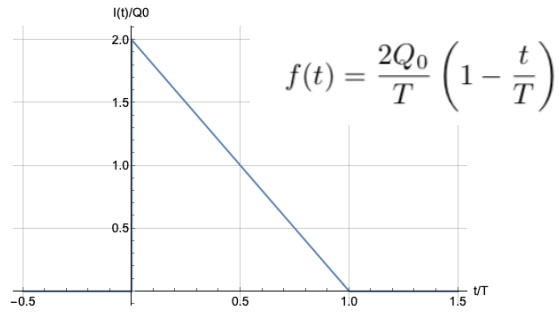
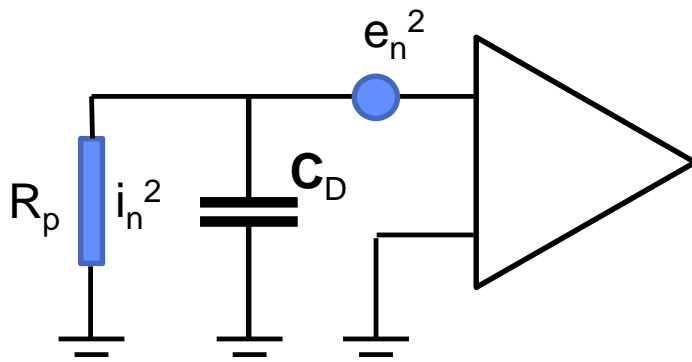
$$\lim_{t_p \rightarrow 0} k(t_p) = \frac{2Q_0}{T}$$

To find the optimum peaking time and best time resolution we therefore have to minimise the function

$$\frac{\sigma(t_p)^2}{k(t_p)^2} \rightarrow \min.$$



Realistic preamp transfer function



Time resolution for 'standard' preamp delta response.

Time resolution with optimum filter

Neglecting parallel noise (which is a good approximation in most practical applications) the optimum electronics peaking time t_p is between T and $1.5T$.

The achieved time resolution is **only about 30% worse** than the best achievable one with the optimum filter !

This will give the smallest noise contribution to the time resolution.

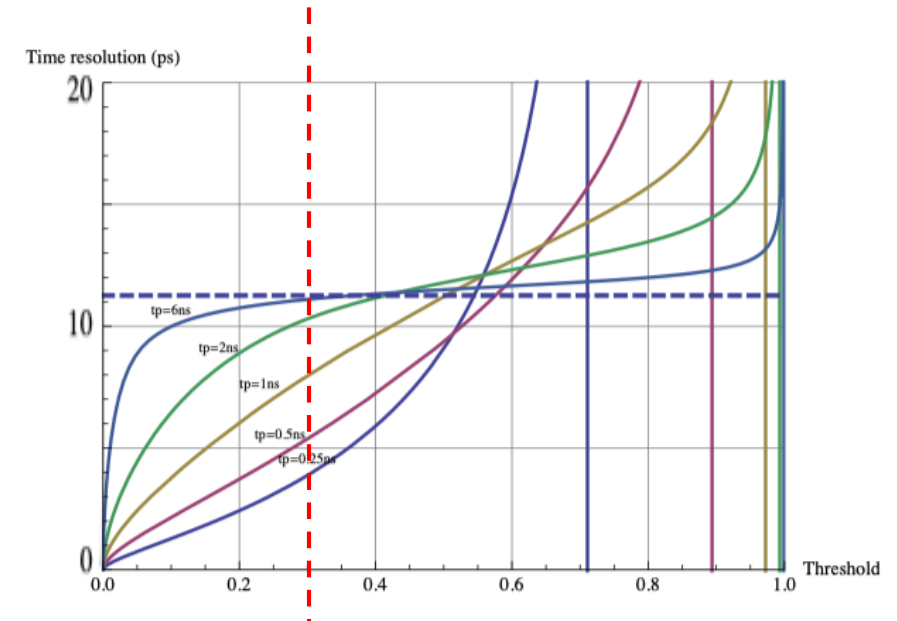
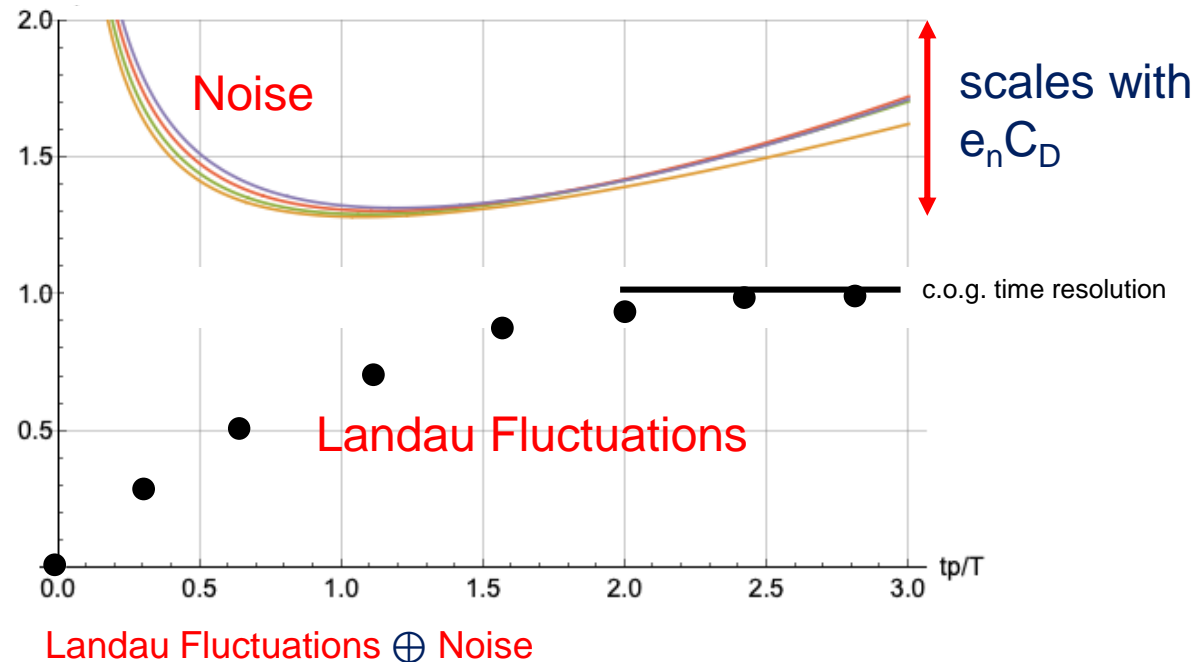
Combined effect of Landau fluctuations and noise

If the noise dominates, the optimum peaking time is about $t_p \sim 1-1.5T$

If the noise is at a similar level to the contribution from Landau fluctuations, the optimum peaking time is still around the same level $t_p \sim 1-1.5T$ and the time resolution is equal to the the c.o.g. time resolution of the silicon sensor.

If the noise is subdominant, shorter peaking times can be improve the time resolution, but with the divergence of the noise contribution at low t_p this will not reach far below the c.o.g. time resolution.

In short: $t_p \sim T$ and $\sigma = \sigma_{\text{c.o.g.}} \oplus \sigma_{\text{noise}}$ give a good order of magnitude for the achievable time resolution



Time resolution of 'standard' silicon sensors

In case noise is not dominant, the time resolution of a silicon sensor is somewhere between zero and the c.o.g. time resolution.

For a silicon detector signal with total duration T , the series noise contribution is minimised for amplifiers of $t_p \sim T$.

For very low noise a time resolution better than the c.o.g. time resolution can be achieved, but the divergence of the noise contribution for $t_p \rightarrow 0$ will limit this improvement.

$$\Delta\tau = w(d) \sqrt{\frac{4}{180} \frac{d^2}{v_1^2} - \frac{7}{180} \frac{d^2}{v_1 v_2} + \frac{4}{180} \frac{d^2}{v_2^2}}$$
$$w(d)^2 = \frac{d}{\lambda} \int_0^\infty \left[\int_0^\infty \frac{n_1^2 p_{\text{clu}}(n_1)}{(n_1 + n)^2} dn_1 \right] p(n, d) dn$$

Effects of finite Pixel Size

Up to now we discussed the situation of a very large pad of size $w \gg d$ i.e. and 'infinitely extended parallel plate geometry'.

Weighting field of a strip in a parallel plate geometry

A uniform charge distribution

Charge moving towards the strip:

$$I_a(x, t) = \frac{\lambda v_1}{V_w} \int_0^d E_w(x, z - v_1 t) \Theta(z/v_1 - t) dz$$

$$= \frac{\lambda v_1}{V_w} [\psi_1(x, 0) - \psi_1(x, d - v_1 t)] \Theta(d/v_1 - t)$$

Charge moving away from the strip:

$$I_b(x, t) = \frac{\lambda v_2}{V_w} \int_0^d E_w(x, z + v_2 t) \Theta((d - z)/v_2 - t) dz$$

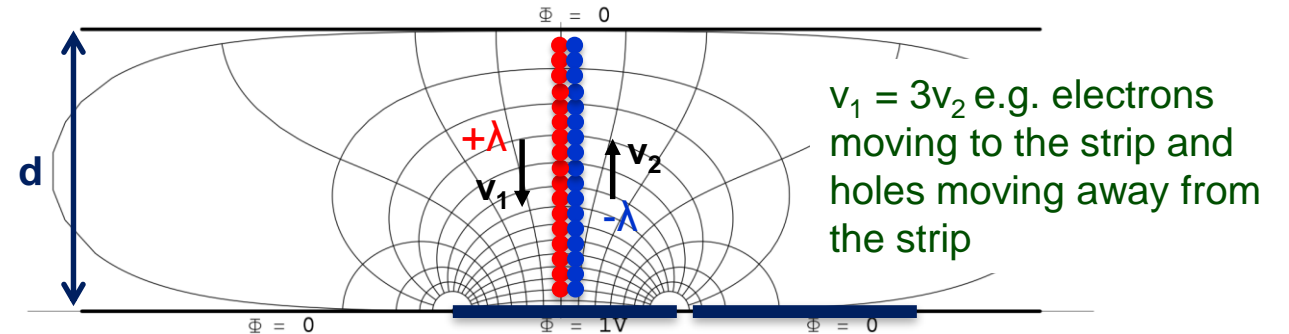
$$= \frac{\lambda v_2}{V_w} \psi_1(x, v_2 t) \Theta(d/v_2 - t)$$

Total induced current on the strip

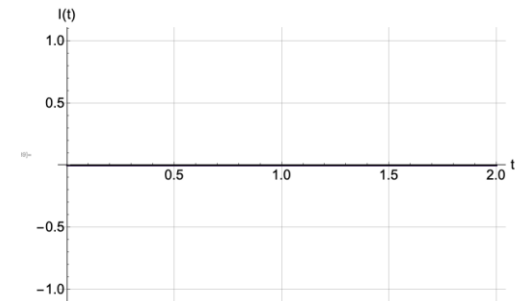
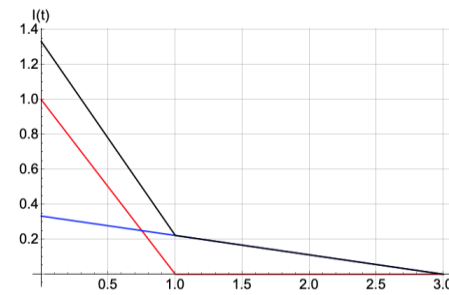
$$I_1(x, t) = I_a(x, t) + I_b(x, t)$$

For very wide strips (parallel plate geometry) the induced charge from the movement of $+\lambda$ and $-\lambda$ is the same and equal to $\lambda d/2$.

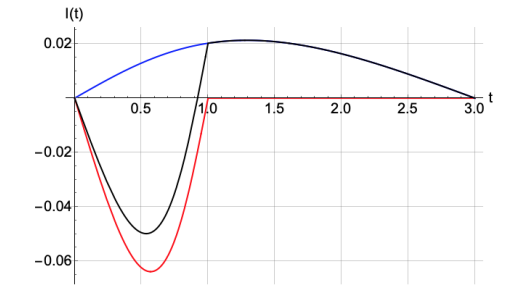
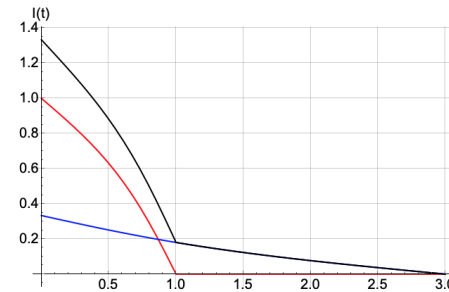
For small strips, the fraction of the signal due to the charges moving towards the strip increases.



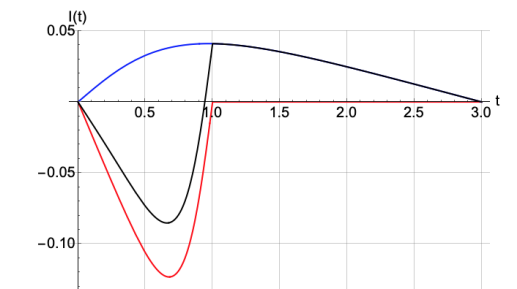
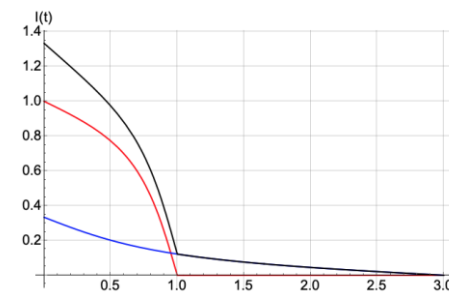
$w \gg d$



$w = d$



$w = d/2$



Weighting field of a strip in a parallel plate geometry

$$I_a(x, t) = \frac{\lambda v_1}{V_w} \int_0^d E_w(x, z - v_1 t) \Theta(z/v_1 - t) dz$$

$$= \frac{\lambda v_1}{V_w} [\psi_1(x, 0) - \psi_1(x, d - v_1 t)] \Theta(d/v_1 - t)$$

$$I_b(x, t) = \frac{\lambda v_2}{V_w} \int_0^d E_w(x, z + v_2 t) \Theta((d - z)/v_2 - t) dz$$

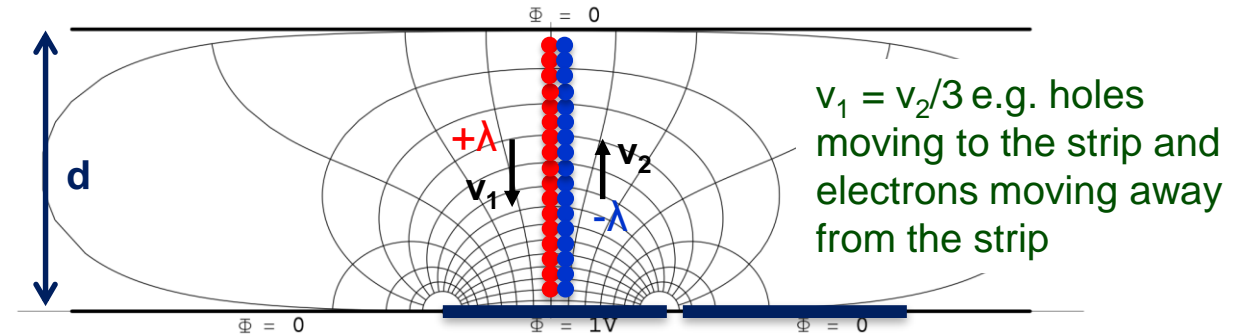
$$= \frac{\lambda v_2}{V_w} \psi_1(x, v_2 t) \Theta(d/v_2 - t)$$

$$I_1(x, t) = I_a(x, t) + I_b(x, t)$$

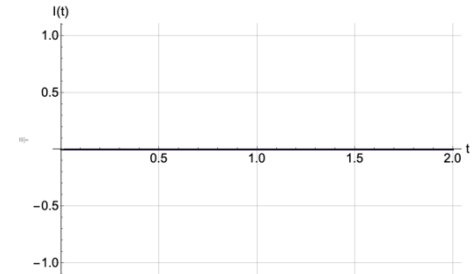
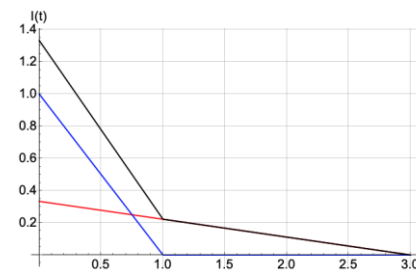
Different positions of the particle inside the pixel will lead to different pulse-shapes.

The varying signal shape will lead to variations in the c.o.g. time and therefore affect the time resolution.

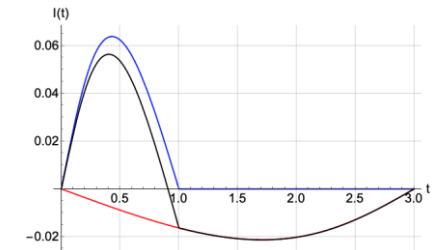
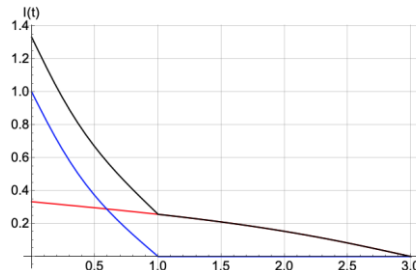
This is also called the 'weighting field effect'.



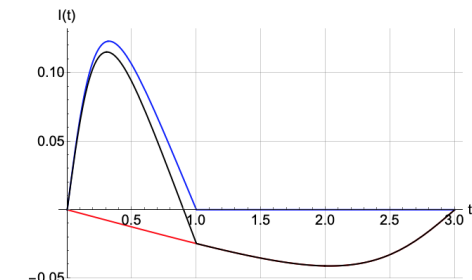
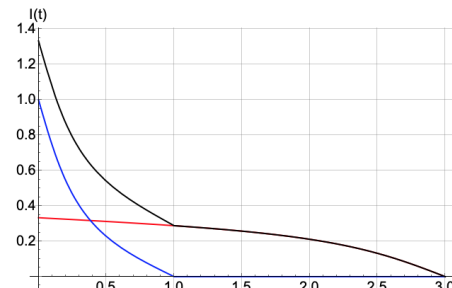
$w \gg d$



$w = d$



$w = d/2$



Weighting field fluctuations

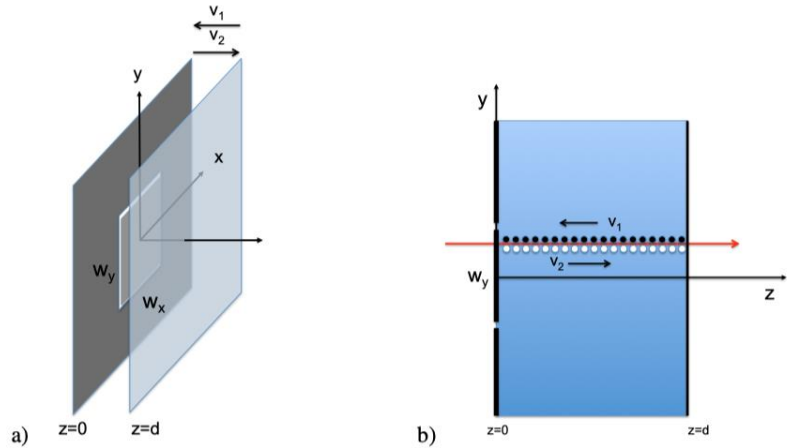
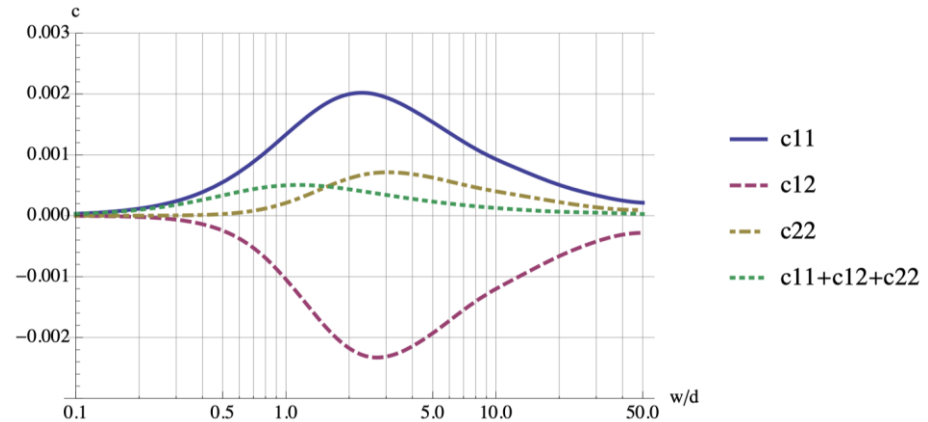
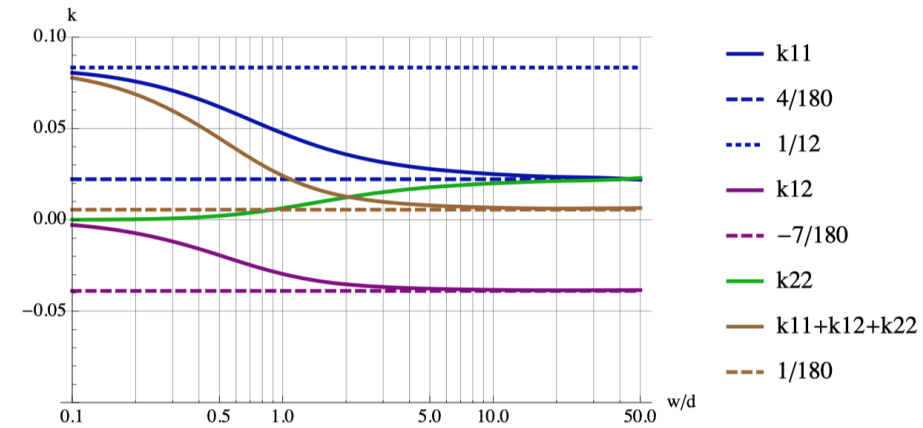


Figure 10. a) A pixel of dimension w_x, w_y centred at $x = y = z = 0$ in a parallel plate geometry of plate distance d . b) Uniform charge deposit of a particle passing the silicon sensor. v_1 is the velocity of charges moving towards the pixel and v_2 is the velocity of charges moving away from the pixel.

$$\Delta_{\tau}^2 = w(d)^2 \left(\frac{k_{11}d^2}{v_1^2} + \frac{k_{12}d^2}{v_1 v_2} + \frac{k_{22}d^2}{v_2^2} \right) + \left(\frac{c_{11}d^2}{v_1^2} + \frac{c_{12}d^2}{v_1 v_2} + \frac{c_{22}d^2}{v_2^2} \right)$$



w/d = pixel size/detector thickness

This weighting field effect is strongly correlated with the Landau fluctuations.

The structure of the expression for the resolution is however similar to the one before.

Weighting field fluctuations

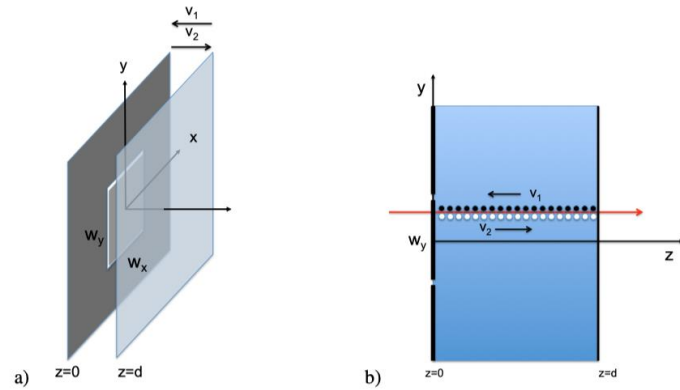


Figure 10. a) A pixel of dimension w_x, w_y centred at $x = y = z = 0$ in a parallel plate geometry of plate distance d . b) Uniform charge deposit of a particle passing the silicon sensor. v_1 is the velocity of charges moving towards the pixel and v_2 is the velocity of charges moving away from the pixel.

Because electrons and holes have different velocities, it makes a significant difference whether the electrons or the holes move to the pixel.

For higher fields (thinner sensors) this difference will decrease.

The dependence on the different parameters is complex.

These fluctuations can dominate the time resolution !

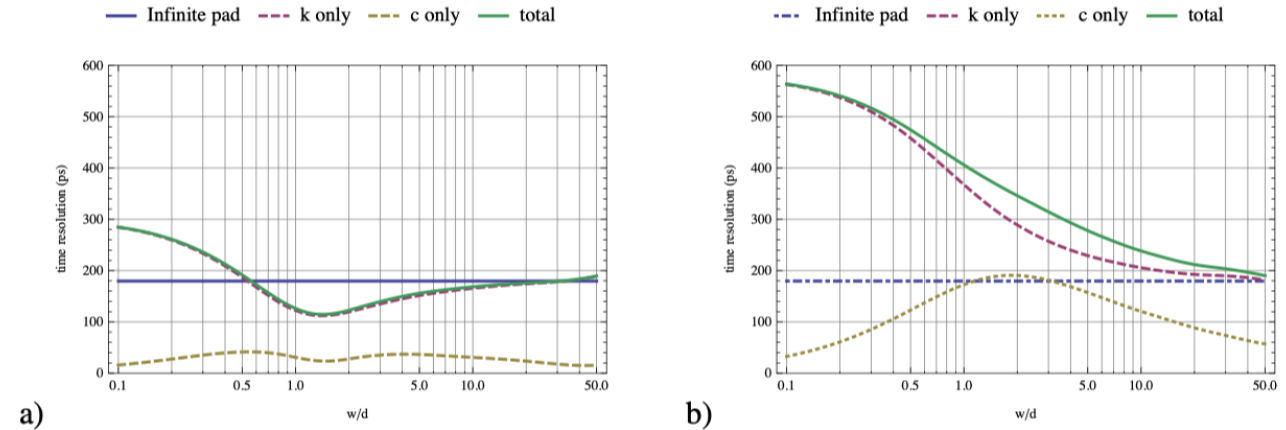


Figure 16. Centroid time resolution for values of $d = 200 \mu\text{m}$ and $V = 200 \text{ V}$ as a function of the pixel size w assuming the Landau theory for the charge deposit. The 'c only' curve refers to the effect from a uniform line charge. In a) the electrons move towards the pixel while in b) the holes move towards the pixel.

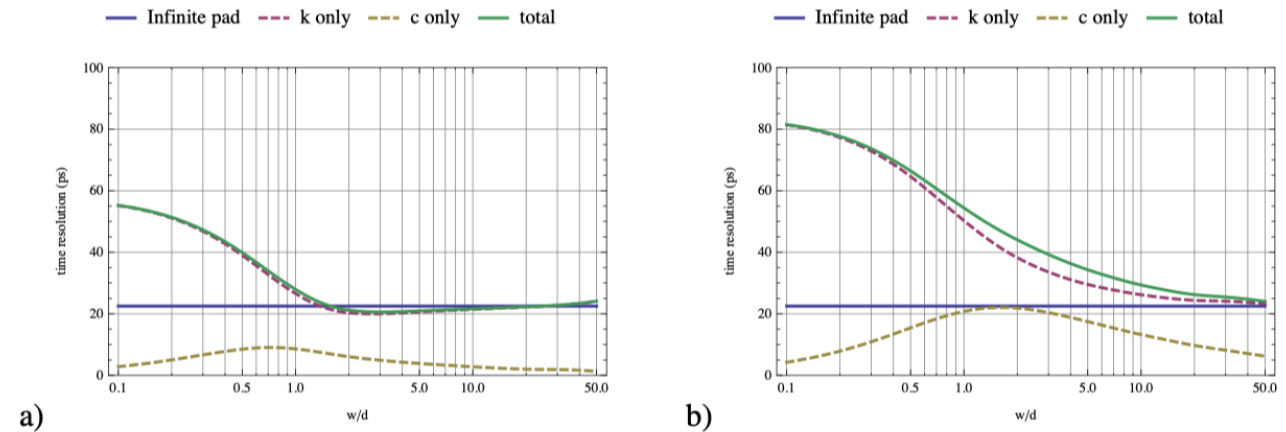


Figure 17. Time resolution for values of $d = 50 \mu\text{m}$ and $V = 200 \text{ V}$ as a function of the pixel size w assuming the Landau theory for the charge deposit. The 'c only' curve refers to the effect from a uniform line charge. In a) the electrons move towards the pixel while in b) the holes move towards the pixel.

Time resolution of 'standard' silicon sensors

Good time resolution demands thin sensors.

Thin sensors give small charge and large capacitance i.e. unfavorable S/N and k/N.

Capacitance can be reduced by making the pixels small.

If the pixel size is in the same order as the sensor thickness, the weighting field fluctuations start to dominate ... and there will be many channels ...

... between a rock and a hard place ...

→ Sensors with internal gain to overcome the noise limit (like gas detectors !)

→ Turn the by sensor 90 degrees and realise a parallel plate geometry in 3D !
(see slide 62, 63)

Time resolution of MAPS with small readout diodes

Up to now we have investigated silicon sensors with e-h drift in a homogeneous electric field perpendicular to the readout electrodes.

One flavour of MAPS sensors uses a small 'collection' electrode to minimise the capacitance and therefore the noise → E.g. ALPIDE

Since the 'weighting field' of the 'readout electrode' is concentrated around the diode, the signal consists to a good approximation of a sequence of delta pulses for each electron arriving at the diode.

→ Arrival time distribution.

The time resolution will be somewhere between the arrival time statistics of the first electron and the center of gravity time of all electron arrival times.

→ Thesis Jan Hasenbichler, to be defended Nov. 2021

Standard process:

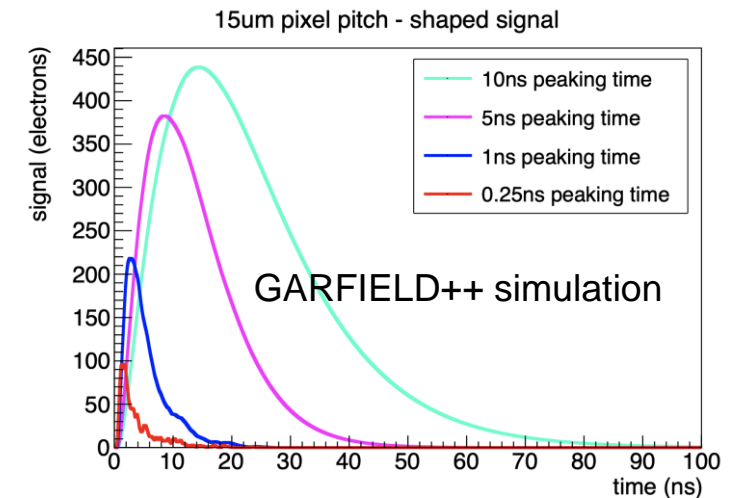
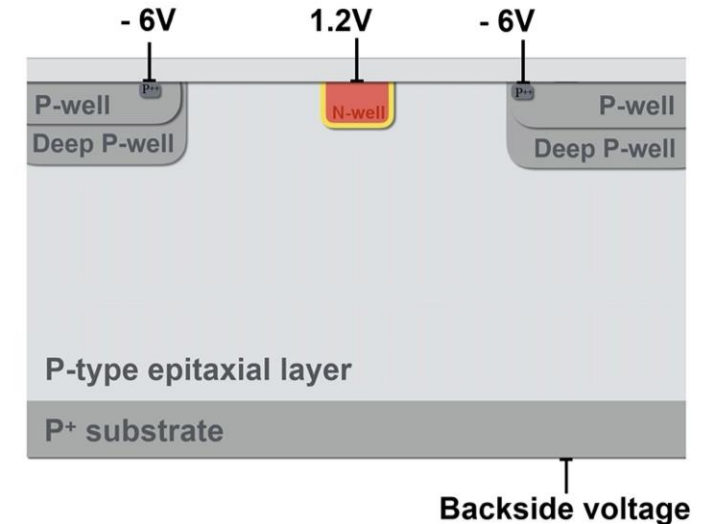


FIGURE 10.1: The simulated shaped signal of one event for the standard flavour with a pixel pitch of 15 μm is shown for peaking times of $\tau = 0.25 \text{ ns}$, 1 ns, 5 ns and 10 ns.

Time resolution of MAPs with small readout diodes

Very fast amplifiers allow in principle excellent time resolution.

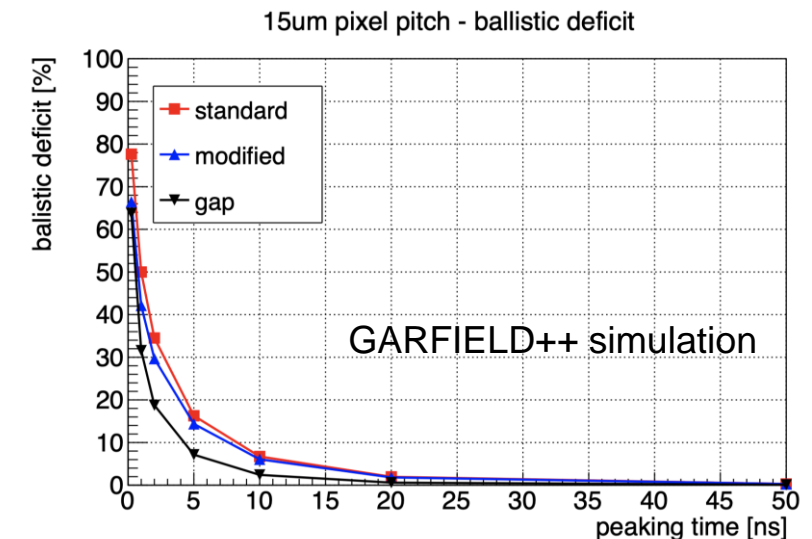
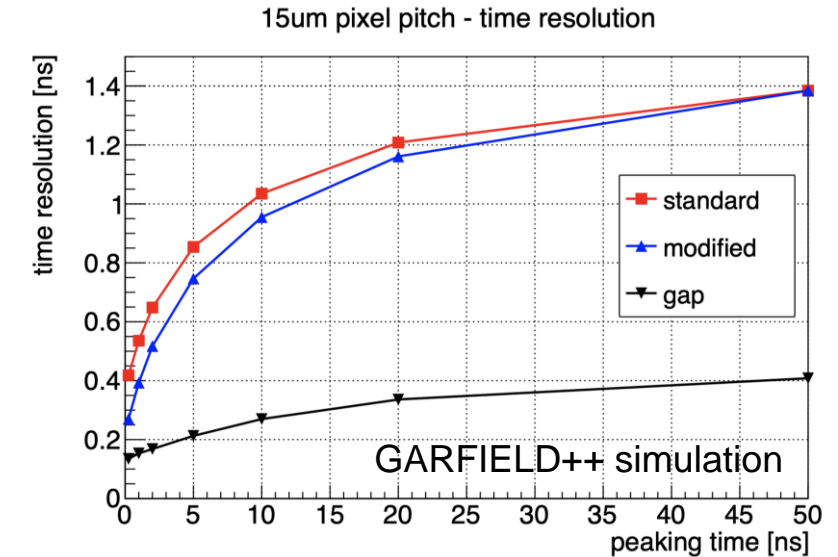
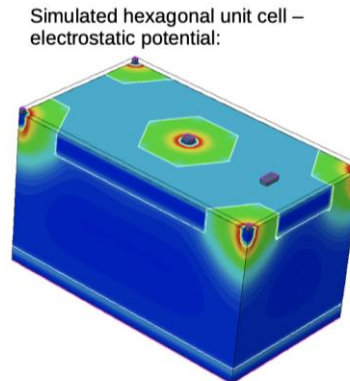
Of course – the ballistic deficit is high and the signal/noise and slope/noise ratio are low.

This puts extreme demands on noises performance of the amplifiers, resulting in significant power consumption.

→ In practise, fast charge collection and amplifier peaking times similar to the total charge collection time will be needed.

400ps seem achievable in these simulations.

Optimized hexagonal pixel geometries:
E.g. Fastpix with <200ps time resolution
→ See slide 63



Time resolution of LGADs

Avalanche Photo Diode, Low Gain Avalanche Diode

IEEE TRANSACTIONS ON ELECTRON DEVICES, JUNE 1972

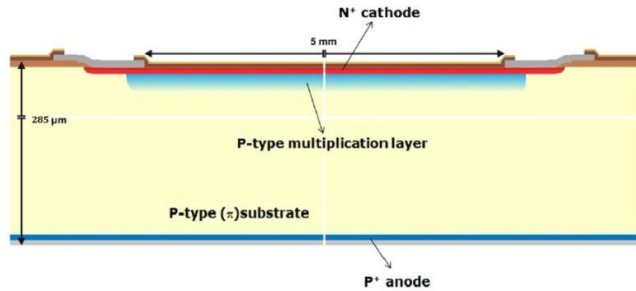


Figure 2.2. Cross-section of the core layout of LGAD. A p-type layer is diffused below the

Idea goes back to the 1960ies.

A high field region is implemented in a silicon sensor by doping.

Electrons will produce an avalanche in this high field region.

The high field region is implemented by doping and related 'space-charge' in the volume.

The sensor is operated in a region where there is electron multiplication but not yet hole multiplication.

This allows to have thin sensors (high field, short signal) but still have enough signal charge to overcome the limitation from noise.

For higher fields \rightarrow electron+hole multiplication \rightarrow avalanche divergence \rightarrow quench resistor \rightarrow SiPM

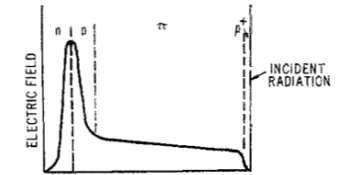
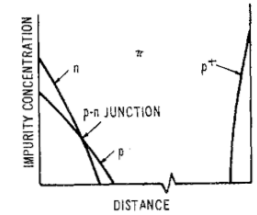
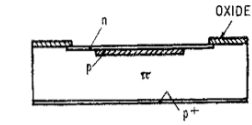
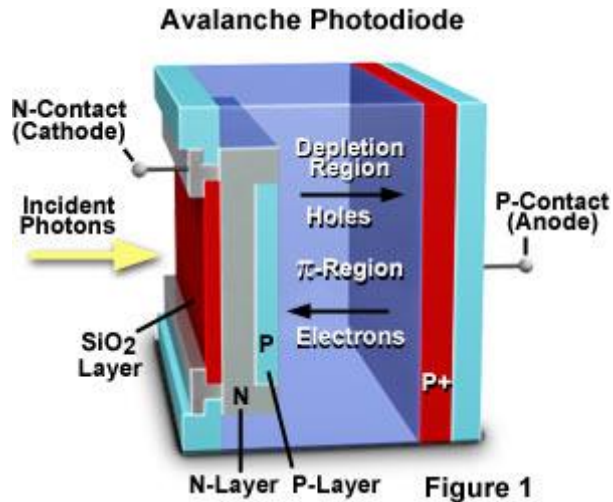
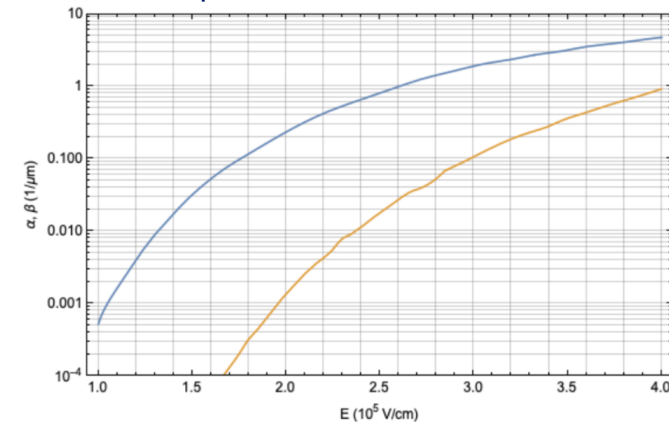


Fig. 1. Sketches of reach-through avalanche-diode structure, impurity-concentration profile, and electric-field distribution.



Electron (alpha) and hole (beta) multiplication coefficient in silicon

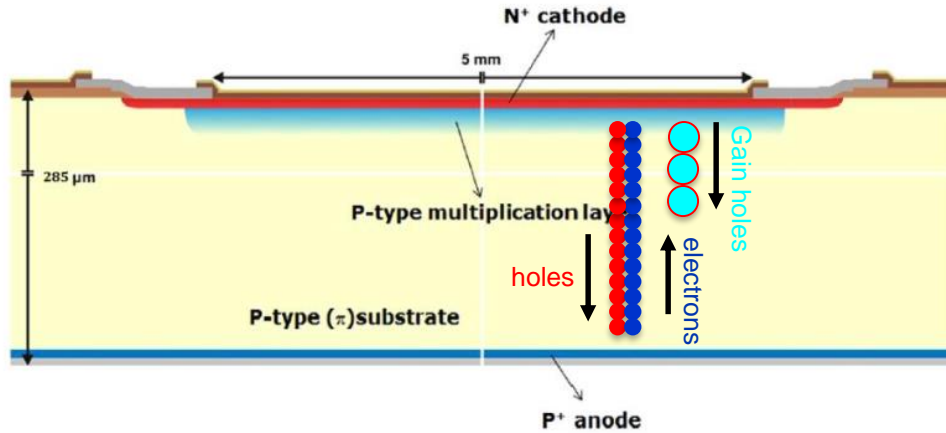


AvalanchePhotoDiode

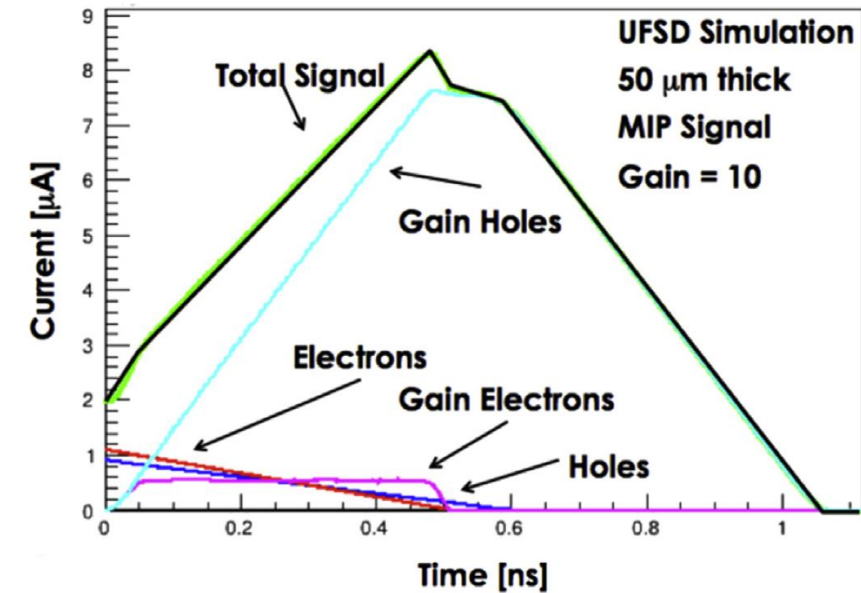
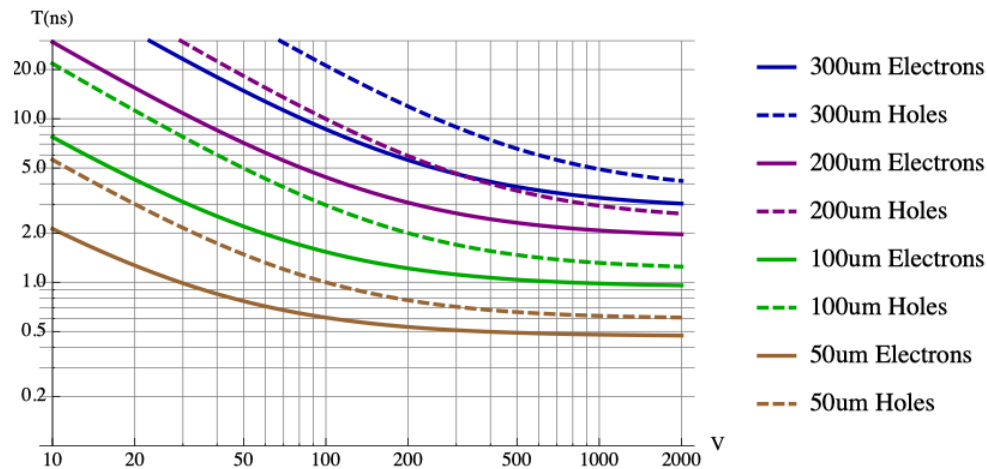
Nuclear Instruments and Methods in Physics Research A 796 (2015) 141–148

Design optimization of ultra-fast silicon detectors

N. Cartiglia^{a,*}, R. Arcidiacono^c, M. Baselga^e, R. Bellan^b, M. Boscardin^f, F. Cenna^a, G.F. Dalla Betta^g, P. Fernandez-Martinez^e, M. Ferrero^{a,b}, D. Flores^e, Z. Galloway^d, V. Greco^e, S. Hidalgo^e, F. Marchetto^a, V. Monaco^b, M. Obertino^c, L. Pancheri^g, G. Paternoster^f, A. Picerno^b, G. Pellegrini^e, D. Quirion^e, F. Ravera^b, R. Sacchi^b, H.F.-W. Sadrozinski^d, A. Seiden^d, A. Solano^b, N. Spencer^d



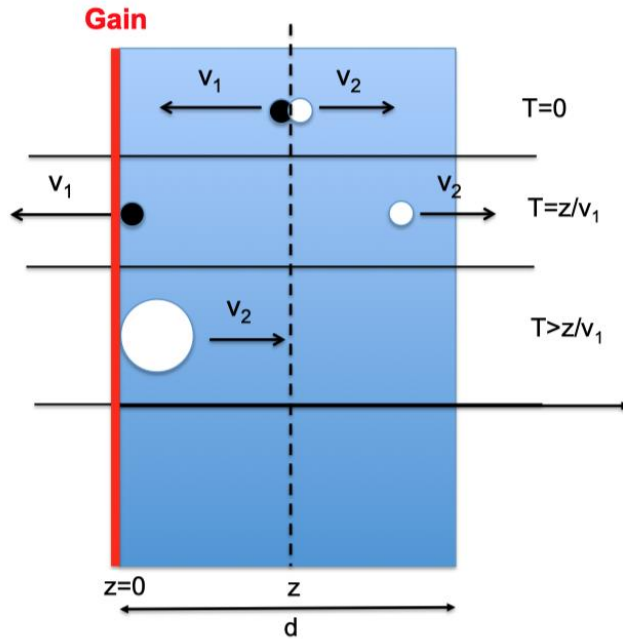
Total drift time for a given sensor thickness



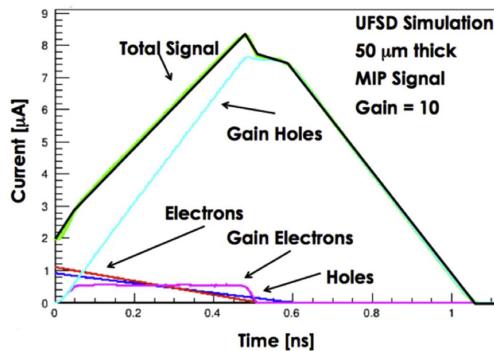
A high field region is implemented in a silicon sensor by doping.

Electrons will produce an avalanche in this high field region.

LGAD



$$w(d)^2 = \frac{d}{\lambda} \int_0^\infty \left[\int_0^\infty \frac{n_1^2 p_{clu}(n_1)}{(n_1 + n)^2} dn_1 \right] p(n, d) dn$$



An e-h pair is produced at position z .

The electron arrives at $z=0$ at time $T=z/v_1$.

The electron multiplies in the high field in the layer at $z=0$ (infinitely thin).

The holes move back to $z=d$ inducing the dominant part of the signal (all in this approximation).

Centroid time resolution for standard silicon sensor:

$$\Delta\tau = w(d) \sqrt{\frac{4}{180} \frac{d^2}{v_1^2} - \frac{7}{180} \frac{d^2}{v_1 v_2} + \frac{4}{180} \frac{d^2}{v_2^2}}$$

Centroid time resolution for LGAD

$$\Delta\tau = w(d) \frac{d}{\sqrt{12} v_1}$$

The signal is now defined by the arrival time distribution of the electrons at the gain layer.

LGAD centroid time resolution

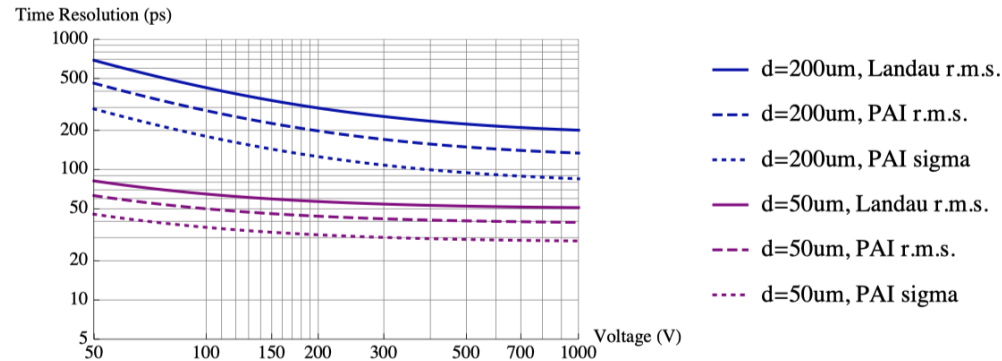


Figure 22. Time resolution for the centroid time from eq. (5.4) for 50, 100, 200, 300 μm silicon sensors with internal gain of electrons, assuming a signal only from gain holes. The three curves for each sensor thickness correspond to the Landau theory, the PAI model and a Gaussian fit to the PAI model.

50um sensor at 200V: 30ps

200um sensor at 200V: 140ps

Standard silicon sensor centroid time resolution

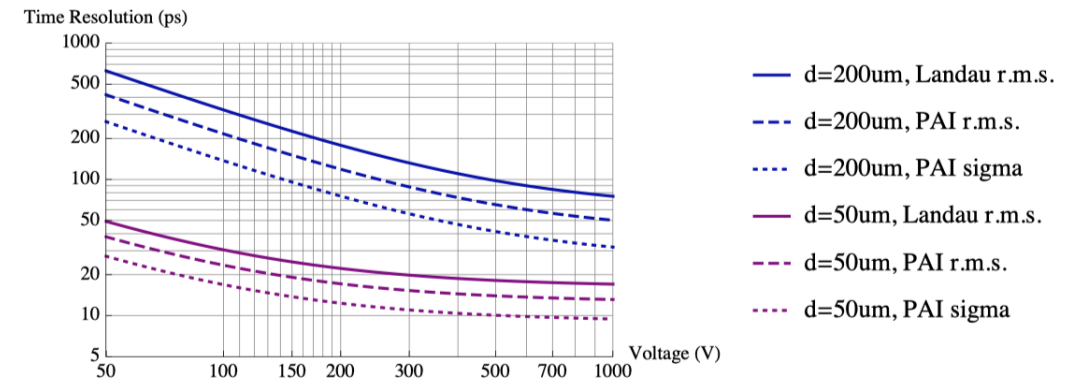


Figure 6. Time resolution from eq. (4.5) for different values of silicon sensor thickness as a function of applied voltage V for the Landau model, the PAI model and a Gaussian fit to the PAI model results.

50um sensor at 200V: 13ps

200um sensor at 200V: 70ps

The c.o.g. time resolution of LGADs is worse than the one for standard silicon sensors due to the very different signal characteristics – essentially an electron arrival time distribution.

Of course – the fact that the signal is larger by a factor 10-15 allows much more relaxed noise requirements, larger pixels etc. ...

LGAD Leading edge discrimination

$$f(x) = x^n e^{n(1-x)} \quad (4.61)$$

The amplifier output signal is then given by the convolution of the induced signal and the amplifier delta response

$$s(n_1, n_2, \dots, n_N, x, y, t) = c \int_0^t f\left(\frac{t-t'}{t_p}\right) i(n_1, n_2, \dots, n_N, x, y, t') dt' \quad (4.62)$$

$$= c q \sum_{k=1}^N n_k g(x, y, k\Delta z, t) \quad (4.63)$$

where $g(x, y, z, t)$ is

$$g(x, y, z, t) = \Theta(z - v_1 t) \int_{\frac{z-v_1 t}{v_1 t_p}}^{\frac{z}{v_1 t_p}} f\left(\frac{v_1 t - z + ud}{v_1 t_p}\right) E_w^z(x/d, y/d, u, w_x/d, w_y/d, 1) du \quad (4.64)$$

$$+ \Theta(v_1 t - z) \int_0^{\frac{z}{v_1 t_p}} f\left(\frac{v_1 t - z + ud}{v_1 t_p}\right) E_w^z(x/d, y/d, u, w_x/d, w_y/d, 1) du$$

$$+ \Theta[(d - z) - v_2 t] \int_{\frac{z}{v_2 t_p}}^{\frac{z+v_2 t}{v_2 t_p}} f\left(\frac{v_2 t + z - ud}{v_2 t_p}\right) E_w^z(x/d, y/d, u, w_x/d, w_y/d, 1) du$$

$$+ \Theta[v_2 t - (d - z)] \int_{\frac{z}{v_2 t_p}}^1 f\left(\frac{v_2 t + z - ud}{v_2 t_p}\right) E_w^z(x/d, y/d, u, w_x/d, w_y/d, 1) du$$

$$\bar{h}(t) = \frac{c}{w_x w_y} \iint \left[\int_0^1 g(x, y, sd, t) ds \right] dx dy \quad (4.66)$$

and

$$\Delta_h^2(t) = w(d)^2 \frac{c^2}{w_x w_y} \iint \left[\int_0^1 g(x, y, sd, t)^2 ds - \left(\int_0^1 g(x, y, sd, t) ds \right)^2 \right] dx dy \quad (4.67)$$

$$+ \frac{c^2}{w_x w_y} \iint \left(\int_0^1 g(x, y, sd, t) ds \right)^2 dx dy - \left[\frac{c}{w_x w_y} \iint \left(\int_0^1 g(x, y, sd, t) ds \right) dx dy \right]^2$$

$$\frac{n^{n+1}}{e^n} \frac{d}{t_p} g(x, y, z, t) = v_2 \Theta(t - z/v_1) \Theta(d/v_2 + z/v_1 - t) \left[n! - \Gamma\left(n+1, \frac{n(v_1 t - z)}{t_p v_1}\right) \right] \quad (5.20)$$

$$- v_2 \Theta(t - d/v_2 - z/v_1) \left[\Gamma\left(n+1, \frac{n(v_1 t - z)}{t_p v_1}\right) - \Gamma\left(n+1, \frac{n(t - d/v_2 - z/v_1)}{t_p}\right) \right]$$

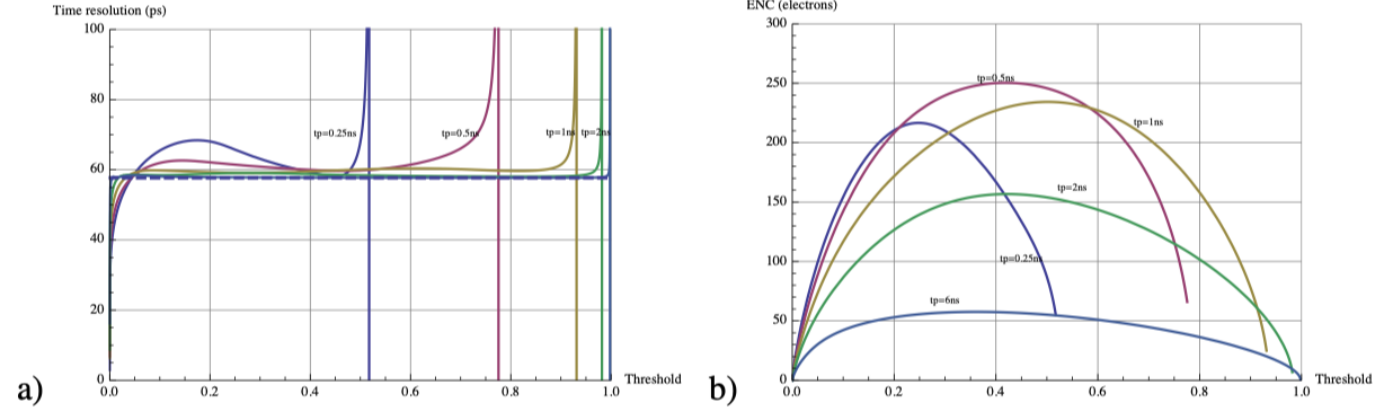


Figure 24. a) Time resolution for a gain sensor of $50\mu\text{m}$ thickness at 200 V bias voltage when applying a threshold to the signal normalized by the total charge, assuming the Landau theory. The values do not improve beyond the centroid time resolution which is indicated by the dashed horizontal line. b) ENC needed to match the noise effect of the time resolution to the effect from the Landau fluctuations.

Standard silicon sensor

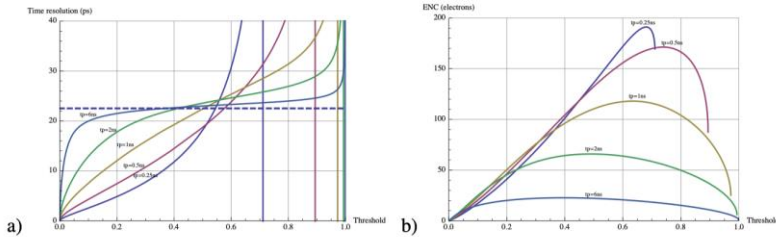


Figure 19. a) Time resolution for a sensor of $50\mu\text{m}$ thickness at 200 V bias voltage. The slewing correction is performed by dividing the signal by the total charge and applying the threshold as a fraction of this charge. b) ENC needed to match the noise contribution to the effect from the Landau fluctuations.

For LGADs the time resolution does not improve over the centroid time resolution when using leading edge discrimination on the signal normalized to the total deposited charge.

While for standard silicon sensors, the leading edge of the signal is proportional to (equal to) the total amount of charge in the sensor, for the LGADs there is no relation between the leading edge and the total charge deposit.

$$\Delta_\tau = w(d) \frac{d}{\sqrt{12}v_1}$$

Weighting field fluctuations

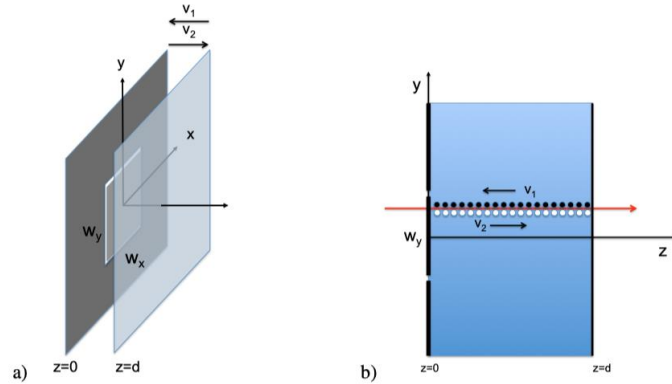


Figure 10. a) A pixel of dimension w_x, w_y centred at $x = y = z = 0$ in a parallel plate geometry of plate distance d . b) Uniform charge deposit of a particle passing the silicon sensor. v_1 is the velocity of charges moving towards the pixel and v_2 is the velocity of charges moving away from the pixel.

The effect of finite pixel size and varying signal shape with the weighting field is de-correlated from the Landau fluctuations, in contrast to the standard silicon sensors.

The expression very basic and universal !

- The Landau fluctuations are related to the total electron drift-time
- The weighting field fluctuations are related to the total hole drift time.

$T_1 = d/v_e$ = total electron drift time

$T_2 = d/v_h$ = total hole drift time

$$\Delta_{\tau}^2 = \overline{\tau^2} - \bar{\tau}^2 = w(d)^2 \frac{d^2}{12 v_1^2} + \frac{d^2}{v_2^2} s_{22} = w(d)^2 \frac{T_1^2}{12} + T_2^2 s_{22}$$

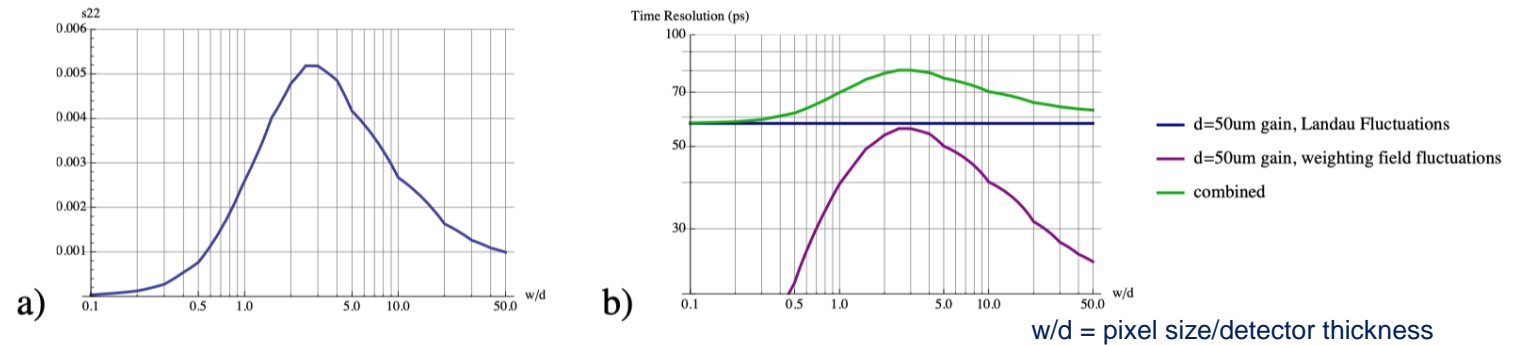


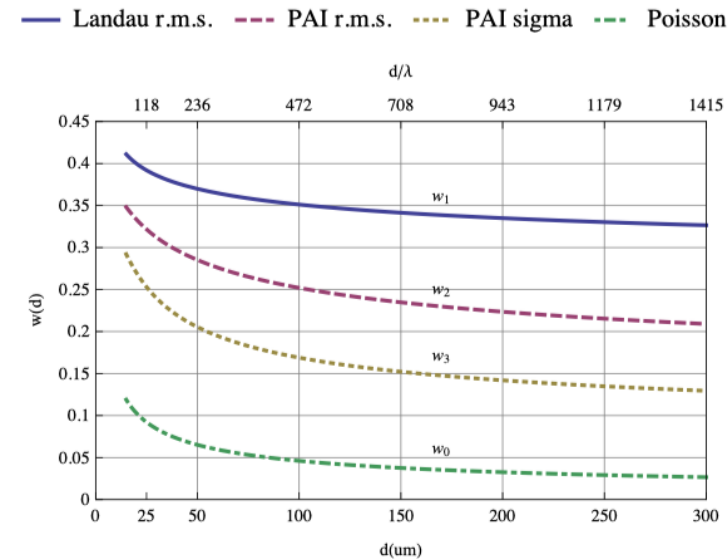
Figure 23. a) Coefficient s_{22} defining the impact of the weighting field on the time resolution. b) Centroid time resolution for a gain sensor of $50 \mu\text{m}$ thickness at 200 V. The horizontal line shows the contribution from Landau fluctuations only, while the other lines show the contribution from weighting field fluctuations as well as the combined effect.

These expressions are valid for perpendicular tracks

Time resolution of LGADs

- Centroid time resolution is around factor 2 worse than for standard silicon sensors.
- The big advantage is of course the much increased signal charge and therefore much relaxed noise specification, which allows very thin sensors for excellent time resolution as well as large pads.
- The resolution cannot be significantly improved when using faster. The centroid time resolution is essentially THE time resolution of the LGAD sensor.
- Weighting field fluctuations and Landau fluctuations are de-correlated.

$$\Delta_{\tau}^2 = \overline{\tau^2} - \bar{\tau}^2 = w(d)^2 \frac{d^2}{12 v_1^2} + \frac{d^2}{v_2^2} s_{22} = w(d)^2 \frac{T_1^2}{12} + T_2^2 s_{22}$$



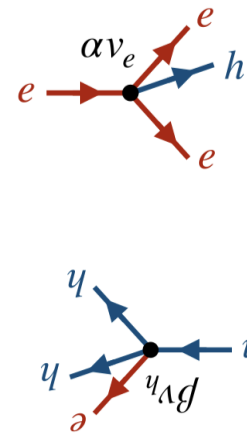
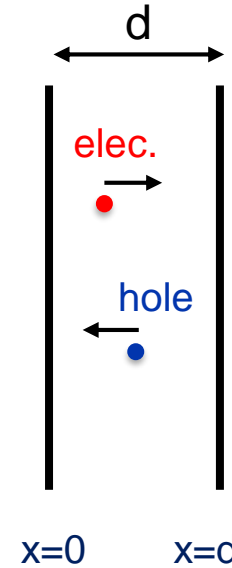
Time resolution of Single Photon Avalanche Diodes (SPADs)

Single Photon Avalanche Diodes

For very large electric fields, also the holes start to contribute to the avalanche.

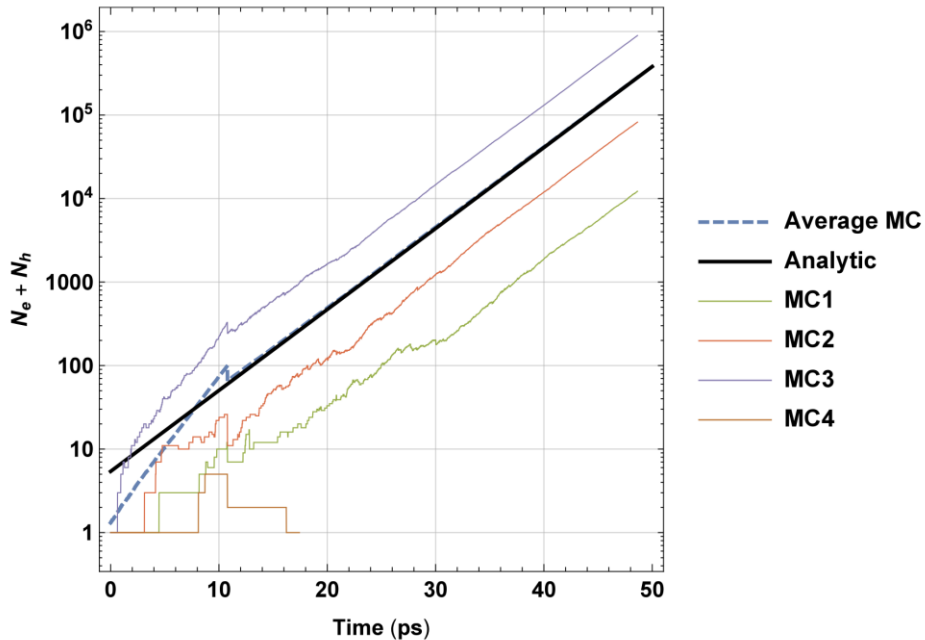
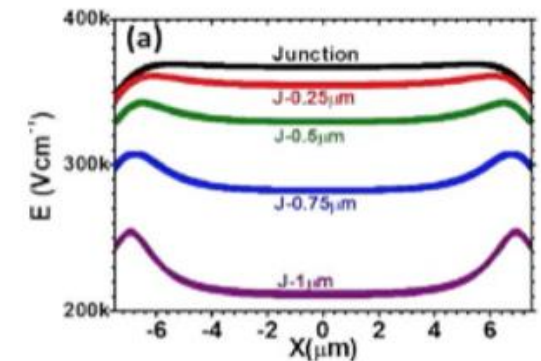
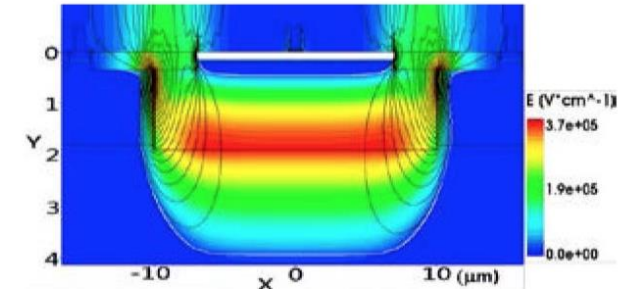
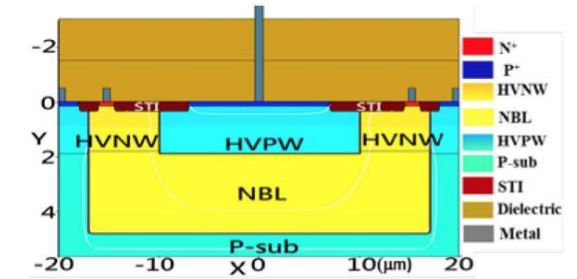
αdx = probability for an electron to produce an additional e-h pair along a distance dx

βdx = probability for a hole to produce an additional e-h pair along a distance dx



SIMULATION OF ELECTRIC FIELD DISTRIBUTION IN CMOS SINGLE PHOTON AVALANCHE DIODES AT BREAKDOWN VOLTAGE

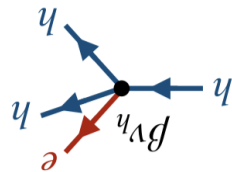
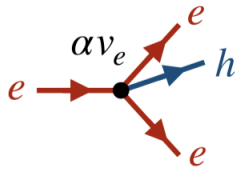
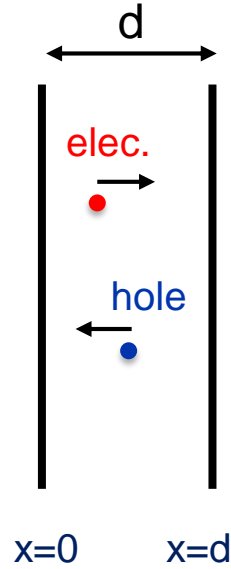
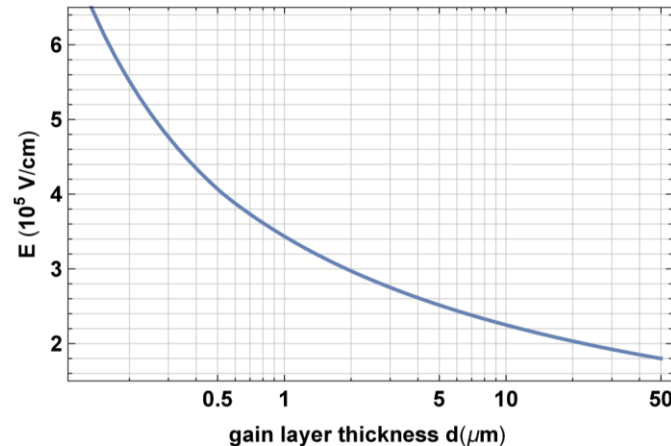
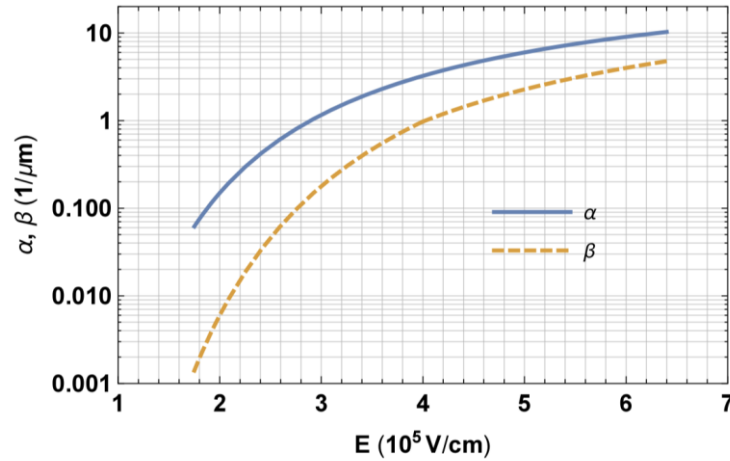
Jau-Yang Wu and Sheng-Di Lin
Department of Electronics Engineering, National Chiao Tung University, Hsinchu, Taiwan
E-mail: judewu.ee95g@nctu.edu.tw



SPADs Breakdown Condition

αdx = probability for an electron to produce an additional e-h pair along a distance dx

βdx = probability for a hole to produce an additional e-h pair along a distance dx



this is different from the notation used in [2]). These charge densities result in local average current densities of $j_e(x, t) = v_e(x)n_e(x, t)$ and $j_h(x, t) = -v_h(x)n_h(x, t)$. By the continuity equation $\partial j / \partial x + \partial n / \partial t = \sigma$, with σ the generation rate, we therefore have

$$\begin{aligned} \frac{\partial n_e(x, t)}{\partial t} + \frac{\partial v_e(x) n_e(x, t)}{\partial x} &= \alpha(x) v_e(x) n_e(x, t) + \beta(x) v_h(x) n_h(x, t) \\ \frac{\partial n_h(x, t)}{\partial t} - \frac{\partial v_h(x) n_h(x, t)}{\partial x} &= \alpha(x) v_e(x) n_e(x, t) + \beta(x) v_h(x) n_h(x, t) \end{aligned} \quad (11)$$

The fact that electrons move to the left and holes move to the right gives the boundary conditions

$$n_e(0, t) = 0 \quad n_h(d, t) = 0 \quad (12)$$

Since Eq. (11) represents a set of linear equations we can use the Ansatz $n_e(x, t) = f(x)e^{St}$ and $n_h(x, t) = g(x)e^{St}$ and we find

$$\begin{aligned} S f(x) + [v_e(x) f(x)]' &= \alpha(x) v_e(x) f(x) + \beta(x) v_h(x) g(x) \\ S g(x) - [v_h(x) g(x)]' &= \alpha(x) v_e(x) f(x) + \beta(x) v_h(x) g(x) \end{aligned} \quad (13)$$

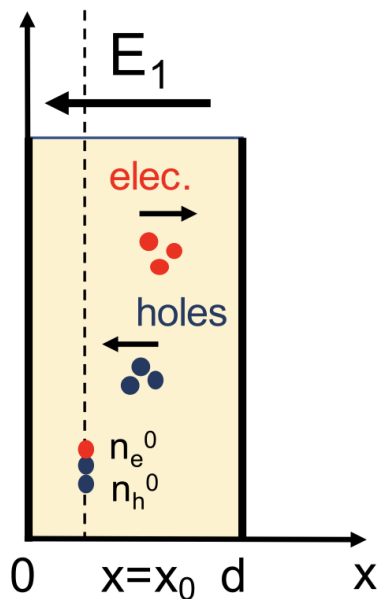
with $f(0) = 0$ and $g(d) = 0$. The multiplication of electrons and holes can lead to a finite amount of total charge in the avalanche ($S < 0$) or it can diverge and cause breakdown ($S > 0$). The boundary between the two regimes is at $S = 0$, so by setting $S = 0$ in the above equations and solving them with the given boundary conditions we find the breakdown condition (Appendix B)

$$\int_0^d \alpha(x) \exp \left[- \int_0^x (\alpha(x') - \beta(x')) dx' \right] dx = 1 \quad (14)$$

The breakdown condition is independent of $v_e(x)$ and $v_h(x)$. This relation is usually derived by evaluating the point at which the gain for a constant current injected into the gain layer diverges [6]. Evaluating the breakdown equation for constant α and β implies that breakdown occurs if

$$d > \frac{1}{\alpha - \beta} \ln \frac{\alpha}{\beta} \quad (15)$$

Solution for the average Signal



$$\begin{aligned}\frac{\partial n_e(x, t)}{\partial t} + \frac{\partial v_e(x) n_e(x, t)}{\partial x} &= \alpha(x) v_e(x) n_e(x, t) + \beta(x) v_h(x) n_h(x, t) \\ \frac{\partial n_h(x, t)}{\partial t} - \frac{\partial v_h(x) n_h(x, t)}{\partial x} &= \alpha(x) v_e(x) n_e(x, t) + \beta(x) v_h(x) n_h(x, t) \\ n_e(0, t) &= 0 \quad n_h(d, t) = 0\end{aligned}$$

A number of n_e^0 electrons and n_h^0 holes are placed at $x=x_0$ at time $t=0$.

What is the average distribution of electrons $n_e(x, t)$ and holes $n_h(x, t)$ in the sensor at time t ?

What is the total number of electron $N_e(t)$ and holes $N_h(t)$ in the sensor at time t ?

Average signal $I(t) = E_W [N_e(t) v_e + N_h(t) v_h]$

Nuclear Inst. and Methods in Physics Research, A 1003 (2021) 165327

The statistics of electron-hole avalanches

P. Windischhofer^{a,*}, W. Riegler^b

^a University of Oxford, United Kingdom
^b CERN, Switzerland

$$\langle n_e(x, t) \rangle = \sum_{\lambda} C(\lambda) f_{\lambda}^e(x, t), \quad \langle n_h(x, t) \rangle = \sum_{\lambda} C(\lambda) f_{\lambda}^h(x, t).$$

$$f_{\lambda}^e(x, t) = e^{\gamma v^* t} e^{ax} \sinh \kappa x,$$

$$f_{\lambda}^h(x, t) = \frac{1}{\beta d} \frac{v_e}{v_h} e^{\gamma v^* t} e^{ax} [\lambda \sinh \kappa x + \bar{\kappa} \cosh \kappa x].$$

$$C(\lambda) = \frac{1}{\mathcal{N}(\lambda, t=0)} [\alpha v_e N_e^0 f_{\lambda}^e(d - x_0, t=0) + \beta v_h N_h^0 f_{\lambda}^h(d - x_0, t=0)]$$

$$\mathcal{N}(\lambda, t) = -e^{2\gamma v^* t} e^{ad} \frac{\alpha d}{2\bar{\kappa}} \frac{v_e}{v_h} (v_e + v_h) (1 + \lambda) \sinh \bar{\kappa}.$$

$$\gamma = \frac{\alpha + \beta}{2} + \frac{\lambda}{d},$$

$$v^* = \frac{2v_e v_h}{v_e + v_h},$$

$$\lambda_t = \gamma v^*,$$

$$a = \frac{v^*}{2} \left(\frac{\alpha}{v_h} - \frac{\beta}{v_e} \right) + \frac{v^*}{2d} \left(\frac{1}{v_h} - \frac{1}{v_e} \right) \lambda,$$

$$\kappa = \frac{1}{d} \bar{\kappa} = \frac{1}{d} \sqrt{\lambda^2 - \alpha \beta d^2},$$

λ must satisfy the 'Eigenvalue' equation:

$$\lambda + \bar{\kappa} \coth \bar{\kappa} = 0,$$

The equation has a finite number ≥ 1 of real solutions and an infinite number of complex valued solutions.

→ For long times, the largest real Eigenvalue λ dominates.

Solution for the average Signal

$$n_e(x, t) = \frac{1}{d} a(x) [n_e^0 u_e(x_0) + n_h^0 u_h(x_0)] e^{\gamma v^* t}$$

$$n_h(x, t) = \frac{1}{d} b(x) [n_e^0 u_e(x_0) + n_h^0 u_h(x_0)] e^{\gamma v^* t}$$

with

$$u_e(x_0) = e^{-a_1 x_0} \sin(k - kx_0/d)$$

$$u_h(x_0) = \frac{e^{-a_1 x_0}}{\alpha d} [k \cos(k - kx_0/d) + \lambda_1 \sin(k - kx_0/d)]$$

$$a(x) = \frac{2v_h k e^{a_1 x} \sin\left(k \frac{x}{d}\right)}{(v_e + v_h)(1 + \lambda_1) \sin k}$$

$$b(x) = \frac{2kv_e e^{a_1 x} [k \cos\left(k \frac{x}{d}\right) + \lambda_1 \sin\left(k \frac{x}{d}\right)]}{(v_e + v_h)\beta d(1 + \lambda_1) \sin k}$$

and the constants v^* , a_1 , γ , k are defined by

$$v^* = \frac{2v_e v_h}{v_e + v_h}$$

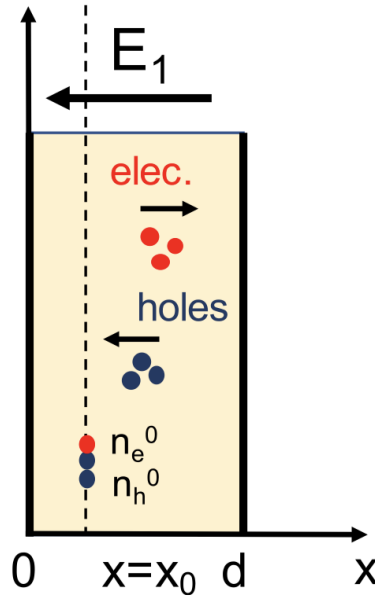
$$a_1 = \frac{\alpha v_e - \beta v_h}{v_e + v_h} + \frac{v_e - v_h}{v_e + v_h} \frac{1}{d} \lambda_1$$

$$\gamma = \frac{\alpha + \beta}{2} + \frac{\lambda_1}{d}$$

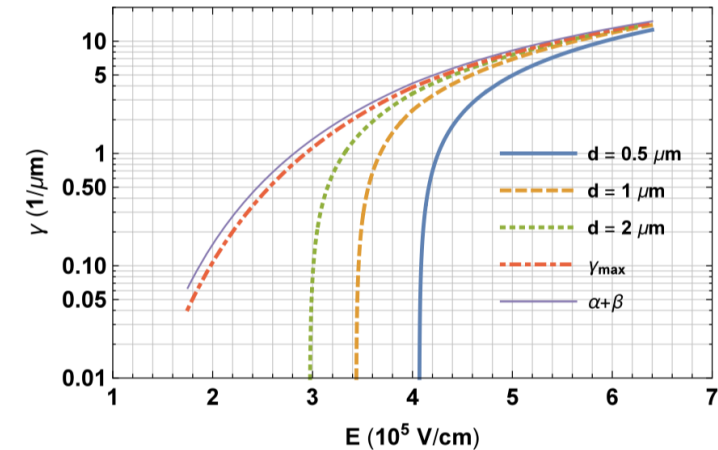
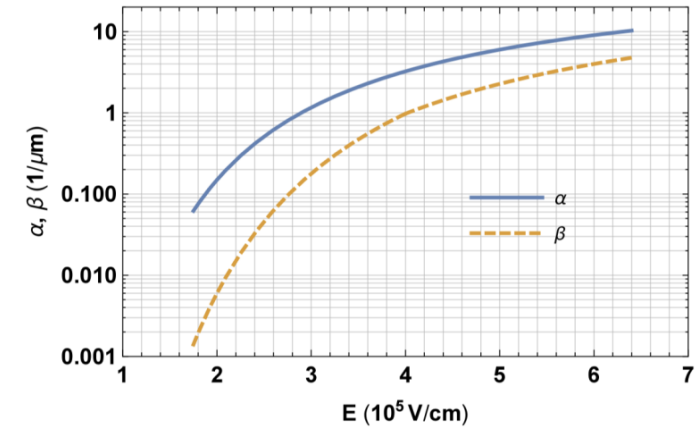
$$k = \sqrt{\alpha\beta d^2 - \lambda_1^2}$$

The parameter λ_1 is the largest real solution of the equation

$$\lambda_1 + \sqrt{\alpha\beta d^2 - \lambda_1^2} \cot \sqrt{\alpha\beta d^2 - \lambda_1^2} = 0$$



$$\begin{aligned} \gamma = 0 & & \alpha\beta d^2 = \frac{\alpha\beta}{(\alpha - \beta)^2} \ln^2 \frac{\beta}{\alpha} \leq 1 \\ \gamma = \frac{\alpha + \beta}{2} - \sqrt{\alpha\beta} & & \alpha\beta d^2 = 1 \\ \gamma = \frac{\alpha + \beta}{2} & & \alpha\beta d^2 = \frac{\pi^2}{4} \approx 2.47 \\ \gamma_{max} = \frac{\alpha + \beta}{2} + \sqrt{\alpha\beta} & & \alpha\beta d^2 \rightarrow \infty \end{aligned}$$



Solution for the average Signal

$$N = \int_0^d n(x, t) dx$$

$$N_e(t) = B_e [n_e^0 u_e(x_0) + n_h^0 u_h(x_0)] e^{\gamma v^* t}$$

$$N_h(t) = B_h [n_e^0 u_e(x_0) + n_h^0 u_h(x_0)] e^{\gamma v^* t}$$

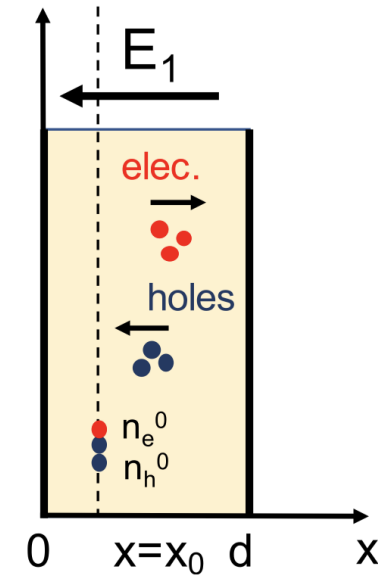
where we have

$$B_e = \frac{2k v_h [e^{a_1 d} (a_1 d - k \cot k) + k \csc k]}{(v_e + v_h)(a_1^2 d^2 + k^2)(1 + \lambda_1)}$$

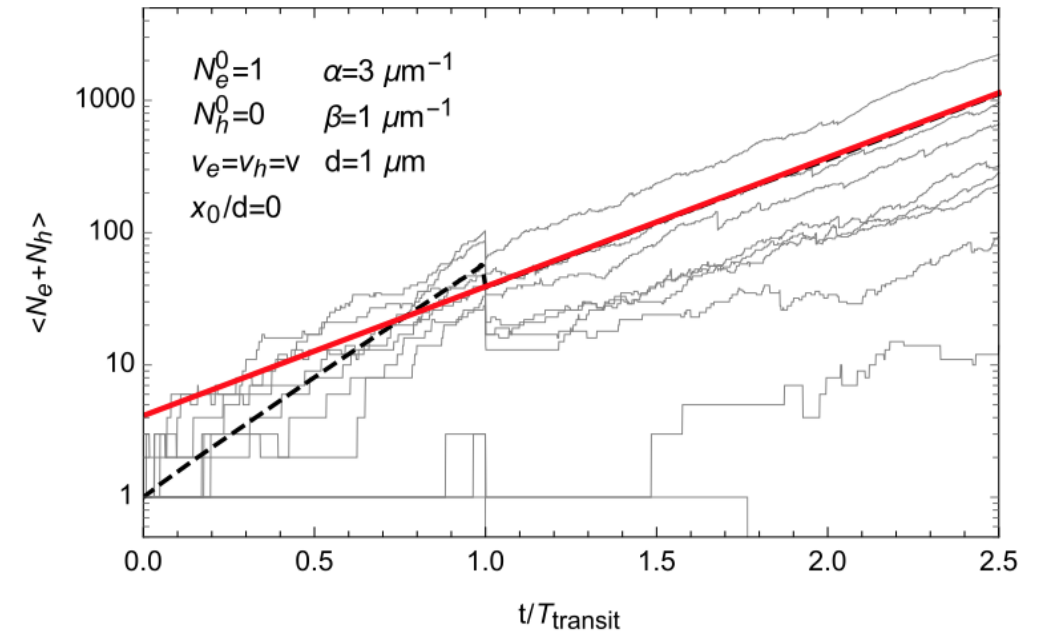
$$B_h = \frac{2k v_e [e^{a_1 d} (k^2 + a_1 d \lambda_1 + k(a_1 d - \lambda_1) \cot k) + k(\lambda_1 - a_1 d) \csc k]}{(v_e + v_h) \beta d (a_1^2 d^2 + k^2)(1 + \lambda_1)}$$

The total induced current becomes

$$\begin{aligned} I(t) &= e_0 \frac{E_w}{V_w} [v_e N_e(t) + v_h N_h(t)] \\ &= e_0 \frac{E_w}{V_w} (v_e B_e + v_h B_h) [n_e^0 u_e(x_0) + n_h^0 u_h(x_0)] e^{\gamma v^* t} \end{aligned}$$



----- MC ——— $N(\lambda_1) e^{\gamma v^* t}$



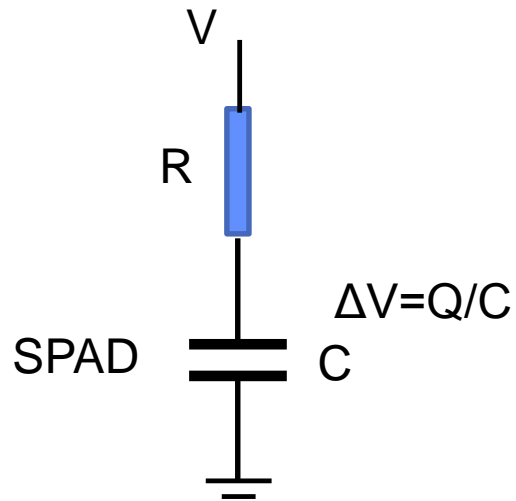
Quenching

The average signal will increase until the number of charges that are deposited on the capacitor lowers the voltage across the diode below the breakdown voltage.

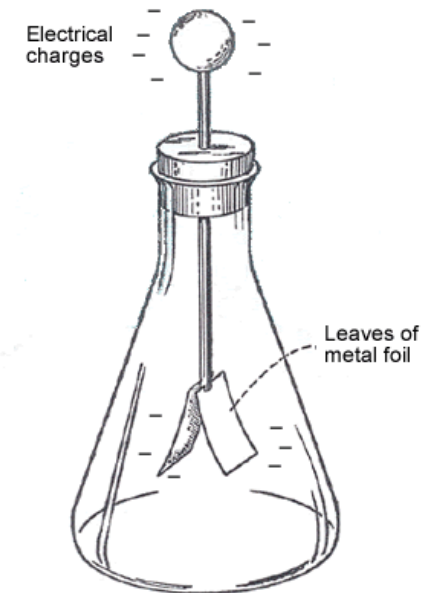
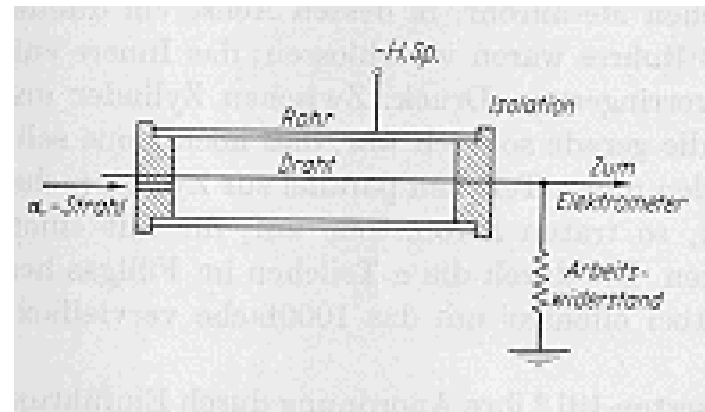
The 'quench' resistor will determine the rate of recharging of the SPAD.

The voltage drop represents the SPAD signal.

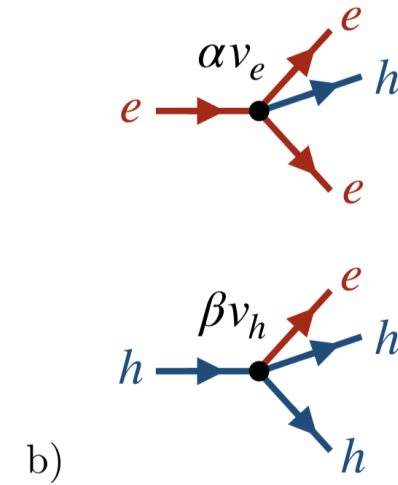
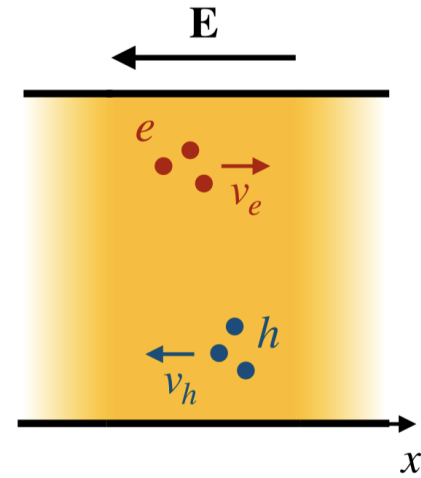
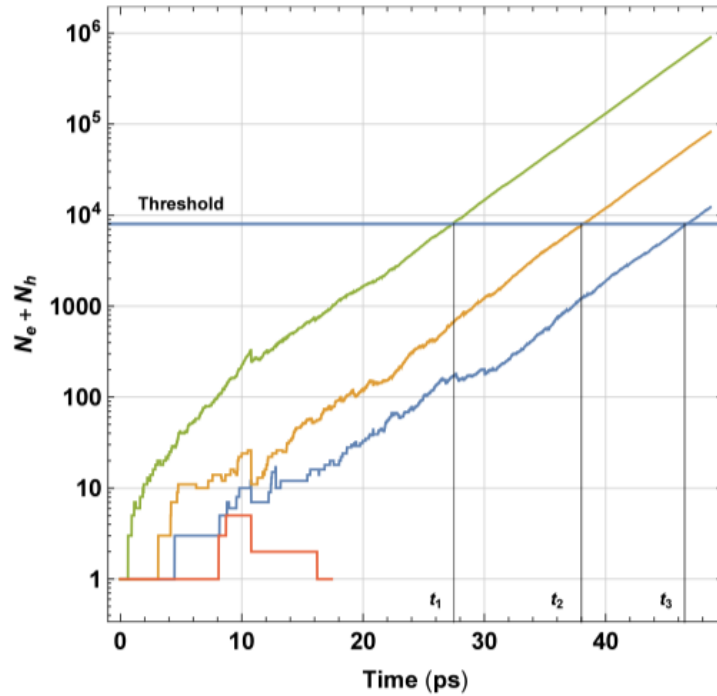
This is the same principle as the Geiger counter, where the divergence of the avalanche is due to electrons and photons (produced in the avalanche and producing more ionization electrons).



Rutherford and Geiger 1908



SPAD time resolution

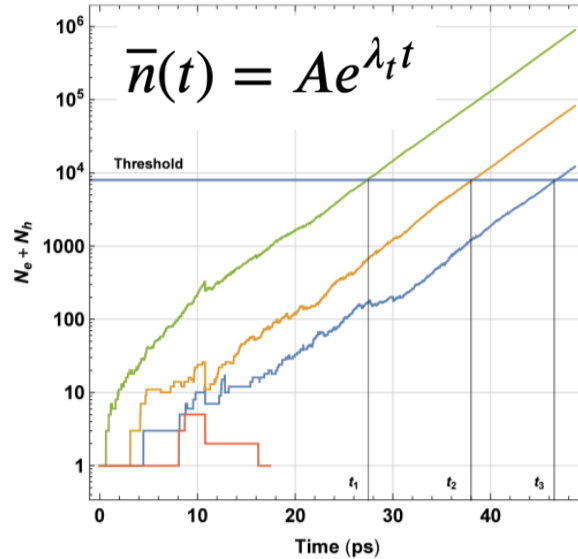


Time measurement by setting a threshold to the diverging avalanche signal.

First investigate a SPAD without boundaries:

- Exact solution exists
- Features are similar to the (much more complicated) SPAD with boundaries

Fluctuations of the avalanche, SPAD without boundary



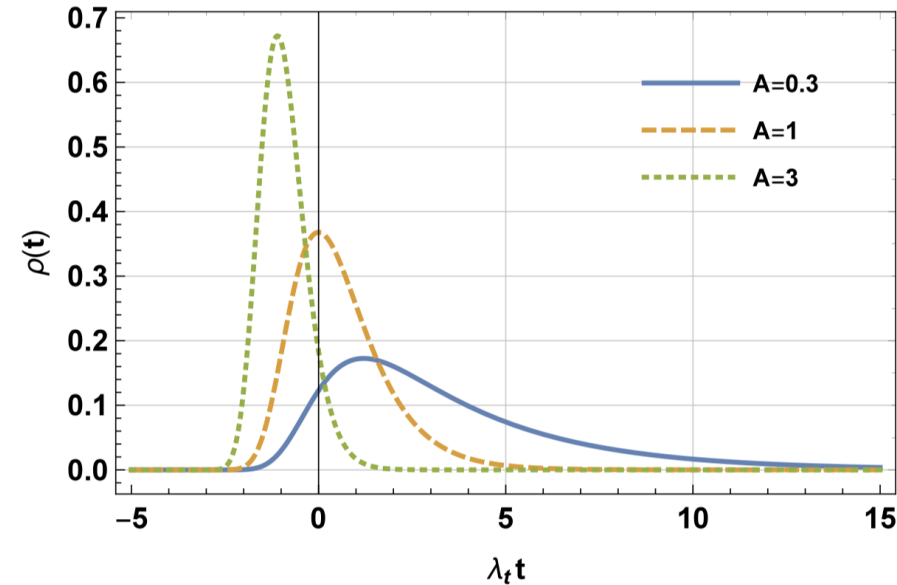
Time response function when placing a threshold of n electrons to the signal.

$$\rho(n, t)dt = \lambda_t \frac{\Gamma(1 + A + n)}{\Gamma(A)\Gamma(1 + n)} \left(\frac{1}{v(t)}\right)^A \left(1 - \frac{1}{v(t)}\right)^n dt$$

$$A = \frac{n_e^0 \alpha v_e + n_h^0 \beta v_h}{\alpha v_e + \beta v_h} \quad v(t) = e^{\lambda_t t} \quad \lambda_t = \alpha v_e + \beta v_h$$

$$\bar{t} = \frac{1}{\lambda_t} [\psi_0(n + A + 1) - \psi_0(A)] \quad \sigma = \frac{1}{\lambda_t} \sqrt{\psi_1(A) - \psi_1(n + A + 1)} \quad (54)$$

where $\psi_0(x) = d \ln \Gamma(z)/dz$ is the digamma function and $\psi_1(x) = d^2 \ln \Gamma(z)/dz^2$ is the trigamma function. For large numbers of n the



Approximation for 'large thresholds'

$$\rho(n, t) = \frac{\lambda_t}{\Gamma(A)} \exp [A \ln n - A \lambda_t t - n e^{-\lambda_t t}]$$

$$\sigma = \frac{1}{\lambda_t} \sqrt{\psi_1(A)}$$

→ Time resolution is independent of the threshold

→ Time resolution is inversely proportional to the 'risetime' of the signal

→ For a single e-h pair, $A=1$ and $\sqrt{\psi_1(A)} = \pi/\sqrt{6} = 1.28=O(1)$

Avalanche fluctuations, SPAD with boundary

Equations for the average electron and hole densities

$$\begin{aligned}\frac{\partial}{\partial t} \langle n_e(x) \rangle + \frac{\partial}{\partial x} v_e(x) \langle n_e(x) \rangle &= \alpha(x) v_e(x) \langle n_e(x) \rangle + \beta(x) v_h(x) \langle n_h(x) \rangle, \\ \frac{\partial}{\partial t} \langle n_h(x) \rangle - \frac{\partial}{\partial x} v_h(x) \langle n_h(x) \rangle &= \alpha(x) v_e(x) \langle n_e(x) \rangle + \beta(x) v_h(x) \langle n_h(x) \rangle.\end{aligned}$$

Nuclear Inst. and Methods in Physics Research, A 1003 (2021) 165327

The statistics of electron–hole avalanches

P. Windischhofer^{a,*}, W. Riegler^b

^a University of Oxford, United Kingdom

^b CERN, Switzerland



... surprisingly complex.

Solution gives important insights:

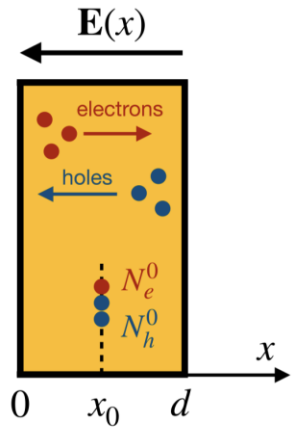
Equations for second moment of the electron and hole densities

$$\begin{aligned}\frac{\partial}{\partial t} \langle n_e(x) n_e(y) \rangle + \frac{\partial}{\partial x} v_e(x) \langle n_e(x) n_e(y) \rangle + \frac{\partial}{\partial y} v_e(y) \langle n_e(x) n_e(y) \rangle \\ = \alpha(x) v_e(x) \delta(x - y) \langle n_e(x) \rangle + \beta(x) v_h(x) \delta(x - y) \langle n_h(y) \rangle \\ + [\alpha(x) v_e(x) + \alpha(y) v_e(y)] \langle n_e(x) n_e(y) \rangle + \beta(y) v_h(y) \langle n_e(x) n_h(y) \rangle \\ + \beta(x) v_h(x) \langle n_e(y) n_h(x) \rangle,\end{aligned}$$

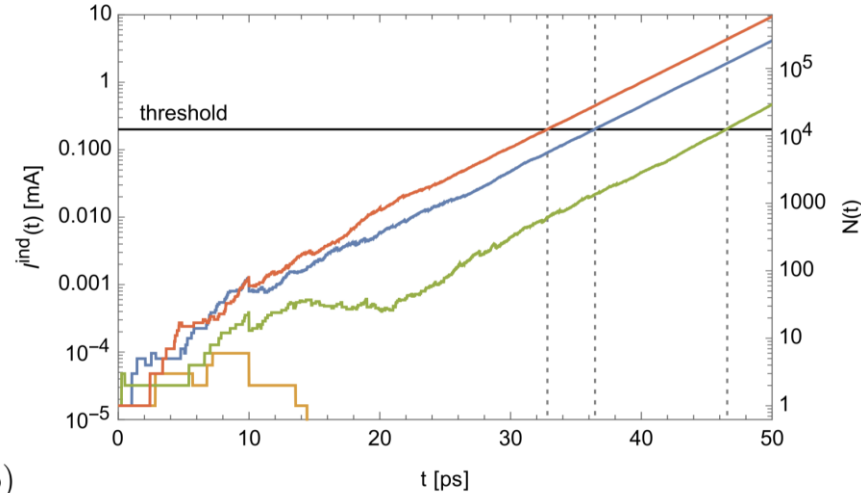
$$\begin{aligned}\frac{\partial}{\partial t} \langle n_h(x) n_h(y) \rangle - \frac{\partial}{\partial x} v_h(x) \langle n_h(x) n_h(y) \rangle - \frac{\partial}{\partial y} v_h(y) \langle n_h(x) n_h(y) \rangle \\ = \alpha(x) v_e(x) \delta(x - y) \langle n_e(y) \rangle + \beta(x) v_h(x) \delta(x - y) \langle n_h(y) \rangle \\ + [\beta(x) v_h(x) + \beta(y) v_h(y)] \langle n_h(x) n_h(y) \rangle \\ + \alpha(y) v_e(y) \langle n_e(y) n_h(x) \rangle + \alpha(x) v_e(x) \langle n_e(x) n_h(y) \rangle,\end{aligned}$$

$$\begin{aligned}\frac{\partial}{\partial t} \langle n_e(x) n_h(y) \rangle + \frac{\partial}{\partial x} v_e(x) \langle n_e(x) n_h(y) \rangle - \frac{\partial}{\partial y} v_h(y) \langle n_e(x) n_h(y) \rangle \\ = \alpha(x) v_e(x) \delta(x - y) \langle n_e(y) \rangle + \beta(x) v_h(x) \delta(x - y) \langle n_h(y) \rangle \\ + \alpha(y) v_e(y) \langle n_e(x) n_e(y) \rangle + \beta(x) v_h(x) \langle n_h(x) n_h(y) \rangle \\ + [\alpha(x) v_e(x) + \beta(y) v_h(y)] \langle n_e(x) n_h(y) \rangle.\end{aligned}$$

Time resolution of SPAD



a)



b)

$$I(t) = e_0 \frac{E_w}{V_w} [v_e N_e(t) + v_h N_h(t)]$$

$$= e_0 \frac{E_w}{V_w} (v_e B_e + v_h B_h) [n_e^0 u_e(x_0) + n_h^0 u_h(x_0)] e^{\gamma v^* t}$$

$$\sigma \approx \frac{\sqrt{\psi_1(A)}}{\gamma v^*}$$

$$v^* = \frac{2v_e v_h}{v_e + v_h}$$

$$A = \frac{n_e^0 \alpha v_e + n_h^0 \beta v_h}{\alpha v_e + \beta v_h}$$

γ determines the exponential growth of the avalanche for long times

$1/\gamma v^*$ determines the time resolution when setting a 'high' threshold to the signal !

The coefficient $\sqrt{\psi_1(A)}$ is $O(1) \rightarrow 1/\gamma v^*$ IS the approximate time resolution of a SPAD

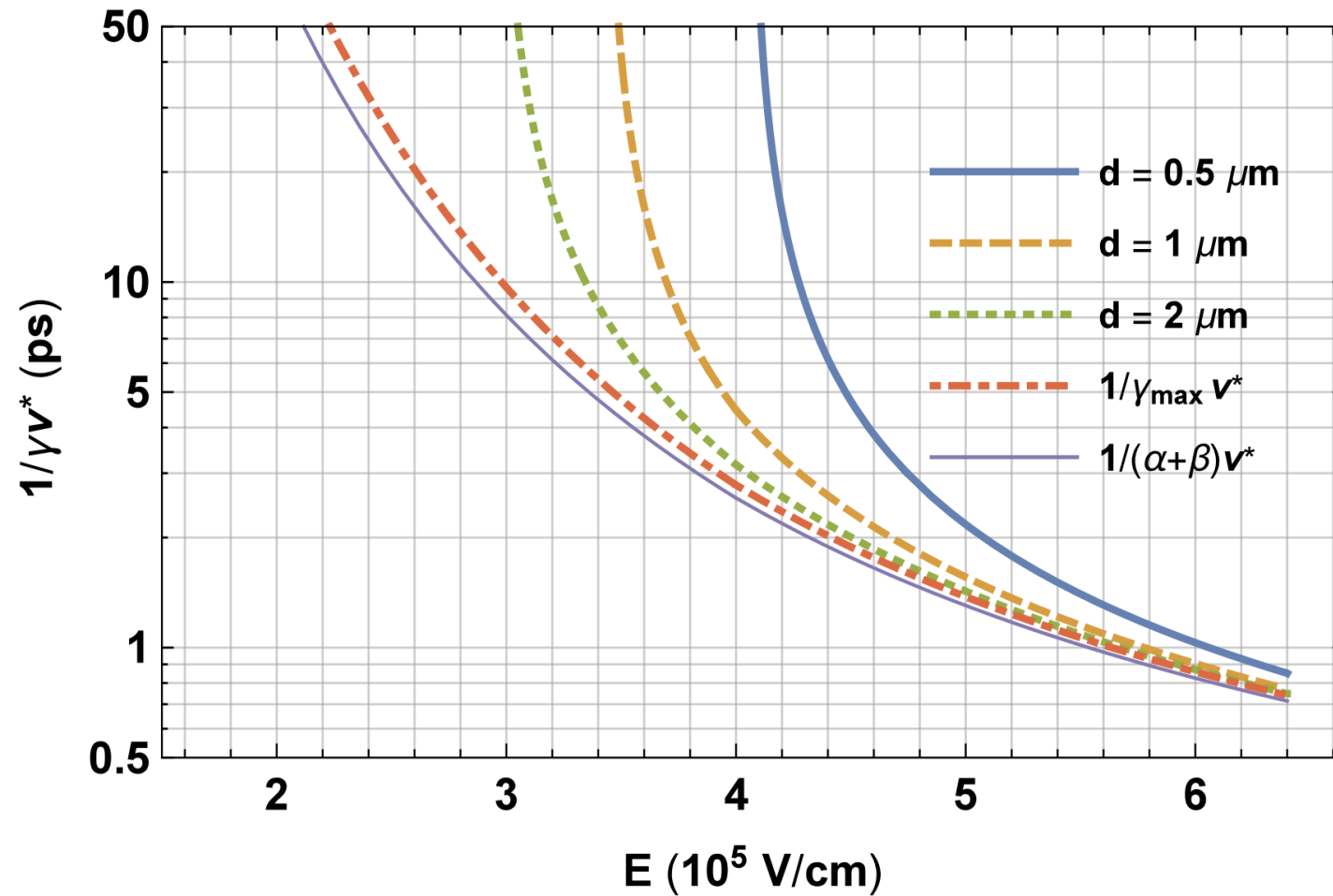
The electron and hole densities become fully correlated over the timescale of $1/\gamma v^*$ i.e. there are no more fluctuations. The fluctuations take place in the very beginning of the avalanches – from there on there is only deterministic grow of the avalanche.

$$C(\lambda_1, \lambda_1, t) \sim C_\infty(\lambda_1, \lambda_1) \left(1 - e^{-\gamma_1 v^* t}\right)$$

Time resolution aSPAD

Approximate r.m.s. SPAD time resolution $1/\gamma v^*$

<10ps is in the cards ...



Other contributions to the time resolution of SPADs

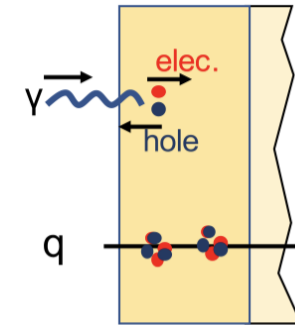
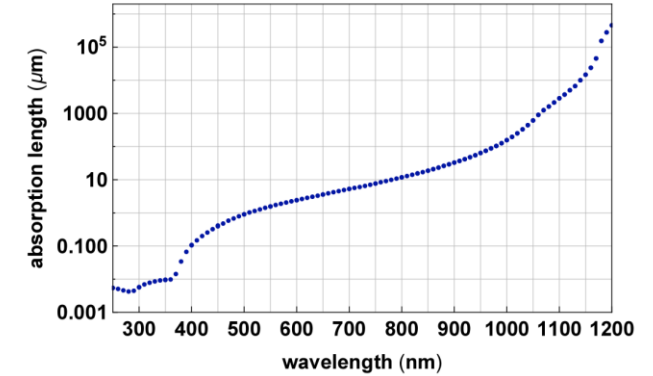
Up to now we assumed a given number of electrons and holes at a given position x_0 .
 → Only avalanche fluctuations are contributing to the time resolution.

For the measurement of single photons, the conversion point in the gain layer can vary.

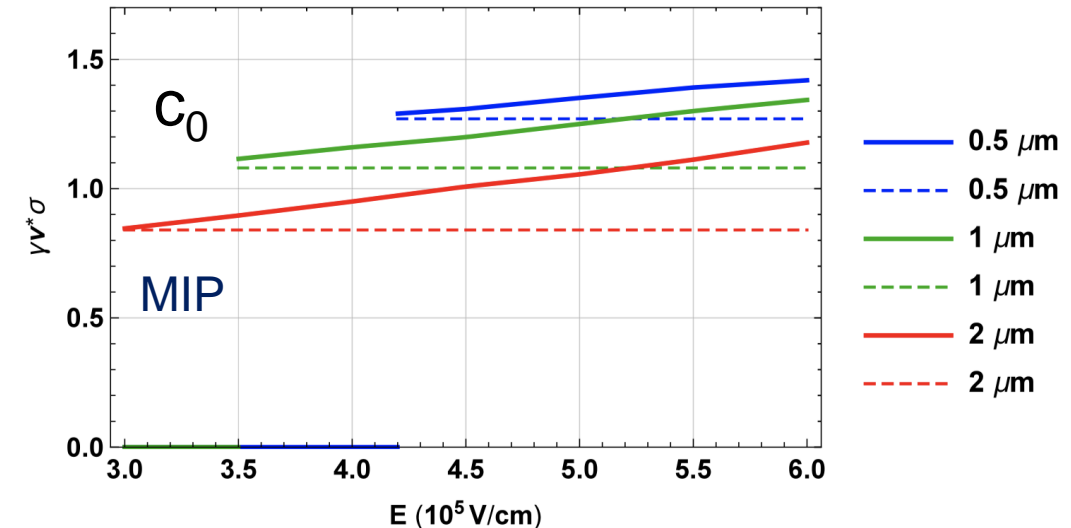
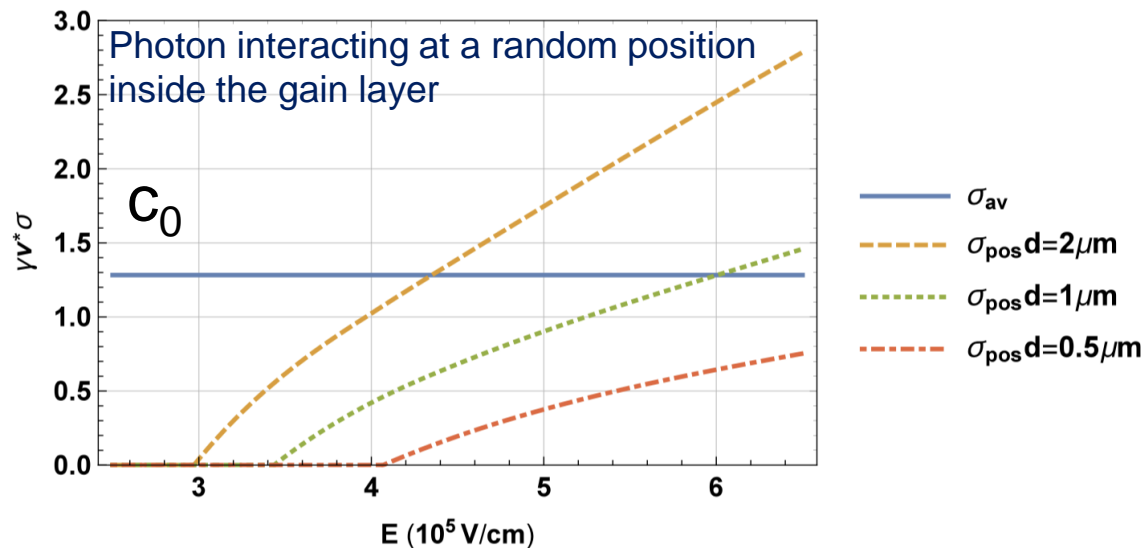
For SPADs with a conversion layer, the arrival time distribution of the electrons at the gain layer will contribute.

For the measurement of charged particles, the Landau fluctuations of the charge deposit will contribute to the time resolution.

Conclusion (see paper): for all these scenarios, the time resolution stays around $\sigma = \frac{c_0}{\gamma v^*}$ with c_0 in the order of 1-3.



Expect excellent time resolution for MIPs



Efficiency of SPADs

Applying a voltage below the breakdown voltage, the avalanche will never diverge and a finite number of electrons and holes will be produced in the avalanche.

Applying a voltage above the breakdown voltage, some avalanches will diverge and some avalanches will only produce a finite amount of charge, typically much too small to be detected.

A SPAD is considered efficient only in case an avalanche diverges.

Probability $P_e(x)$ for single electron at position x to produces a diverging avalanche and
Probability $P_h(x)$ for single electron at position x to produces a diverging avalanche

$$\frac{d P_e(x)}{d x} = -\alpha(x)[1 - P_e(x)] [P_e(x) + P_h(x) - P_e(x)P_h(x)]$$
$$\frac{d P_h(x)}{d x} = \beta(x)[1 - P_h(x)] [P_e(x) + P_h(x) - P_e(x)P_h(x)]$$

$$P_e(d) = 0 \text{ and } P_h(0) = 0.$$

[8] W. Oldham, R. Samuelson, P. Antognetti, Triggering phenomena in avalanche diodes, IEEE 19 (9) (1972) 1056–1060.

[9] R.J. McIntyre, On the avalanche initiation probability of avalanche diodes above the breakdown voltage, IEEE Trans. Electron. Dev. 20 (7) (1973) 637–641.

Efficiency of SPADs

Solution for a SPAD of thickness d

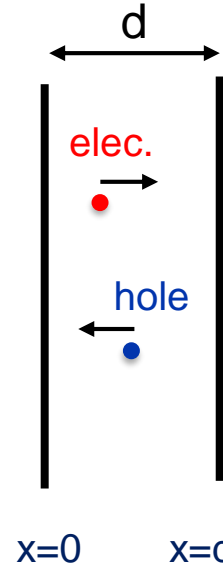
$$P(x) = \frac{p_0}{p_0 + [1 - p_0]e^{(\alpha-\beta)x}}$$

$$P_e(x) = 1 - e^{-\alpha(d-x)} \left[\frac{(1 - p_0)e^{(\alpha-\beta)d} + p_0}{(1 - p_0)e^{(\alpha-\beta)x} + p_0} \right]^{\frac{\alpha}{\alpha-\beta}}$$

$$P_h(x) = 1 - e^{-\beta x} \left[(1 - p_0)e^{(\alpha-\beta)x} + p_0 \right]^{\frac{\beta}{\alpha-\beta}}$$

Eq. (41) that determines p_0 reads as

$$e^{-(\alpha-\beta)d} = \frac{1}{p_0} \left[(1 - p_0)^{1-\frac{\beta}{\alpha}} - (1 - p_0) \right]$$



Efficiencies for single electrons and holes.

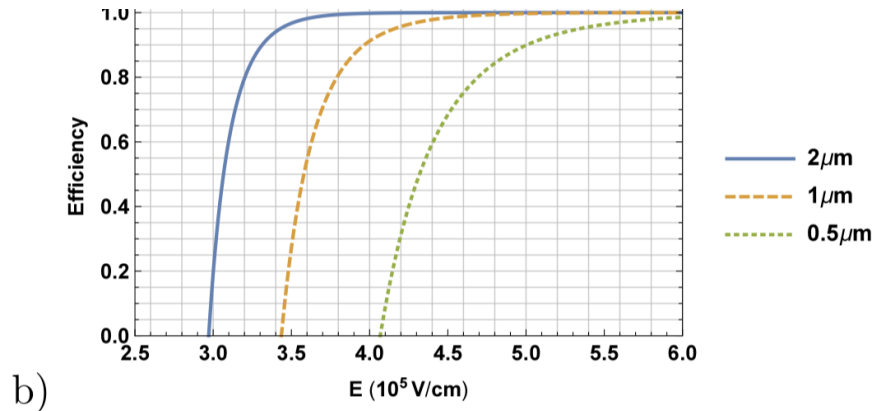
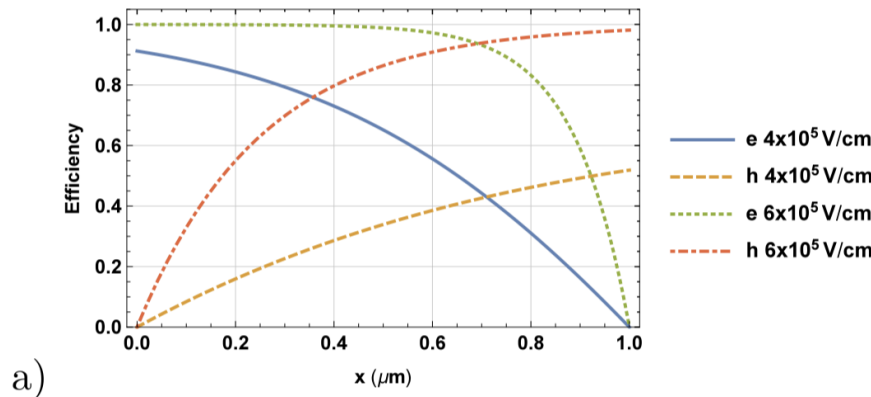


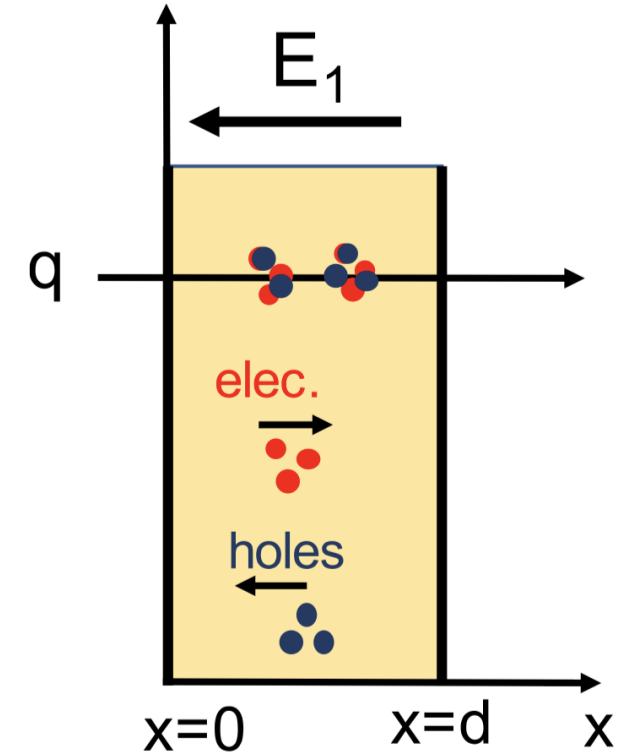
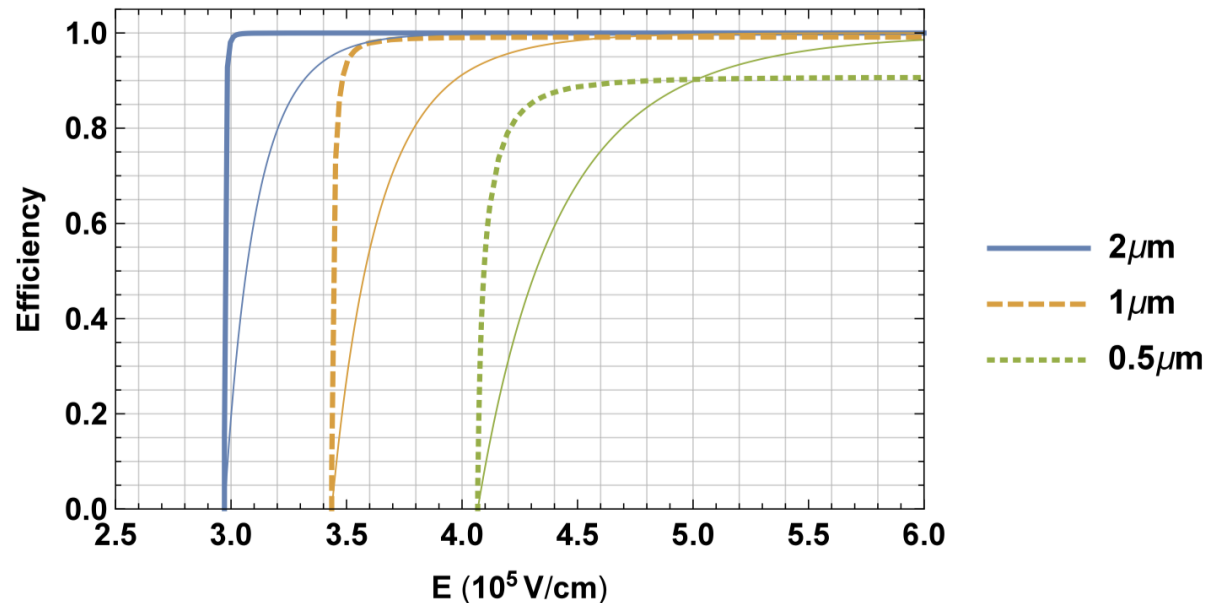
Fig. 10. (a) Breakdown probability (efficiency) for a single electron and a single hole deposited at position x inside a gain layer of $d = 1 \mu\text{m}$ for two values of the electric field. (b) Breakdown probability p_0 (efficiency) for a single electron placed at $x = 0$ for different values of the gain layer thickness d .

Efficiency of SPADs for MIPS

Solution for a SPAD of thickness d

$$Q(x) = 1 - P(x) = \frac{1}{1 + \frac{p_0}{1-p_0} \exp \left[- \int_0^x (\alpha(x') - \beta(x')) dx' \right]}$$

$$p = 1 - \exp \left[- \frac{1}{\lambda} \left(d - \sum_{n=1}^{\infty} p_{clu}(n) \int_0^d Q(x)^n dx \right) \right]$$



Once a MIP leaves a cluster in a SPAD that is biased above the breakdown voltage, there is a quite high probability that a diverging avalanche is produced.

$$\text{Efficiency} \sim 1 - \exp[-d/\lambda]$$

Garfield and Garfield++

[CERN](#) [Consult](#) [Writups](#) [Garfield](#)

Garfield - simulation of gaseous detectors

Responsible at CERN: [Rob Veenhof](#)
Manual Type: User Guide
Version: 9
Author: Rob Veenhof
Reference: W5050

Created: 1 Sep 1984
Last Update: 7 Sep 2010
Verified: 7 Sep 2010
Valid until: further notice
Support Level: [High](#)

What Garfield does

Garfield is a computer program for the detailed simulation of two- and three-dimensional drift chambers.

Fields

Originally, the program was written for two-dimensional chambers made of wires and planes, such as drift chambers, TPCs and multiwire counters. For many of these configurations, exact fields are known. This is not the case for three dimensional configurations, not even for seemingly simple arrangements like two crossing wires. Furthermore, dielectric media and complex electrode shapes are difficult to handle with analytic techniques. To handle such increasingly popular detectors, Garfield is interfaced with the [neBEM](#) program. Garfield also accepts two and three dimensional field maps computed by finite element programs such as [Ansys](#), [Maxwell](#), [Tosca](#), [QuickField](#) and [FEMLAB](#) as basis for its calculations. The finite element technique can handle nearly arbitrary electrode shapes as well as dielectrics.

Transport and ionisation in gas mixtures

An interface to the [Magboltz](#) program is provided for the computation of electron transport properties in nearly arbitrary gas mixtures. Garfield also has an interface with the [Heed](#) program to simulate ionisation of gas molecules by particles traversing the chamber.

Transport of particles, including diffusion, avalanches and current induction is treated in three dimensions irrespective of the technique used to compute the fields.

Applications


The program can calculate for instance the following:

- field maps, contour plots and 3-dimensional impressions;
- the wire sag that results from electrostatic and gravitational forces;
- optimum potential settings to achieve various conditions;
- plots of electron and ion drift lines;
- x(t)-relations, drift time tables and arrival time distributions;
- signals induced by charged particles traversing a chamber, taking both electron pulse and ion tail into account.

Related information

- [help facility](#) with examples for nearly every command, which can be consulted from within the program and via WWW
- [technical notes](#) on specific areas of the program and on related topics
- [bug reports](#)
- [examples](#) that illustrate the use of the program
- [CNL articles](#) (up to 2000)
- [news](#) (from March 2005)
- [running](#) the program at CERN
- [source files](#) of the program

Last updated on 8/2/11.



DISSERTATION

Microscopic Simulation of Particle Detectors

ausgeführt zum Zwecke der Erlangung des akademischen Grades eines
Doktors der technischen Wissenschaften unter der Leitung von

Univ. Prof. Dipl.-Ing. Dr. Christian Fabjan
E 141
Atominstitut der österreichischen Universitäten

eingereicht an der Technischen Universität Wien
Fakultät für Physik

von


Dipl.-Ing. Heinrich Schindler
Matrikel-Nr. 0225800
Mechtlerstr. 17, 2100 Korneuburg

CERN-THESIS-2012-208
13/12/2012

Diese Arbeit wurde unterstützt vom
Österreichischen Bundesministerium für Wissenschaft und Forschung.

Wien, im Oktober 2012

Garfield++ User Guide



Version 2020.5

H. Schindler

July 2020

Magboltz and Heed

Magboltz - transport of electrons in gas mixtures

Responsible at CERN: [Rob Veenhof](#)

Manual Type: Source files, cross sections

Versions: 11.10

Author: [Stephen Biagi](#)

Reference: none

Created: 20 May 1995

Last Update: 3 Nov 2020

Verified: 3 Nov 2020

Valid until: further notice

Support Level: [Normal](#)

Magboltz

Magboltz solves the Boltzmann transport equations for electrons in gas mixtures under the influence of electric and magnetic fields.

Further information:

- [LXCAT](#) cross section compilation;
- The [cross sections](#) used by Magboltz 7.1, interfaced with Garfield 9 (current default)
- How to [use](#) Magboltz

Magboltz source files:

- Source [file](#) for version 7.1 (default since 13/4/2005);
- Source [file](#) for version 8.9.1 (edition of 27 Sep 2010, reinstoring GeH₄ and SiH₄ and improving C₂H₂F₄);
- Source [file](#) for version 8.9.2 (edition of 14 Nov 2010, hydrogen update);
- Source [file](#) for version 8.9.3 (edition of 24 Feb 2011, xenon ionisation cross section corrected);
- Source [file](#) for version 8.9.4 (edition of 25 May 2011, xenon ionisation cross section changed at threshold);
- Source [file](#) for version 8.9.5 (edition of 12 Jun 2011, TMA);
- Source [file](#) for version 8.9.6 (edition of 27 Aug 2011, update of low energy argon excitation cross sections);
- Source [file](#) for version 8.9.7 (edition of 25 Sep 2011, krypton update);
- The source file for version 9.0.1 (edition of 12 May 2012) was corrected with version 9.0.3;
- Source [file](#) for version 9.0.3 (edition of 28 Aug 2013);
- The source file for version 10.0.1 (edition of 24 Apr 2013) was corrected with version 10.0.2;
- Source [file](#) for version 10.0.2 (edition of 28 Aug 2013);
- Source [file](#) for version 10.0.4 (edition of 17 Jun 2014);
- Source [file](#) for version 10.6 (edition of 3 Dec 2014);
- Source [file](#) for version 10.13 (edition of 5 Oct 2015);
- Source [file](#) for version 10.14 (edition of 12 Jan 2016);
- Source [file](#) for version 11.1 (edition of 14 Dec 2016);
- Source [file](#) for version 11.2 (edition of 19 Oct 2017);
- Source [file](#) for version 11.3 (edition of 29 Nov 2017);
- Source [file](#) for version 11.4 (edition of 29 Apr 2018);
- Source [file](#) for version 11.5 (edition of 23 Oct 2018);
- Source [file](#) for version 11.6 (edition of 13 Nov 2018);
- Source [file](#) for version 11.7 (edition of 26 Feb 2019);
- Source [file](#) for version 11.9 (edition of 30 Aug 2019);
- Source [file](#) for version 11.10 (edition of 3 Nov 2020).

<https://magboltz.web.cern.ch/magboltz/>



Nuclear Instruments and Methods in Physics Research Section A: Accelerators, Spectrometers, Detectors and Associated Equipment

Volume 554, Issues 1–3, 1 December 2005, Pages 474–493



Modeling of ionization produced by fast charged particles in gases

I.B. Smirnov

Show more

Share Cite

<https://doi.org/10.1016/j.nima.2005.08.064>

[Get rights and content](#)

<https://doi.org/10.1016/j.nima.2005.08.064>

Timing simulations for silicon with GARFIELD++

Interfacing to GEANT:



Interfacing Geant4, Garfield++ and Degrad for the simulation of gaseous detectors

Dorothea Pfeiffer^{a,b,*}, Lennert De Keukeleere^{c,d}, Carlos Azevedo^e, Francesca Belloni^f, Stephen Biagi^g, Vladimir Grichine^h, Leendert Hayenⁱ, Andrei R. Hanu^h, Ivana Hřivnáčová^j, Vladimir Ivanchenko^{k,l}, Vladyslav Krylov^{k,l}, Heinrich Schindler^k, Rob Veenhof^{k,m}

Jan Hasenbichler (CERN TU-Vienna): monolithic silicon detectors (ALPIDE), cluster size, efficiency, time resolution

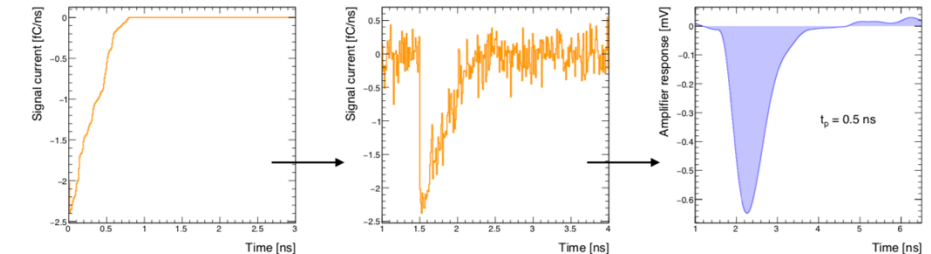
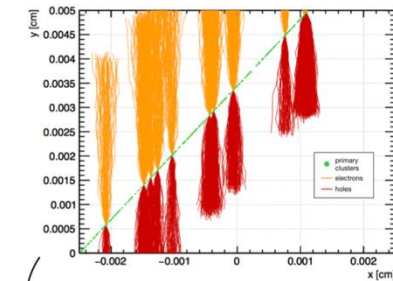
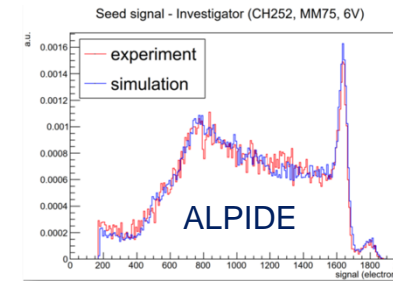
Ann Wang (Harvard University): time resolution of silicon detectors, LGADs, frontend electronics, noise

Francesca Carnesecchi (Bologna): time resolution of LGADs

Marius Maehlum Halvorse: time resolution of silicon sensors

H. Schindler & EPFL group of E. Charbon: time resolution and efficiency of SPADs

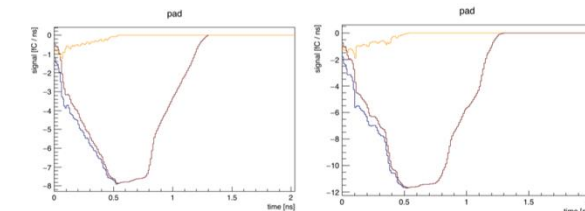
D. Janssens & INFN Torino group of N. Cartiglia: time resolution and efficiency of AC-LGADs



```
void Sensor::AddWhiteNoise(const
double enc, const bool poisson,
const double q0)
```

```
double
UnipolarShaper(const
double t) const;
```

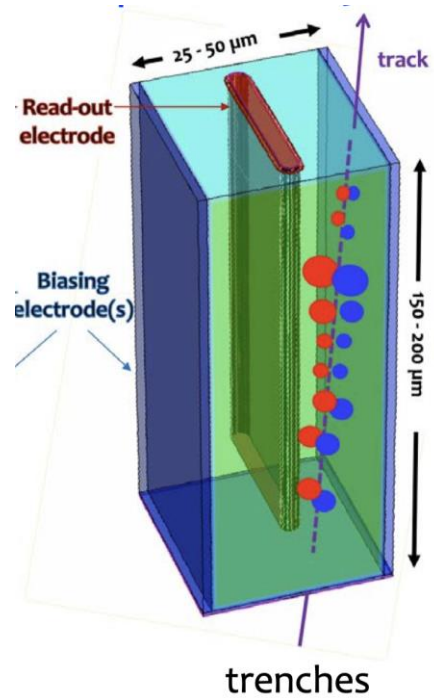
LGAD



- * orange = primary electron signal (no primary hole signal)
- * brown = avalanche hole signal
- * blue = total

Thank You !

3D sensor realising a parallel plate geometry, TimeSPOT



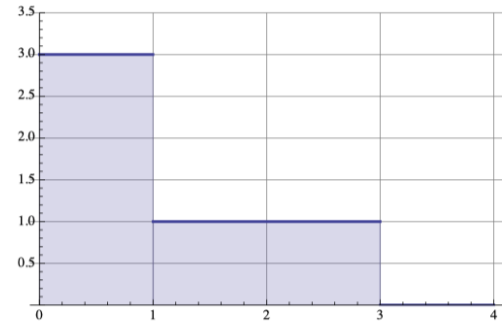
Total charge from the 200μm sensor but timing characteristics from a 25μm sensor !

L. Anderlini et al., *Intrinsic time resolution of 3D-trench silicon pixels for charged particle detection*. JINST 15, P09029, 2020.

D. Brundu et al., *Accurate modelling of 3D-trench silicon sensor with enhanced timing performance and comparison with test beam measurements*. JINST 16, P09028, 2021.

For a perfectly perpendicular track:
'box' signals from electrons and holes.

Landau fluctuations affect just the total pulse-height, which can be corrected.



$$i(t) = -\frac{qv_1}{d}\Theta(z/v_1 - t) - \frac{qv_2}{d}\Theta((d-z)/v_2 - t)$$

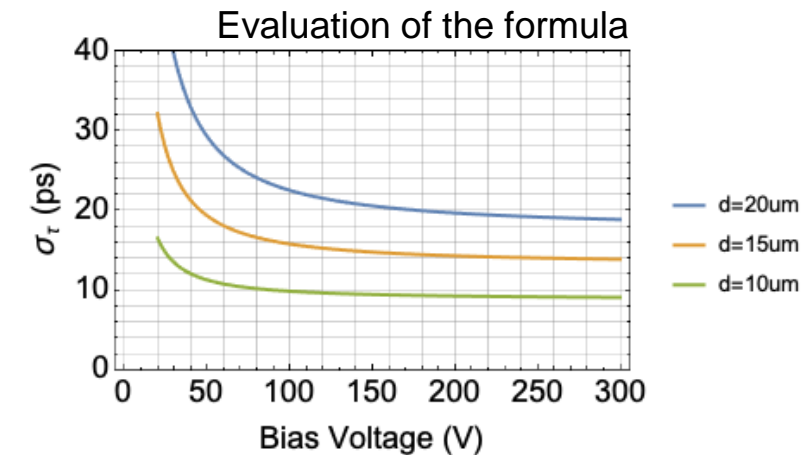
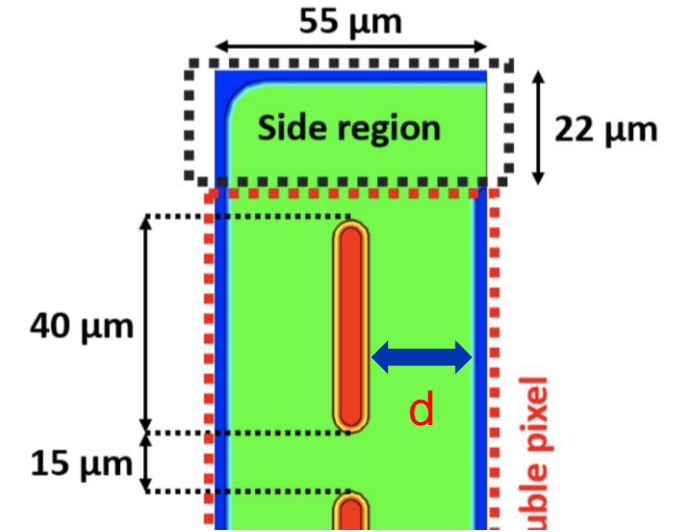
c.o.g. time of the signal

$$\tau(z) = \frac{1}{2d} \left(\frac{z^2}{v_e} + \frac{(d-z)^2}{v_h} \right)$$

Variance of the c.o.g. Time for uniform distribution of tracks

$$\bar{\tau} = \frac{1}{d} \int_0^d \tau(z) dz \quad \overline{\tau^2} = \frac{1}{d} \int_0^d \tau(z)^2 dz$$

$$\sigma_\tau = \sqrt{\overline{\tau^2} - \bar{\tau}^2} = \sqrt{\frac{4}{180} \frac{d^2}{v_e^2} - \frac{7}{180} \frac{d^2}{v_e v_h} + \frac{4}{180} \frac{d^2}{v_h^2}}$$



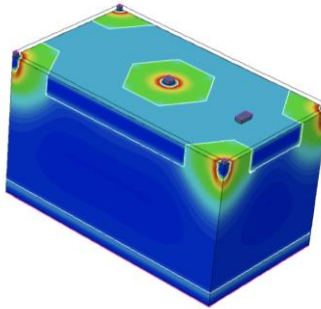
→ 10-20ps achievable and indeed achieved !

FASTPIX: a monolithic CMOS Sensor with <200ps timing

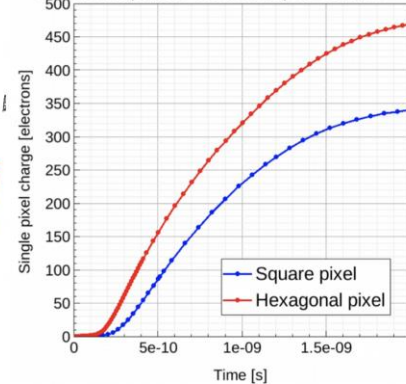
Sensor Optimization for FASTPIX

- Hexagonal design reduces the number of neighbors and charge sharing → higher efficiency
- Hexagonal design minimizes the edge regions while maintaining area for circuitry → faster charge collection
- Other optimised parameters include opening of p-wells, size of collection electrode, deep n-implant... to optimise charge collection and capacitance
→ see M. Munker at [iWoRiD 2021](#) for details on sensor optimisation
- Optimisations important not only for timing, but also for efficiency and radiation tolerance

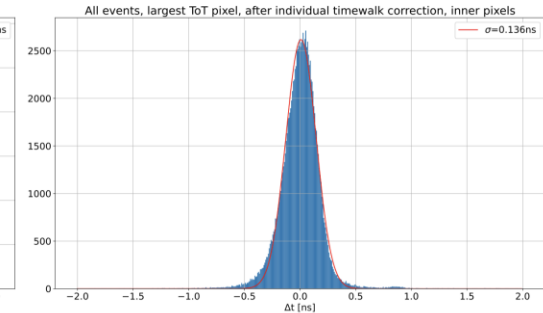
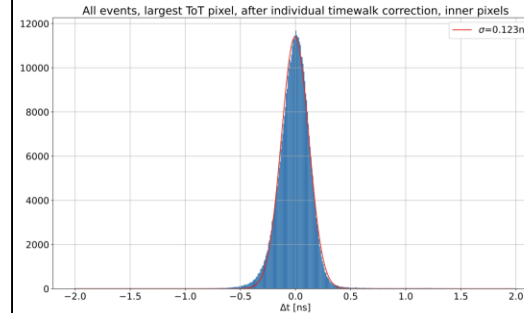
Simulated hexagonal unit cell – electrostatic potential:



Comparison hexagonal to square pixel cell charge vs. time for particle incident at pixel corner:



Test-beam Measurements



Wafer 18
-6V/-6V pwell/
backside

20x20 μm²
matrix (left)
70e threshold

10x10 μm²
matrix (right)
50e threshold

- Timing after timewalk correction on 20μm (left) and 10μm (right) matrix
- Pixel-by-pixel correction for best results, reaching below 200ps resolution
- 10μm matrix is operated at lower threshold with a few Hz noise rate
- Larger cluster sizes for 10μm leads to lower average seed charge and thereby more time walk and makes decoding more difficult

[WORKSHOP ON PICO-SECOND TIMING DETECTORS FOR PHYSICS](#)

9–11 Sep 2021

University of Zurich

Eric Buschmann

<https://indico.cern.ch/event/861104/contributions/4503032/>

< 200ps achieved with a MAPS sensor !